Supporting Information

Multifaceted Antibacterial Action of Dihydrofurocoumarins Against Drug-Resistant *Escherichia coli*: Biofilm Inhibition, Membrane Disruption, Metabolic Dysfunction, and Oxidative Stress Damage

Anmol Jain, Kamaldeep Paul*

[a]Department of Chemistry and Biochemistry, Thapar Institute of Engineering and Technology, Patiala-147004, Punjab, India

[b]TIET-VT, Centre of Excellence in Emerging Materials, Thapar Institute of Engineering and Technology, Patiala-147004, Punjab, India

*Email: kpaul@thapar.edu

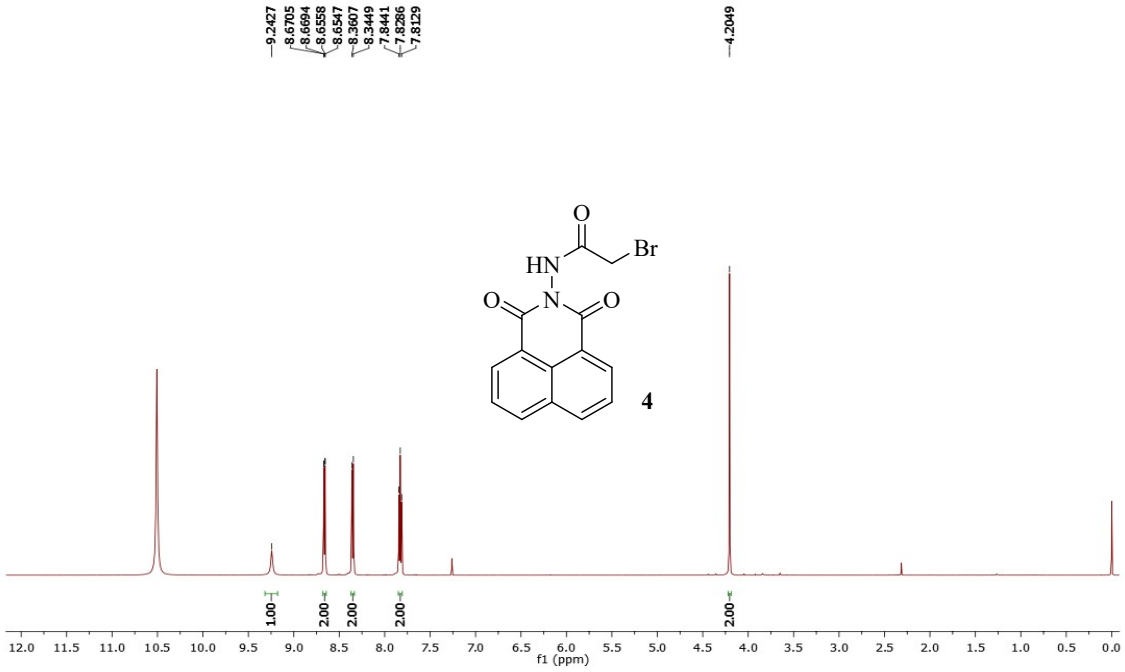

Figure S1: ^{1}H NMR spectrum of 2-bromo-*N*-(1,3-dioxo-1*H*-benzo[*de*]isoquinolin-2(3*H*)-yl)acetamide (4)

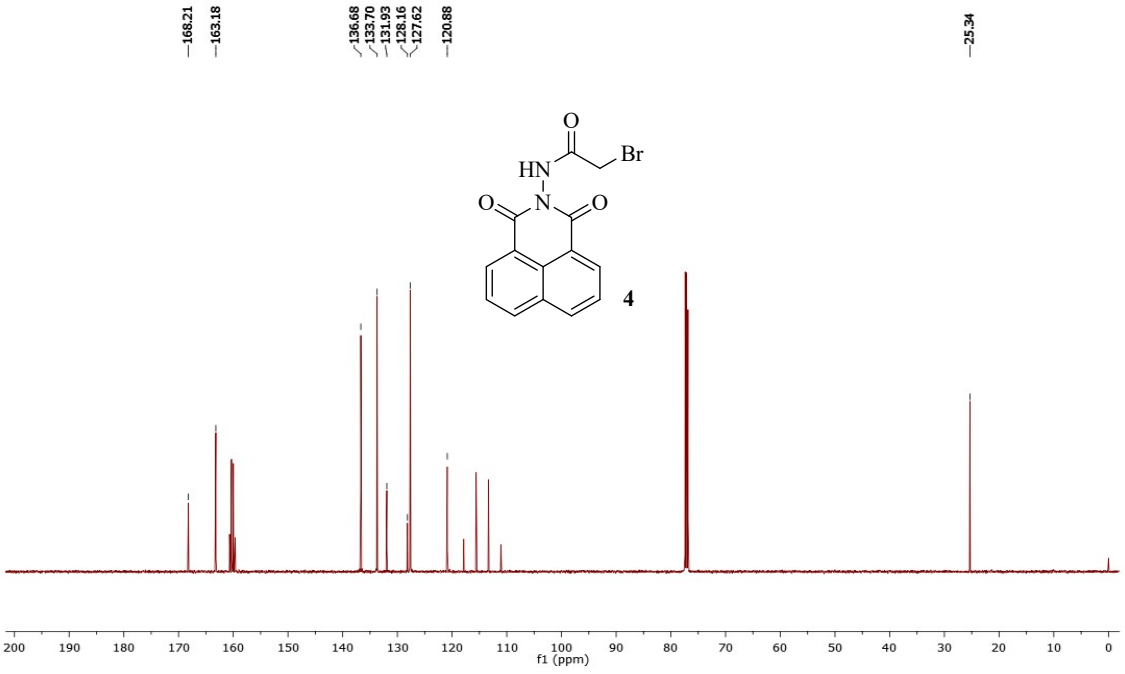

Figure S2: ^{13}C NMR spectrum of 2-bromo-*N*-(1,3-dioxo-1*H*-benzo[*de*]isoquinolin-2(3*H*)-yl)acetamide (4)

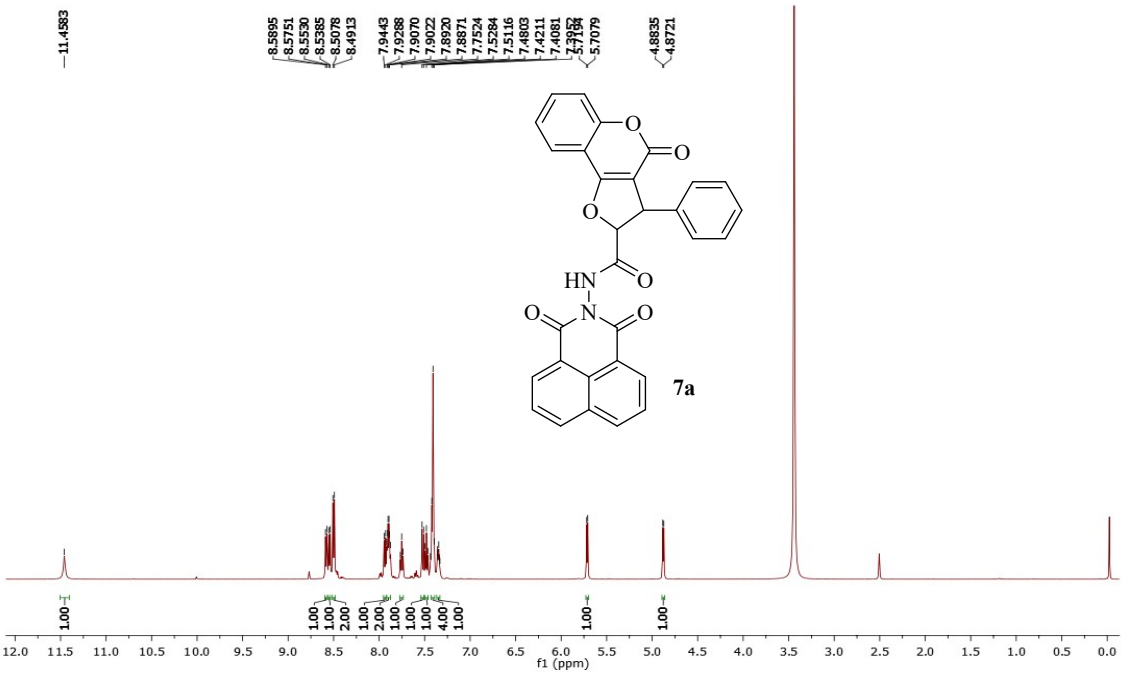

Figure S3: ^{1}H NMR spectrum of *N*-(1,3-dioxo-1*H*-benzo[*de*]isoquinolin-2(3*H*)-yl)-4-oxo-3-phenyl-2,3-dihydro-4*H*-furo[3,2-*c*]chromene-2-carboxamide (7a)

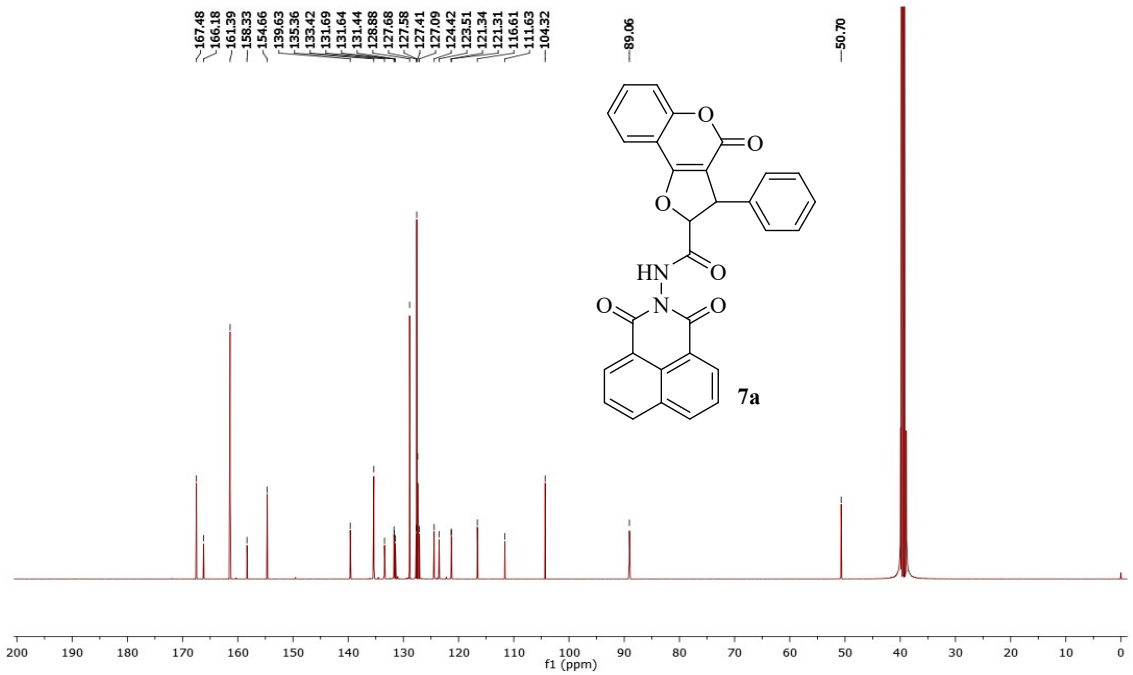

Figure S4: ^{13}C NMR spectrum of *N*-(1,3-dioxo-1*H*-benzo[*de*]isoquinolin-2(3*H*)-yl)-4-oxo-3-phenyl-2,3-dihydro-4*H*-furo[3,2-*c*]chromene-2-carboxamide (7a)

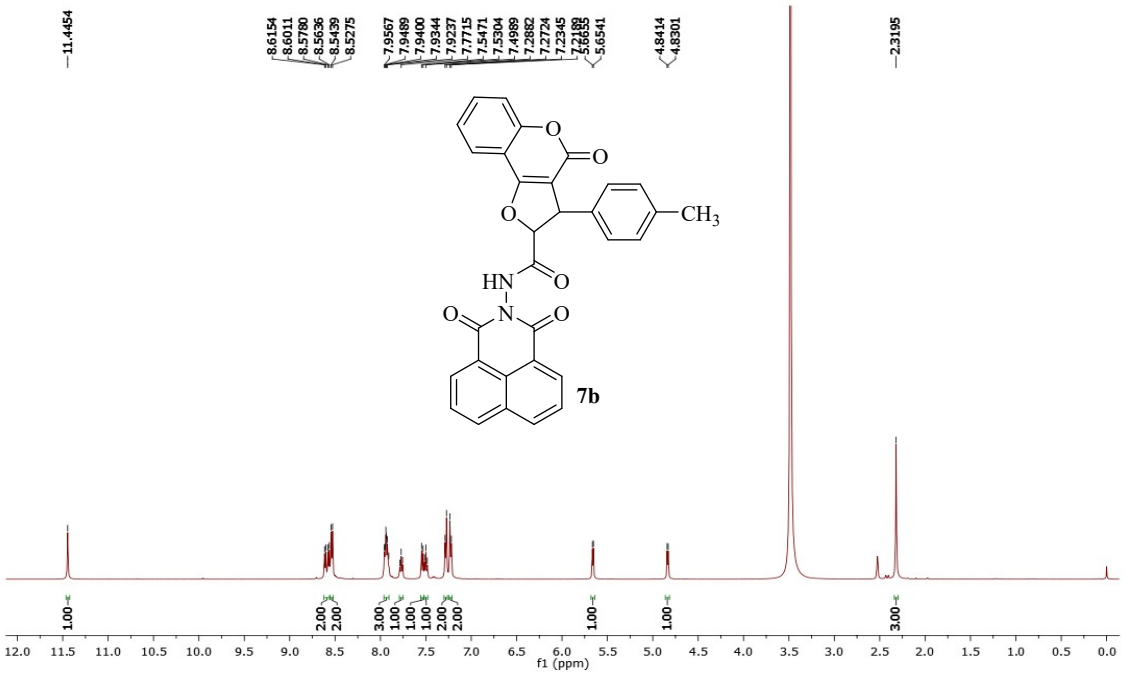

Figure S5: ^{1}H NMR spectrum of *N*-(1,3-dioxo-1*H*-benzo[*de*]isoquinolin-2(3*H*)-yl)-4-oxo-3-(*p*-tolyl)-2,3-dihydro-4*H*-furo[3,2-*c*]chromene-2-carboxamide (7b)

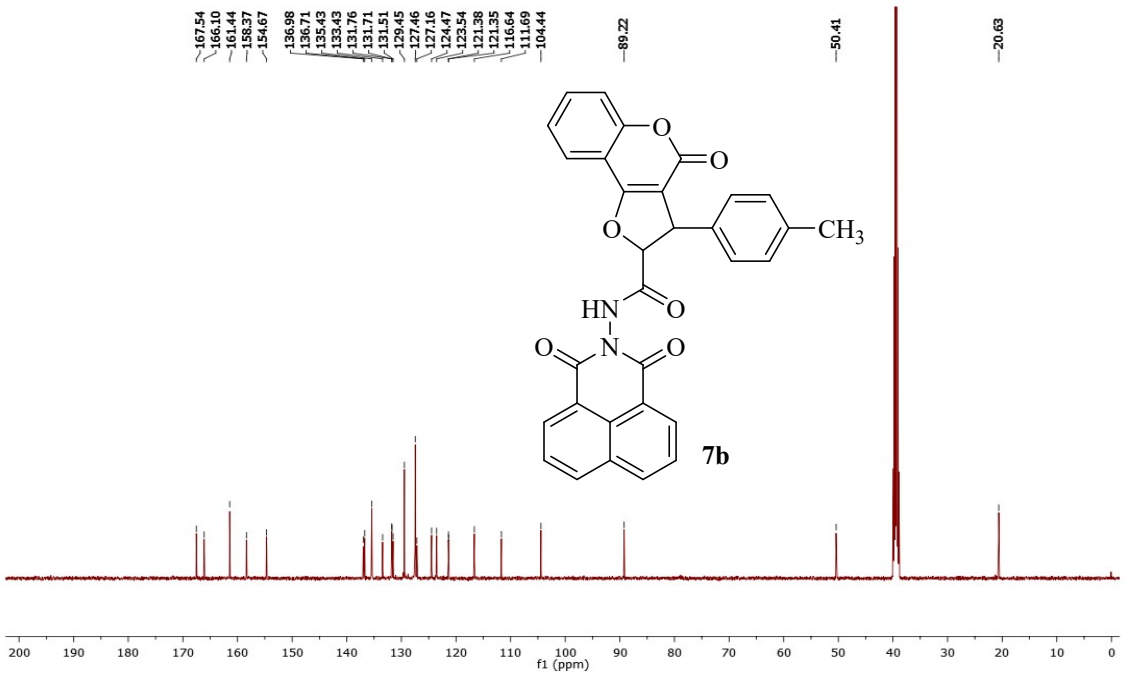

Figure S6: ^{13}C NMR spectrum of *N*-(1,3-dioxo-1*H*-benzo[*de*]isoquinolin-2(3*H*)-yl)-4-oxo-3-(*p*-tolyl)-2,3-dihydro-4*H*-furo[3,2-*c*]chromene-2-carboxamide (7b)

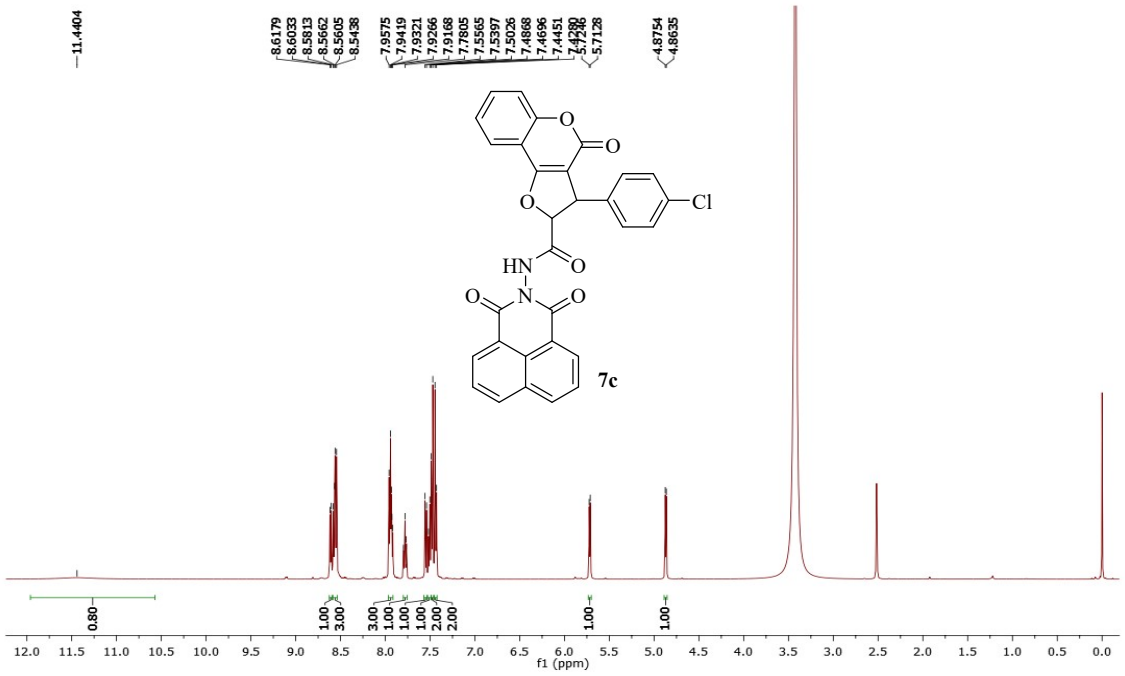

Figure S7: ^{1}H NMR spectrum of 3-(4-chlorophenyl)-*N*-(1,3-dioxo-1*H*-benzo[*de*]isoquinolin-2(3*H*)-yl)-4-oxo-2,3-dihydro-4*H*-furo[3,2-*c*]chromene-2-carboxamide (7c)

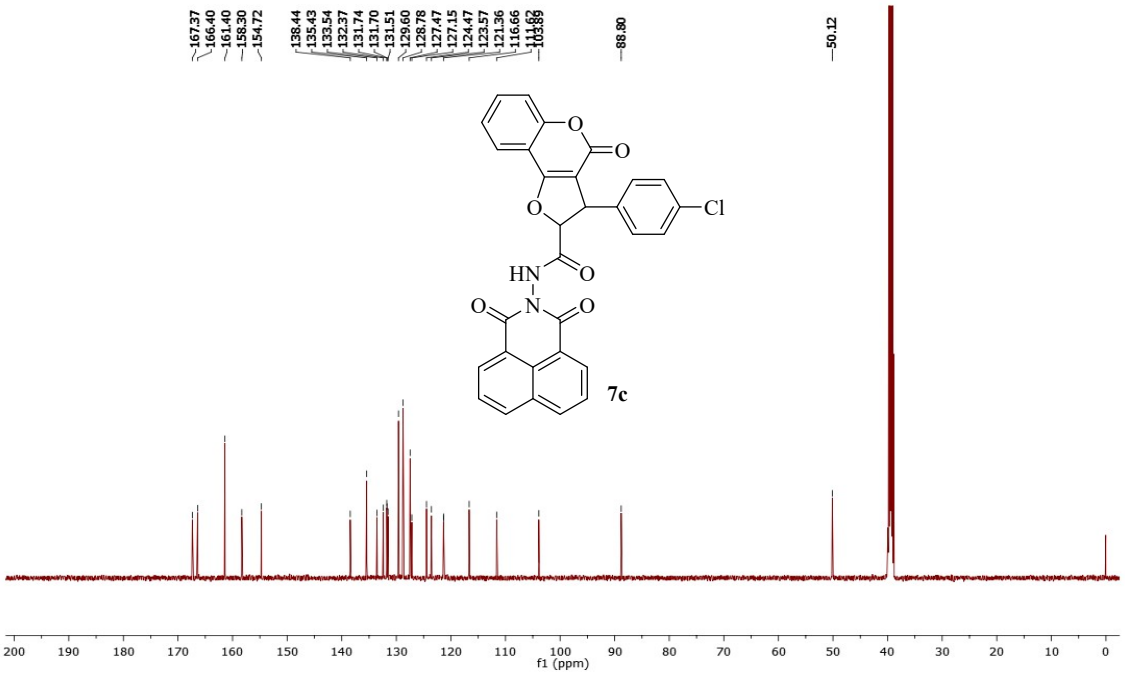

Figure S8: ^{13}C NMR spectrum of 3-(4-chlorophenyl)-*N*-(1,3-dioxo-1*H*-benzo[*de*]isoquinolin -2(3*H*)-yl)-4-oxo-2,3-dihydro-4*H*-furo[3,2-*c*]chromene-2-carboxamide (7c)

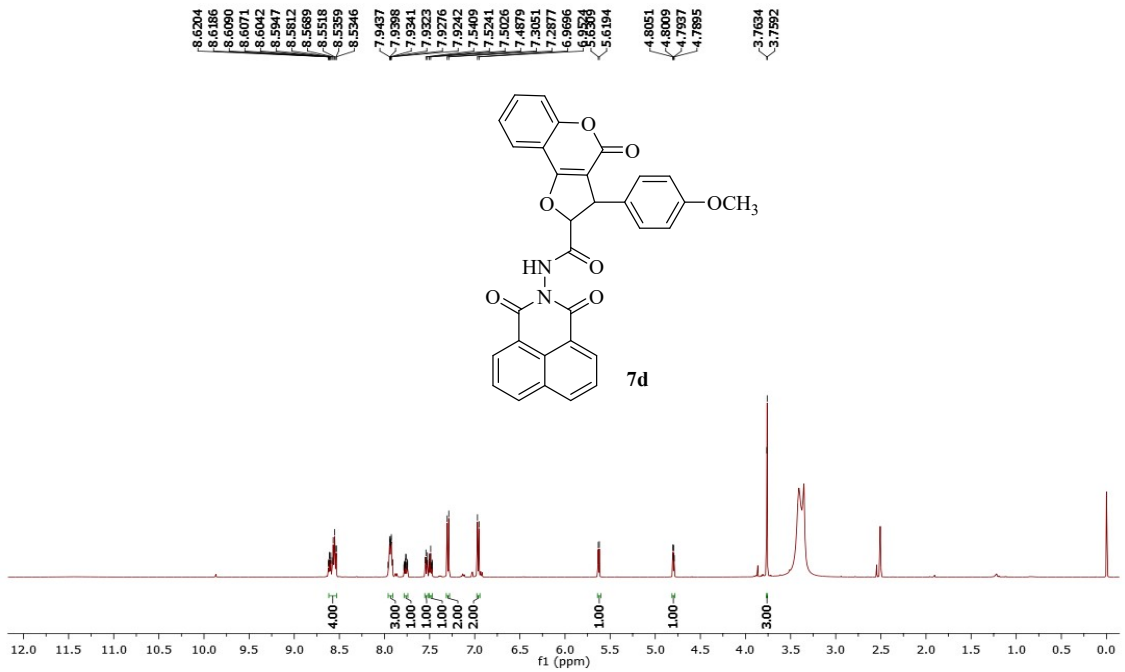

Figure S9: ^{1}H NMR spectrum of *N*-(1,3-dioxo-1*H*-benzo[*de*]isoquinolin-2(3*H*)-yl)-3-(4-methoxyphenyl)-4-oxo-2,3-dihydro-4*H*-furo[3,2-*c*]chromene-2-carboxamide (7d)

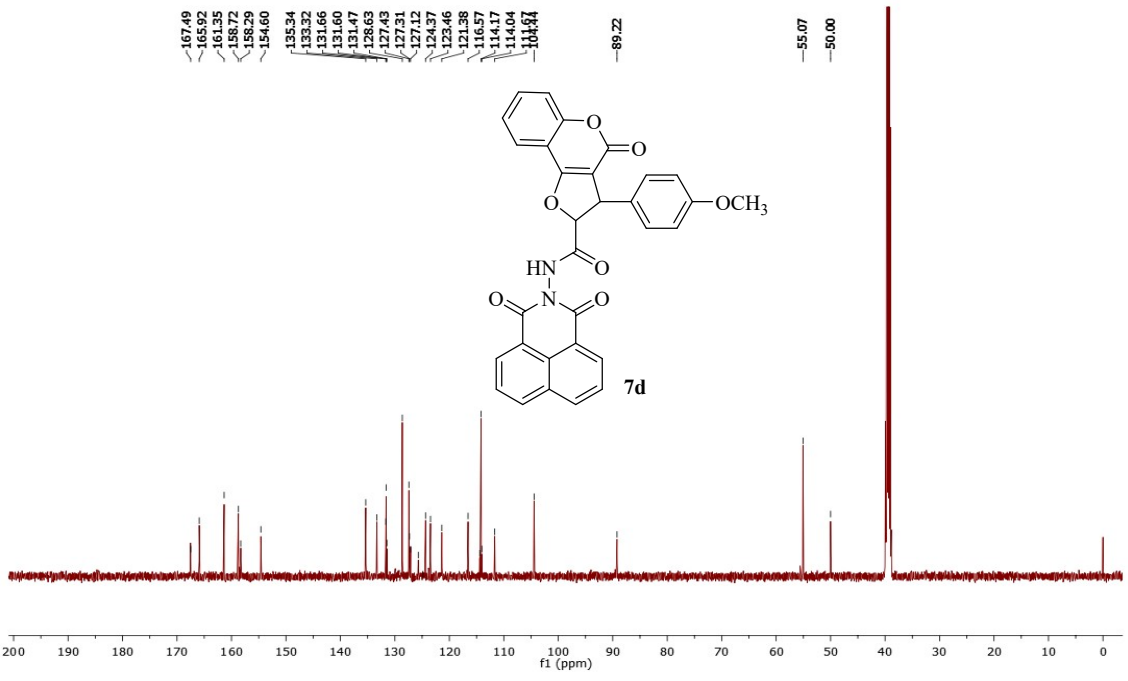

Figure S10: ^{13}C NMR spectrum of *N*-(1,3-dioxo-1*H*-benzo[*de*]isoquinolin-2(3*H*)-yl)-3-(4-methoxyphenyl)-4-oxo-2,3-dihydro-4*H*-furo[3,2-*c*]chromene-2-carboxamide (7d)

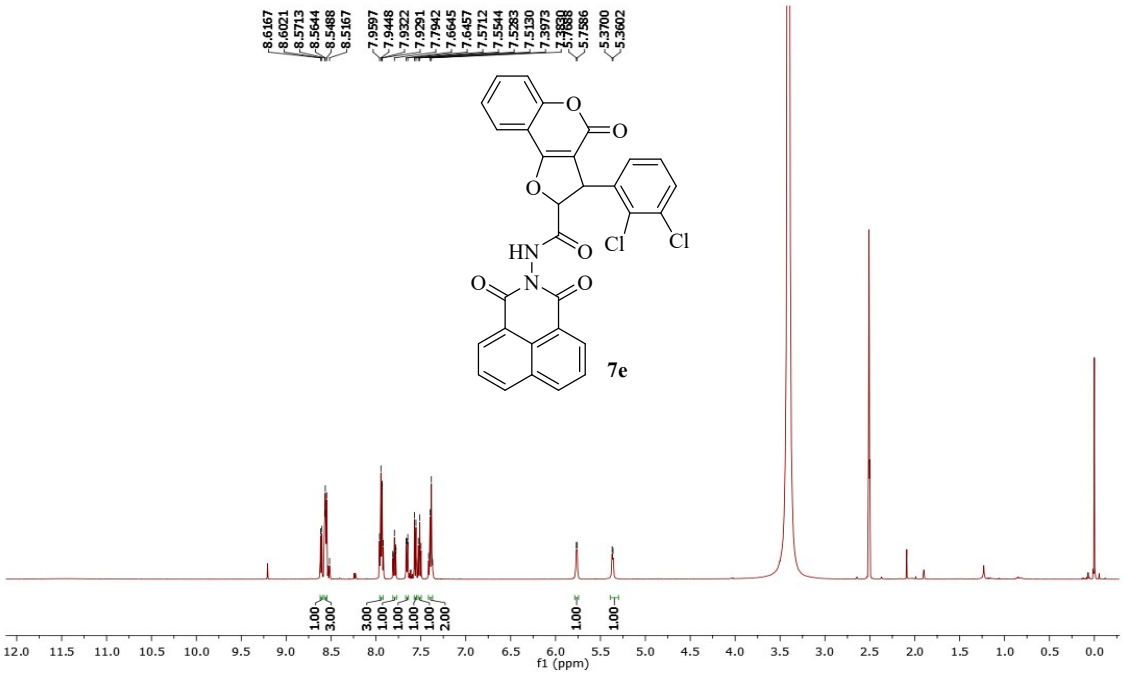

Figure S11: ^{1}H NMR spectrum of 3-(2,3-dichlorophenyl)-*N*-(1,3-dioxo-1*H*-benzo[*de*] isoquinolin-2(3*H*)-yl)-4-oxo-2,3-dihydro-4*H*-furo[3,2-*c*]chromene-2-carboxamide (7e)

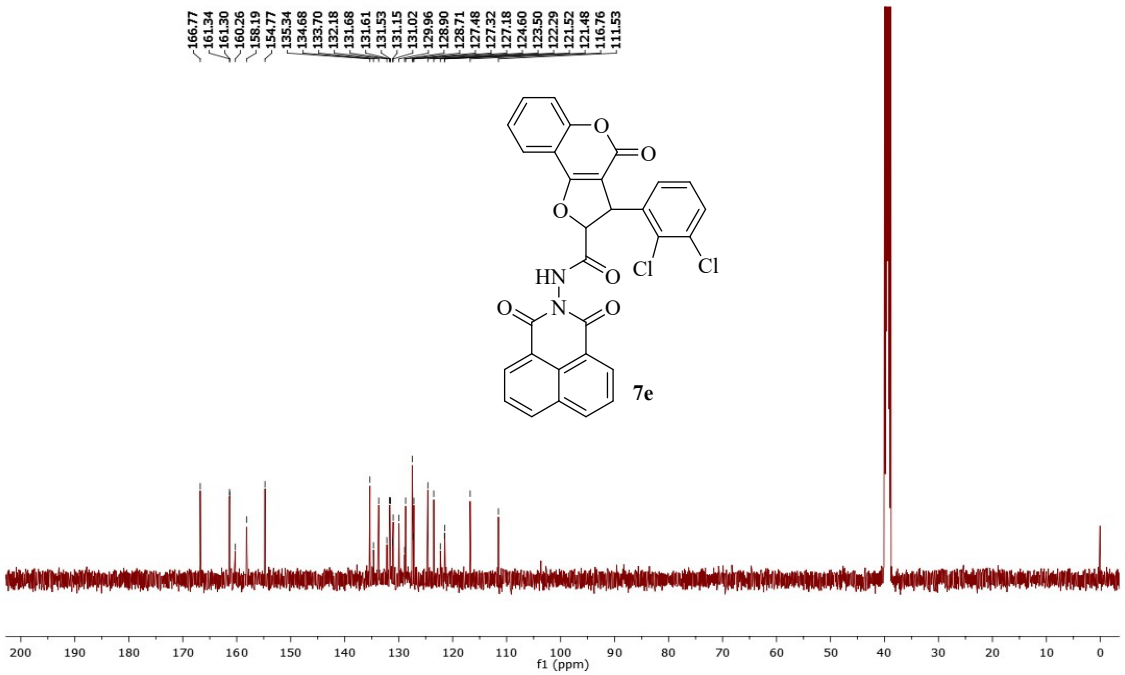

Figure S12: ^{13}C NMR spectrum of 3-(2,3-dichlorophenyl)-*N*-(1,3-dioxo-1*H*-benzo[de] isoquinolin-2(3*H*)-yl)-4-oxo-2,3-dihydro-4*H*-furo[3,2-*c*]chromene-2-carboxamide (7e)

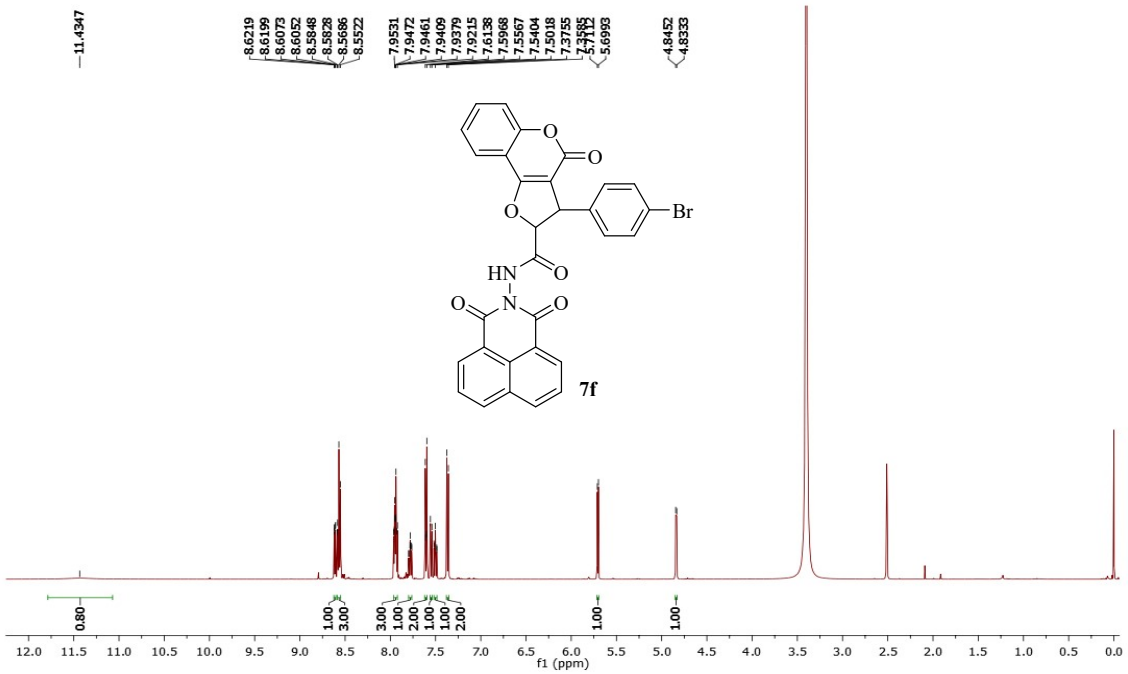

Figure S13: ^{1}H NMR spectrum of 3-(4-bromophenyl)-*N*-(1,3-dioxo-1*H*-benzo[*de*] isoquinolin-2(3*H*)-yl)-4-oxo-2,3-dihydro-4*H*-furo[3,2-*c*]chromene-2-carboxamide (7f)

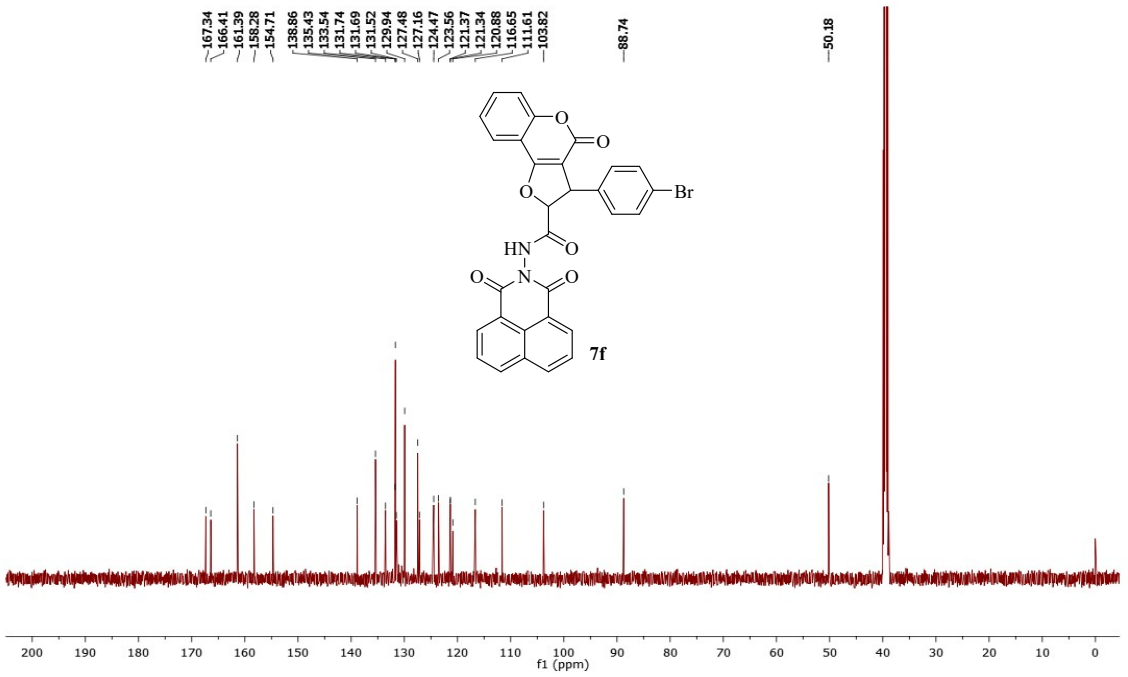

Figure S14: ^{13}C NMR spectrum of 3-(4-bromophenyl)-*N*-(1,3-dioxo-1*H*-benzo[*de*] isoquinolin-2(3*H*)-yl)-4-oxo-2,3-dihydro-4*H*-furo[3,2-*c*]chromene-2-carboxamide (7f)

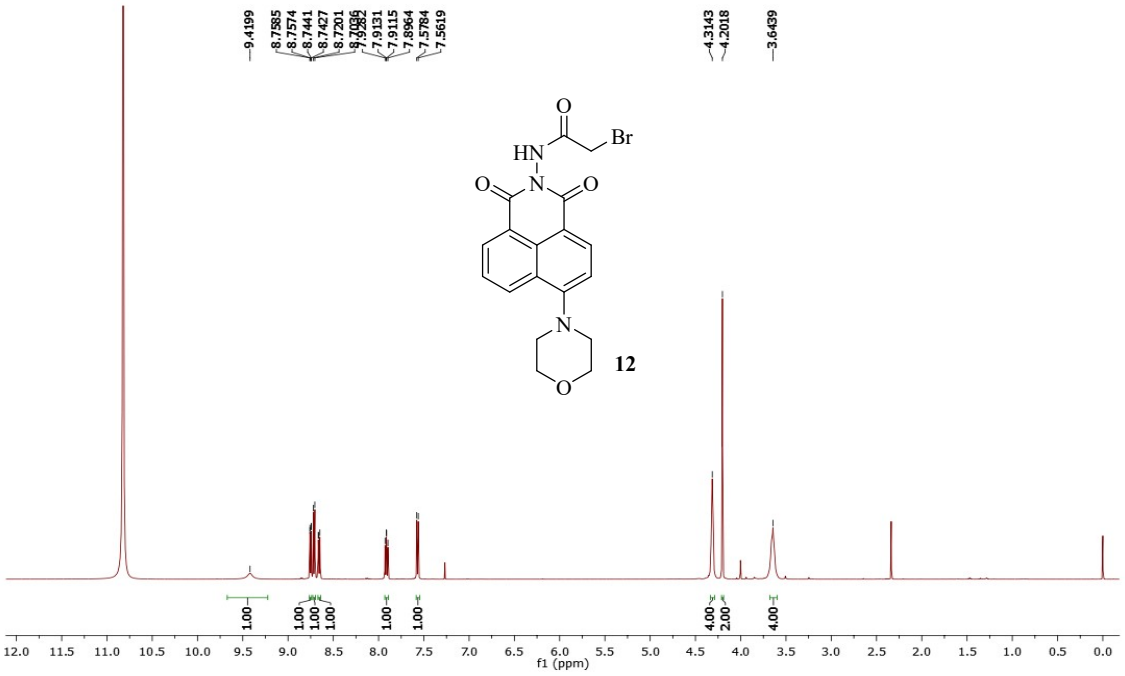

Figure S15: ^{1}H NMR spectrum of 2-bromo-*N*-(6-morpholino-1,3-dioxo-1*H*-benzo[*de*]isoquinolin-2(3*H*)-yl)acetamide (12)

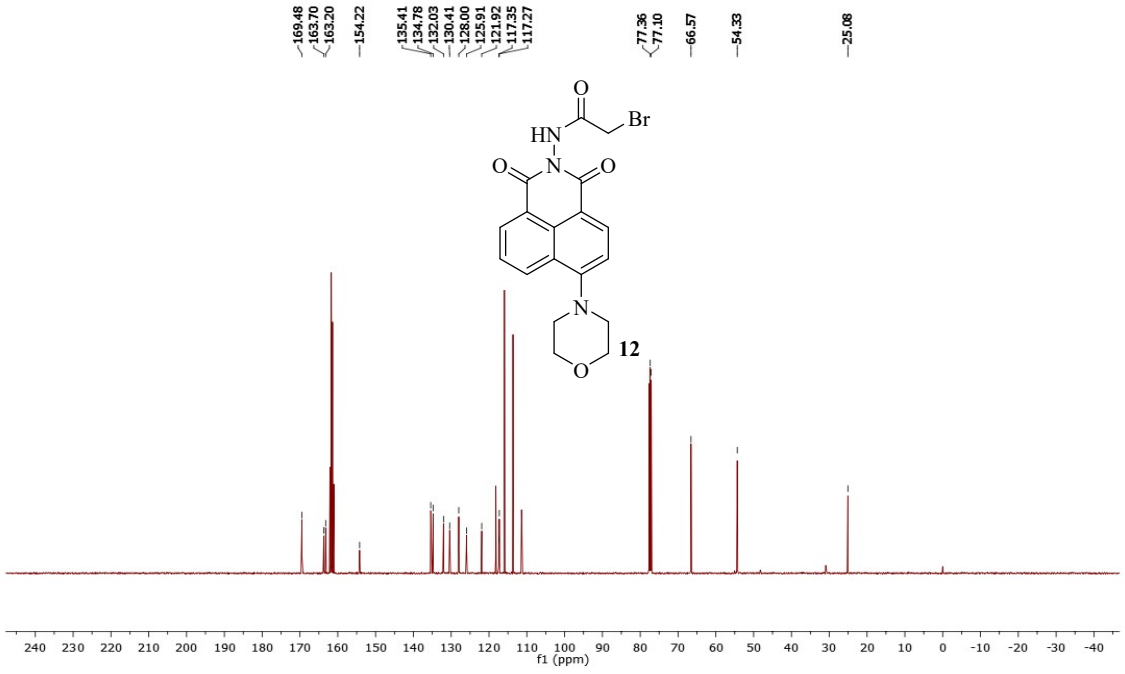

Figure S16: ^{13}C NMR spectrum of 2-bromo-*N*-(6-morpholino-1,3-dioxo-1*H*-benzo[*de*]isoquinolin-2(3*H*)-yl)acetamide (12)

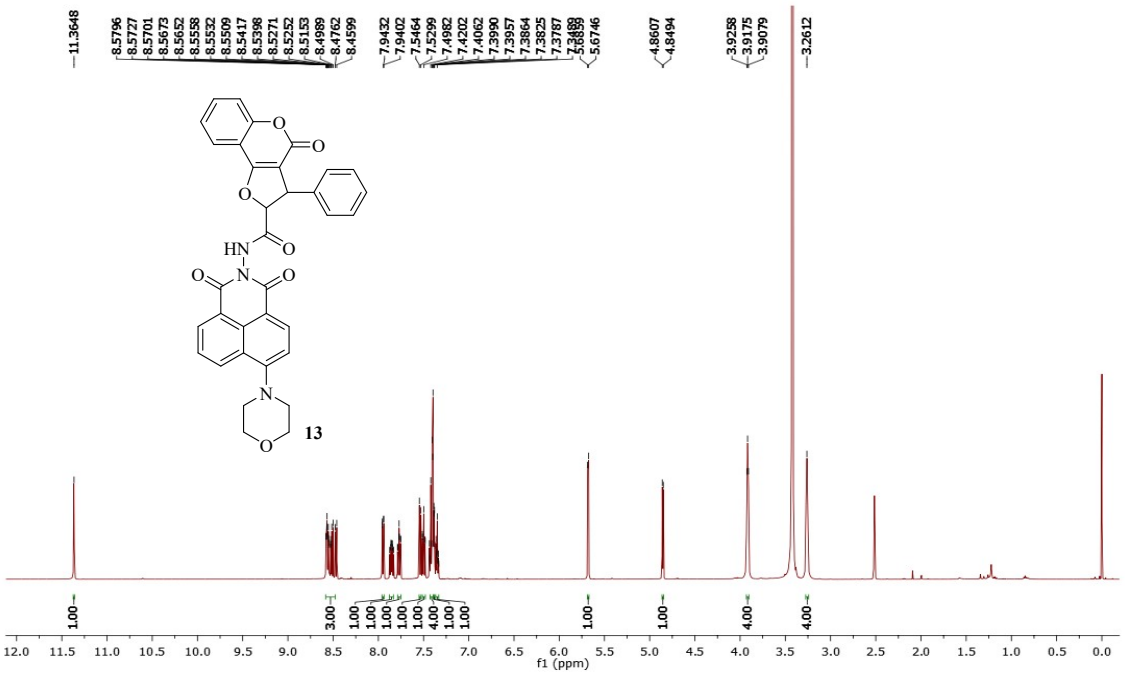

Figure S17: ^{1}H NMR spectrum of *N*-(6-morpholino-1,3-dioxo-1*H*-benzo[*de*]isoquinolin-2(3*H*)-yl)-4-oxo-3-phenyl-2,3-dihydro-4*H*-furo[3,2-*c*]chromene-2-carboxamide (13)

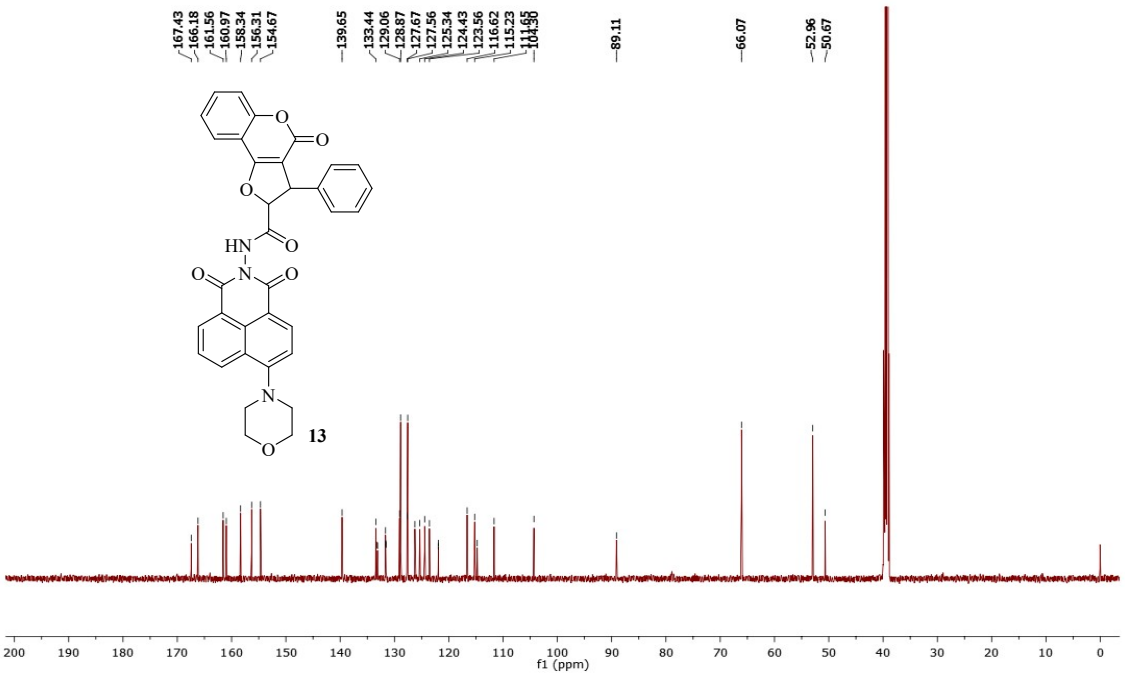

Figure S18: ^{13}C NMR spectrum of *N*-(6-morpholino-1,3-dioxo-1*H*-benzo[*de*]isoquinolin-2(3*H*)-yl)-4-oxo-3-phenyl-2,3-dihydro-4*H*-furo[3,2-*c*]chromene-2-carboxamide (13)

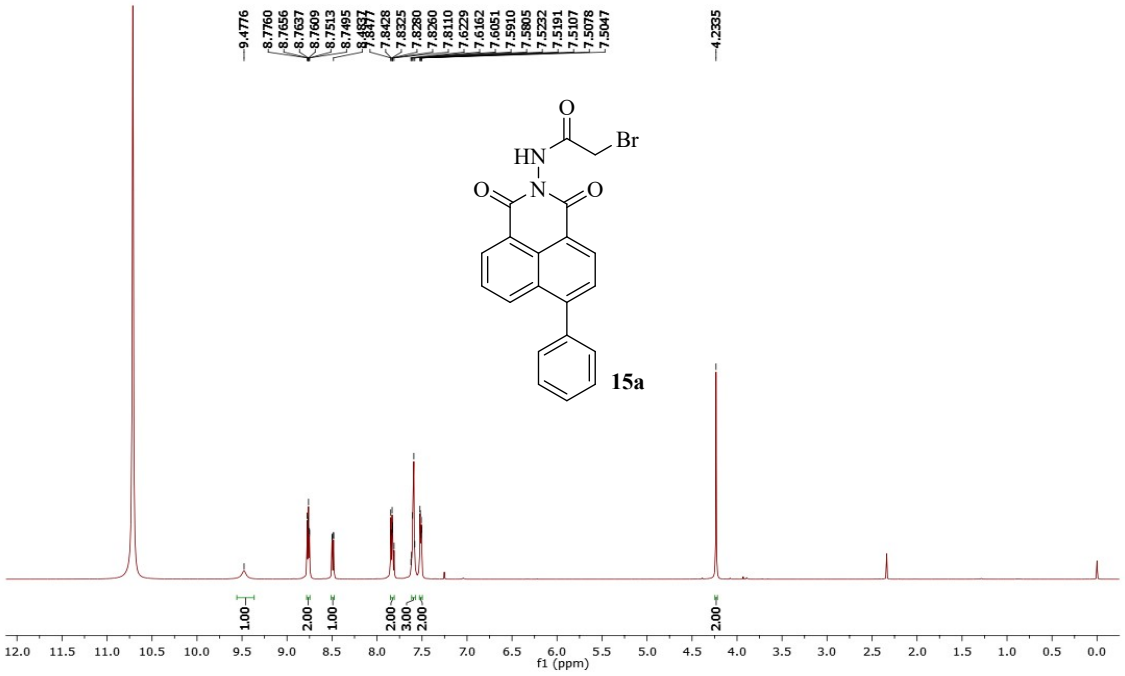

Figure S19: ^{1}H NMR spectrum of 2-bromo-*N*-(1,3-dioxo-6-phenyl-1*H* benzo[*de*]isoquinolin-2(3*H*)-yl)acetamide (15a)

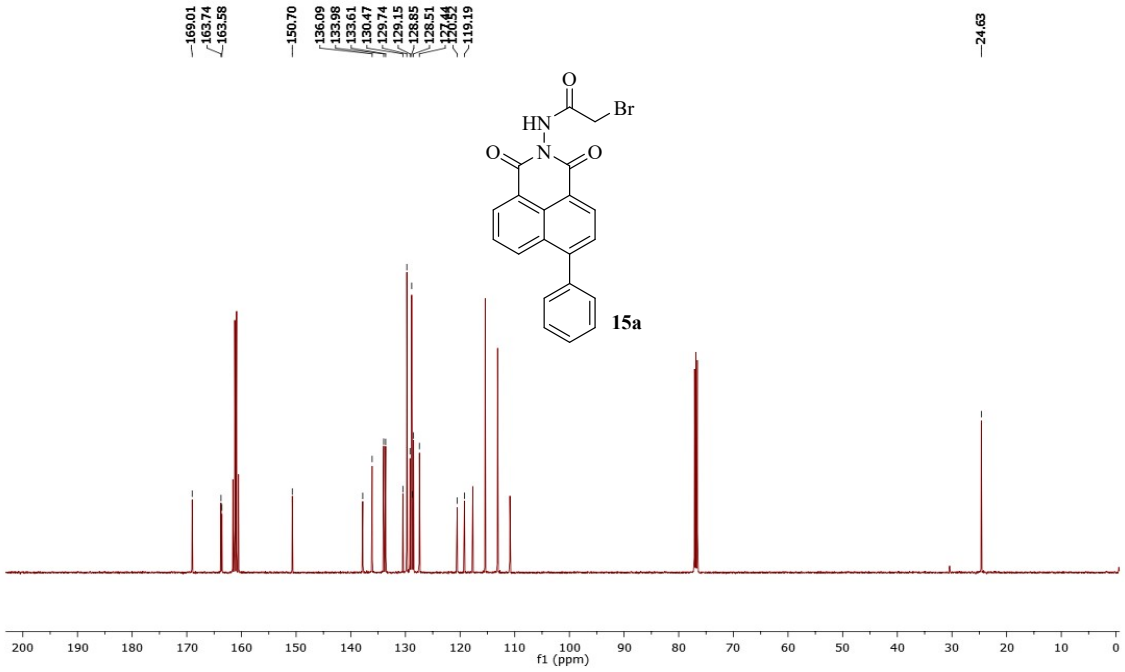

Figure S20: ^{13}C NMR spectrum of 2-bromo-*N*-(1,3-dioxo-6-phenyl-1*H* benzo[*de*]isoquinolin- 2(3*H*)-yl)acetamide (15a)

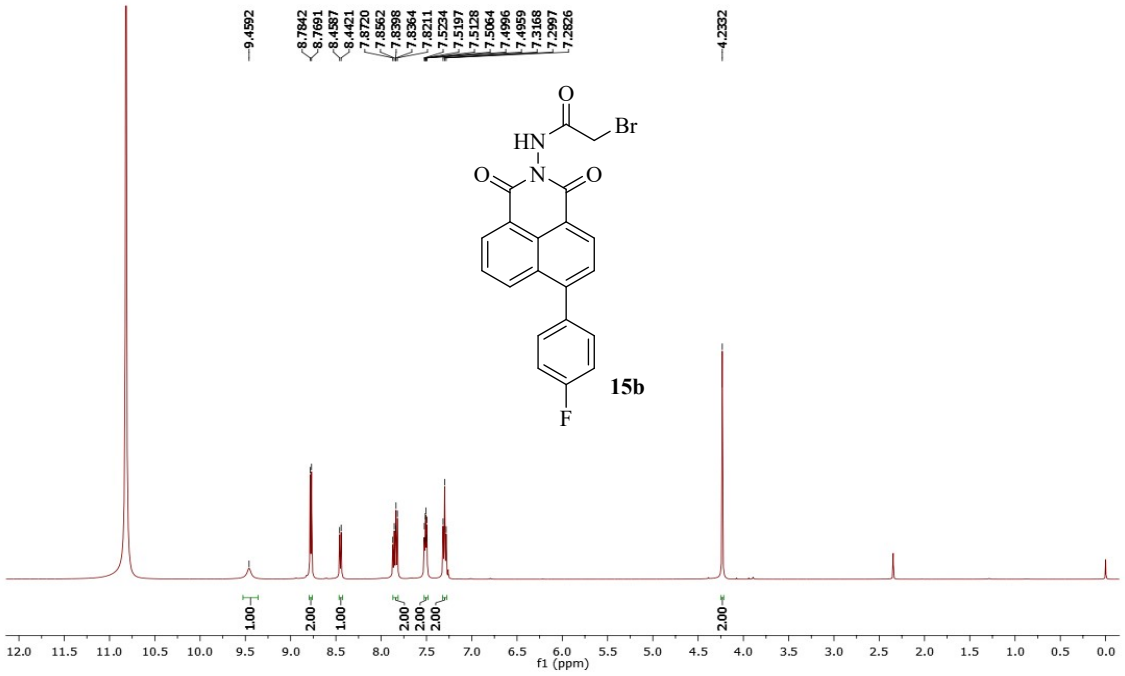

Figure S21: ^{1}H NMR spectrum of 2-bromo-*N*-(6-(4-fluorophenyl)-1,3-dioxo-1*H*-benzo[*de*]isoquinolin-2(3*H*)-yl)acetamide (15b)

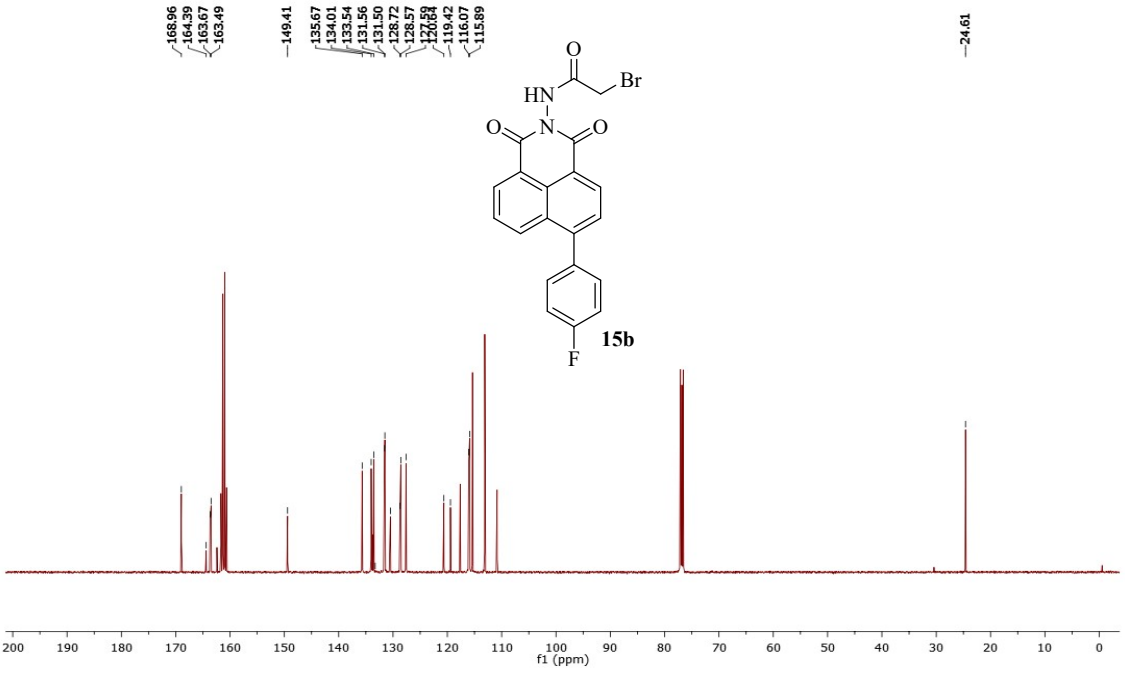

Figure S22: ^{13}C NMR spectrum of 2-bromo-*N*-(6-(4-fluorophenyl)-1,3-dioxo-1*H*-benzo[*de*]isoquinolin-2(3*H*)-yl)acetamide (15b)

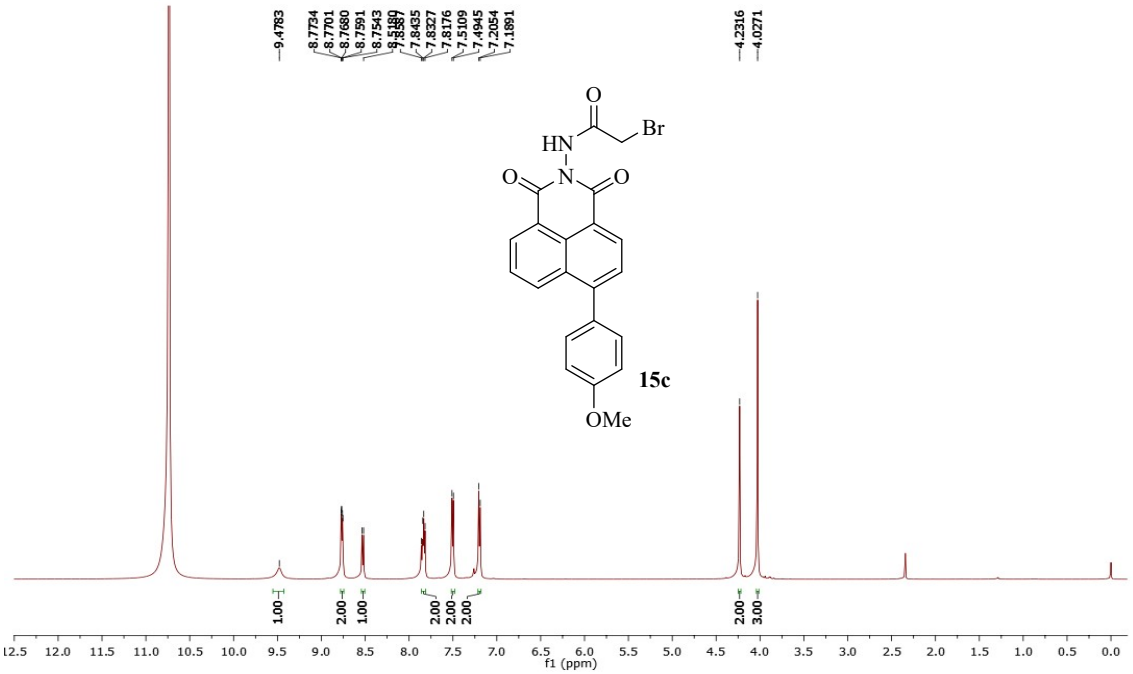

Figure S23: ^{1}H NMR spectrum of 2-bromo-*N*-(6-(4-methoxyphenyl)-1,3-dioxo-1*H*-benzo[*de*]isoquinolin-2(3*H*)-yl)acetamide (15c)

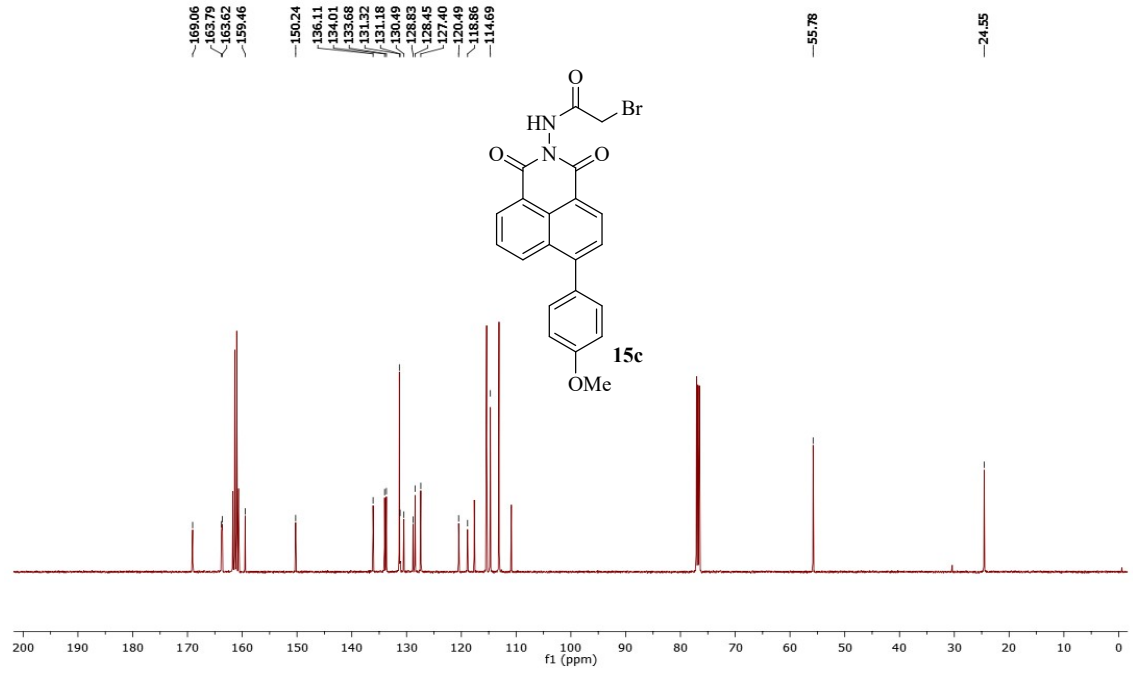

Figure S24: ^{13}C NMR spectrum of 2-bromo-*N*-(6-(4-methoxyphenyl)-1,3-dioxo-1*H*-benzo[*de*]isoquinolin-2(3*H*)-yl)acetamide (15c)

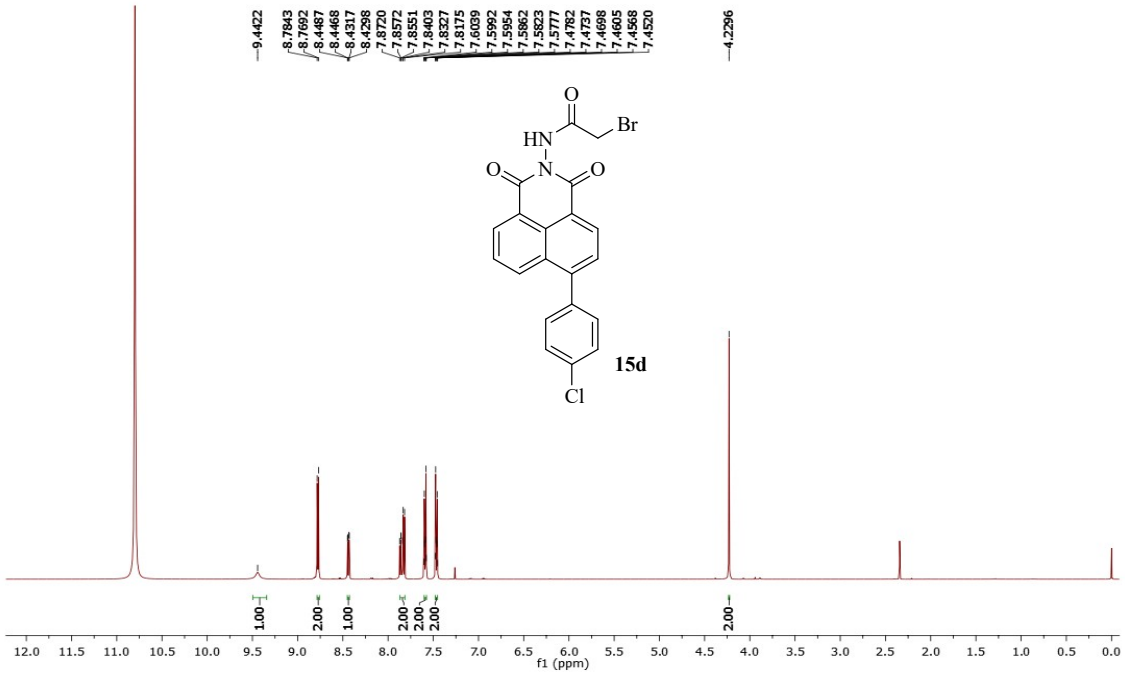

Figure S25: ^{1}H NMR spectrum of 2-bromo-*N*-(6-(4-chlorophenyl)-1,3-dioxo-1*H*-benzo[*de*]isoquinolin-2(3*H*)-yl)acetamide (15d)

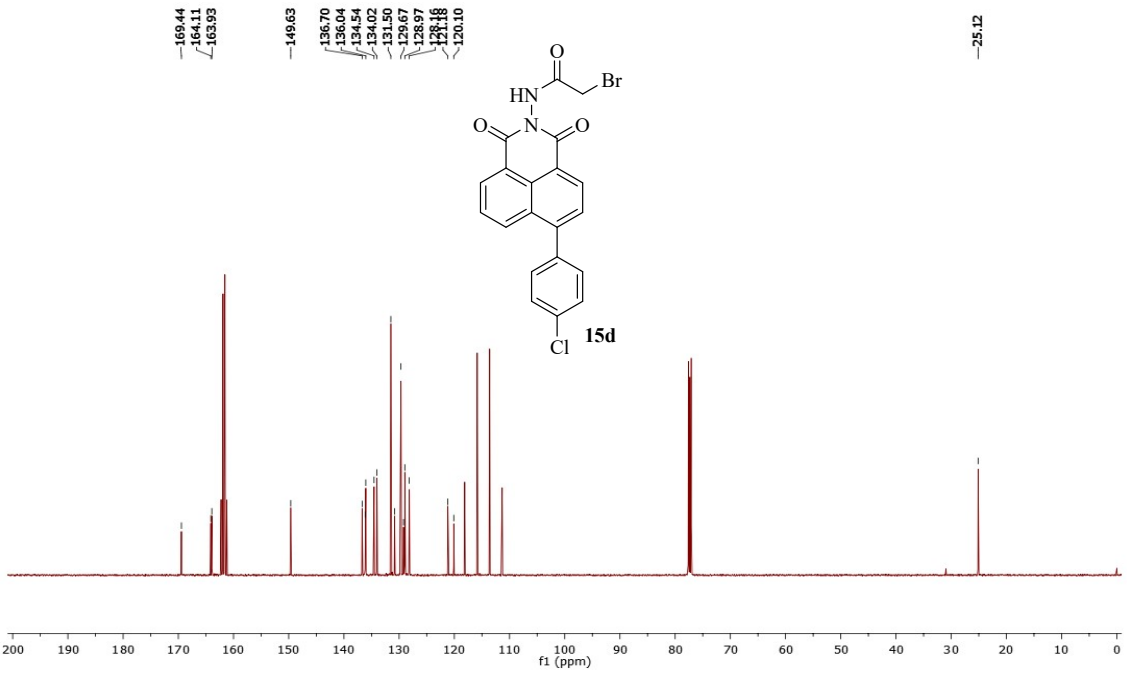

Figure S26: ^{13}C NMR spectrum of 2-bromo-*N*-(6-(4-chlorophenyl)-1,3-dioxo-1*H*-benzo[*de*]isoquinolin-2(3*H*)-yl)acetamide (15d)

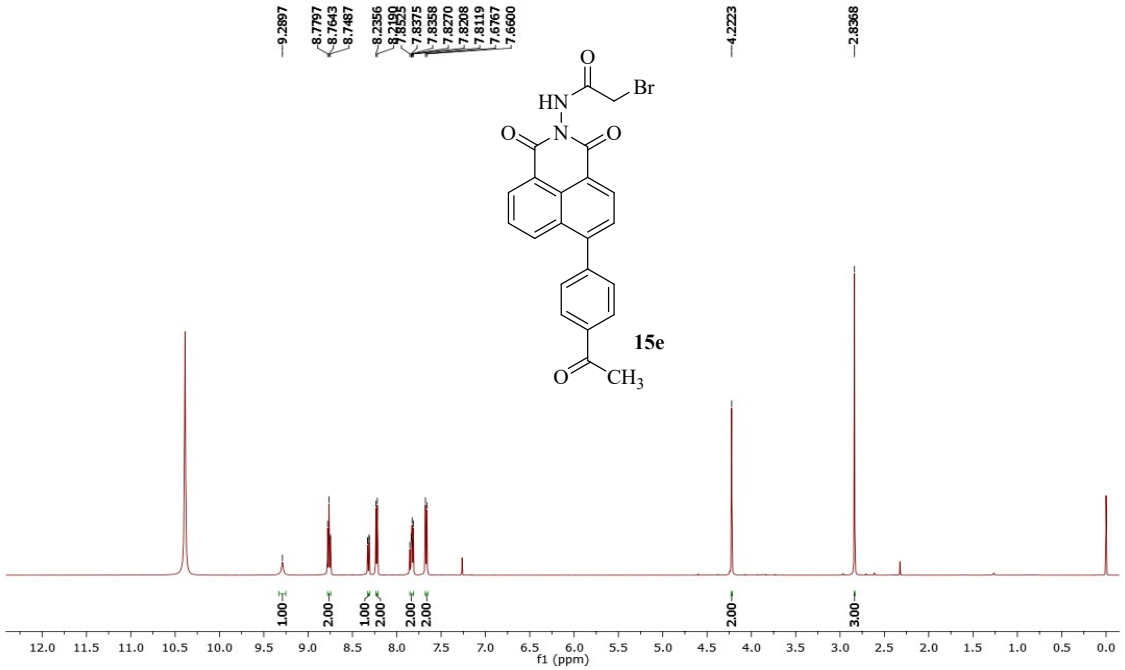

Figure S27: ^{1}H NMR spectrum of *N*-(6-(4-acetylphenyl)-1,3-dioxo-1*H*-benzo[*de*]isoquinolin-2(3*H*)-yl)-2-bromoacetamide (15e)

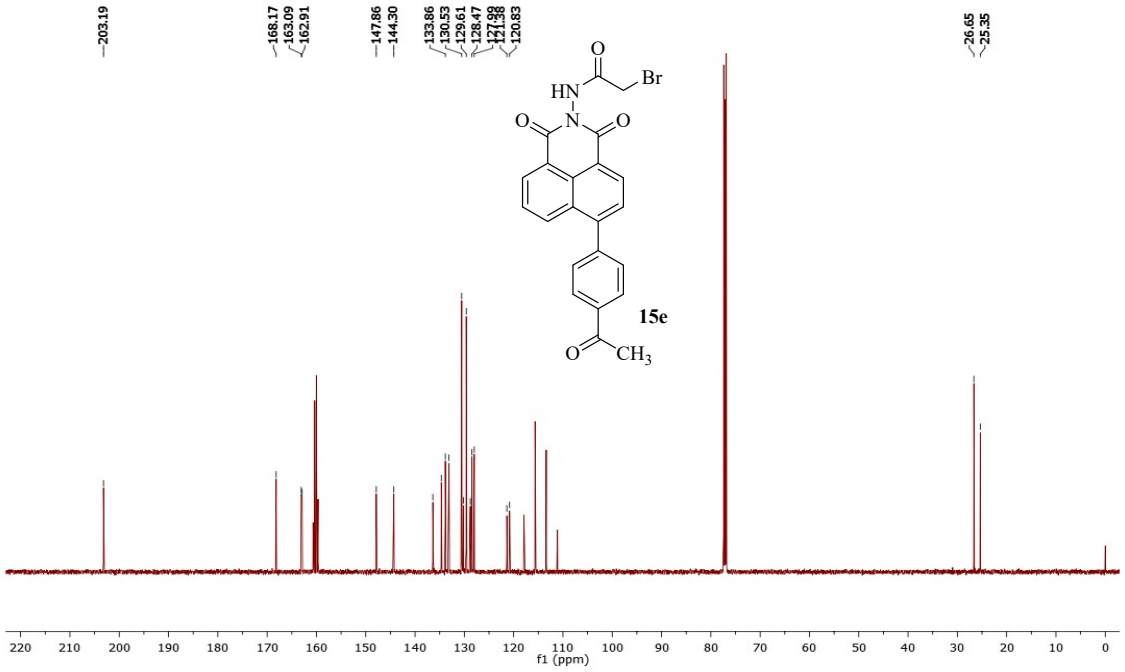

Figure S28: ^{13}C NMR spectrum of *N*-(6-(4-acetylphenyl)-1,3-dioxo-1*H*-benzo[*de*]isoquinolin-2(3*H*)-yl)-2-bromoacetamide (15e)

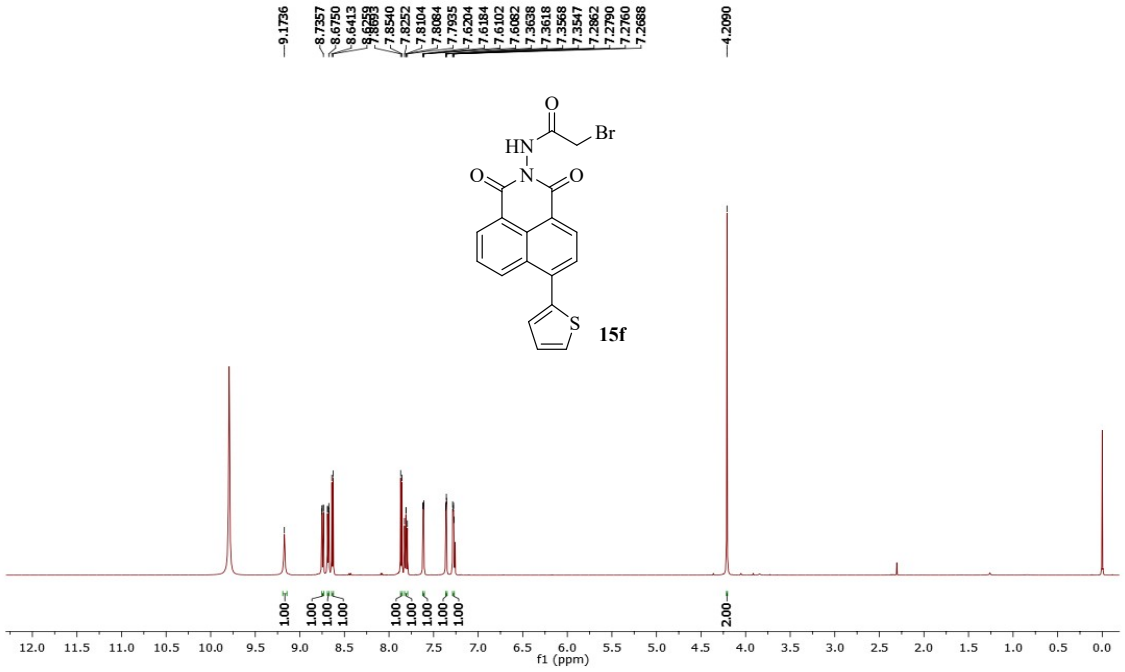

Figure S29: ^{1}H NMR spectrum of 2-bromo-*N*-(1,3-dioxo-6-(thiophen-2-yl)-1*H*-benzo[*de*]isoquinolin-2(3*H*)-yl)acetamide (15f)

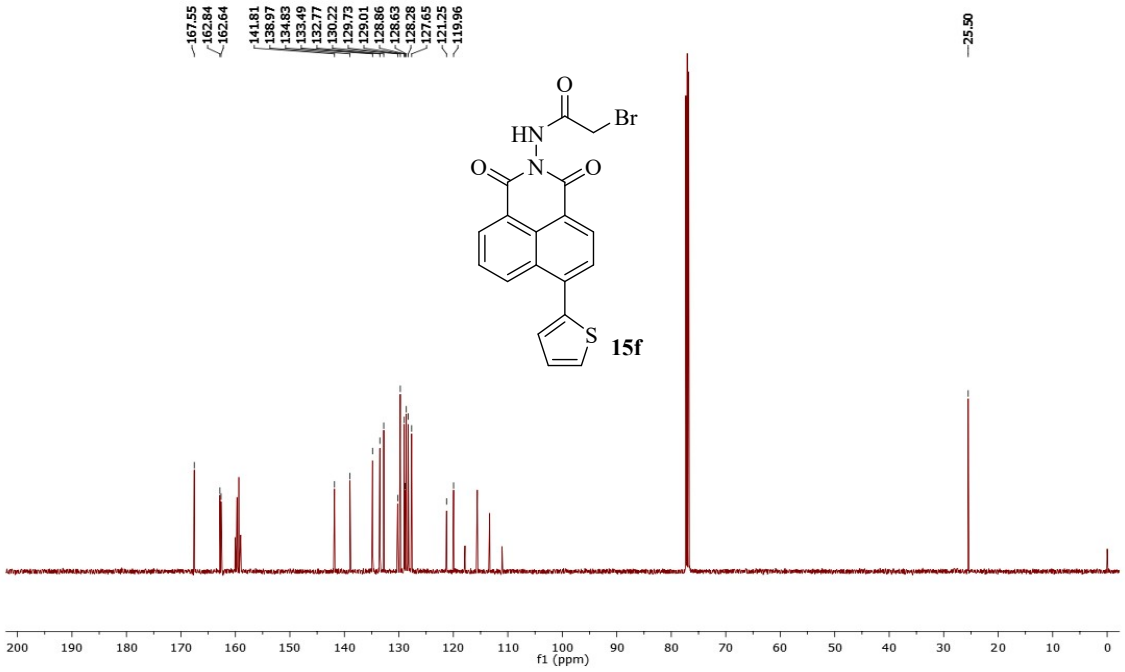

Figure S30: ^{13}C NMR spectrum of 2-bromo-*N*-(1,3-dioxo-6-(thiophen-2-yl)-1*H*-benzo[*de*]isoquinolin-2(3*H*)-yl)acetamide (15f)

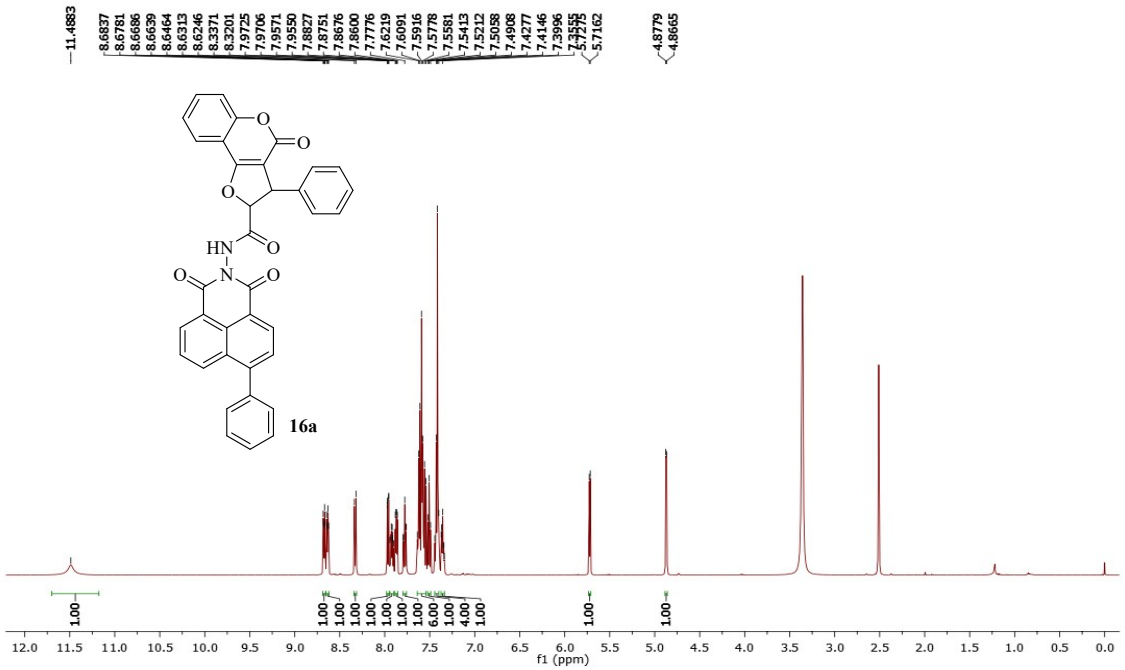

Figure S31: ^{1}H NMR spectrum of *N*-(1,3-dioxo-6-phenyl-1*H*-benzo[*de*]isoquinolin-2(3*H*)-yl)-4-oxo-3-phenyl-2,3-dihydro-4*H*-furo[3,2-*c*]chromene-2-carboxamide (16a)

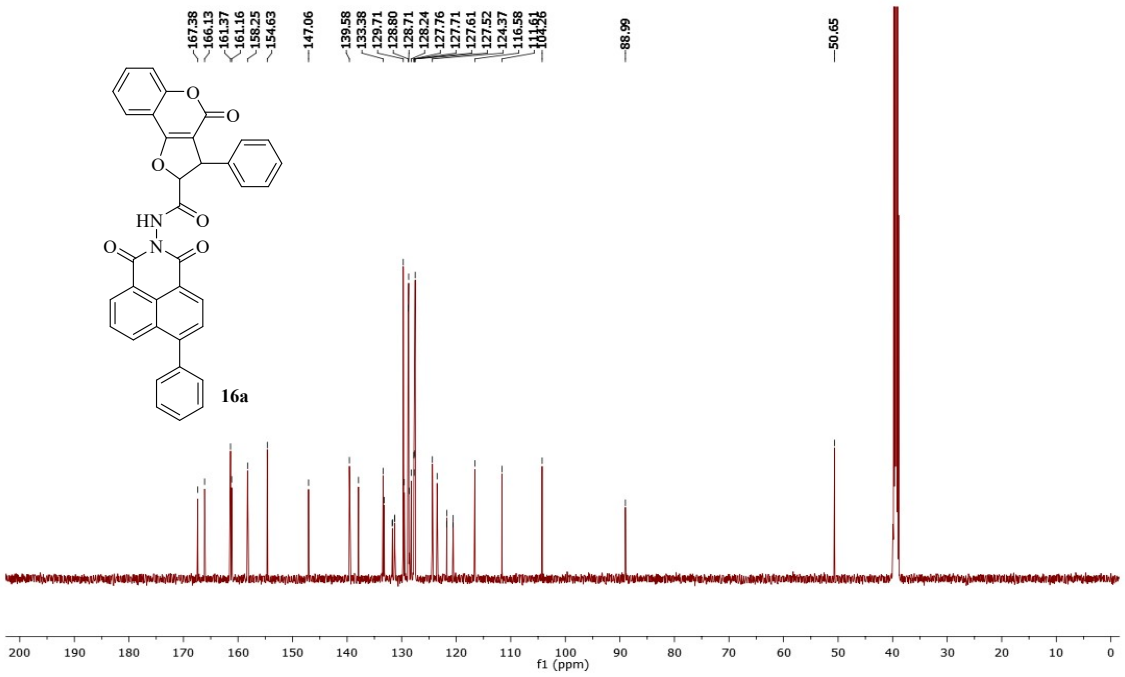

Figure S32: ^{13}C NMR spectrum of *N*-(1,3-dioxo-6-phenyl-1*H*-benzo[*de*]isoquinolin-2(3*H*)-yl)-4-oxo-3-phenyl-2,3-dihydro-4*H*-furo[3,2-*c*]chromene-2-carboxamide (16a)

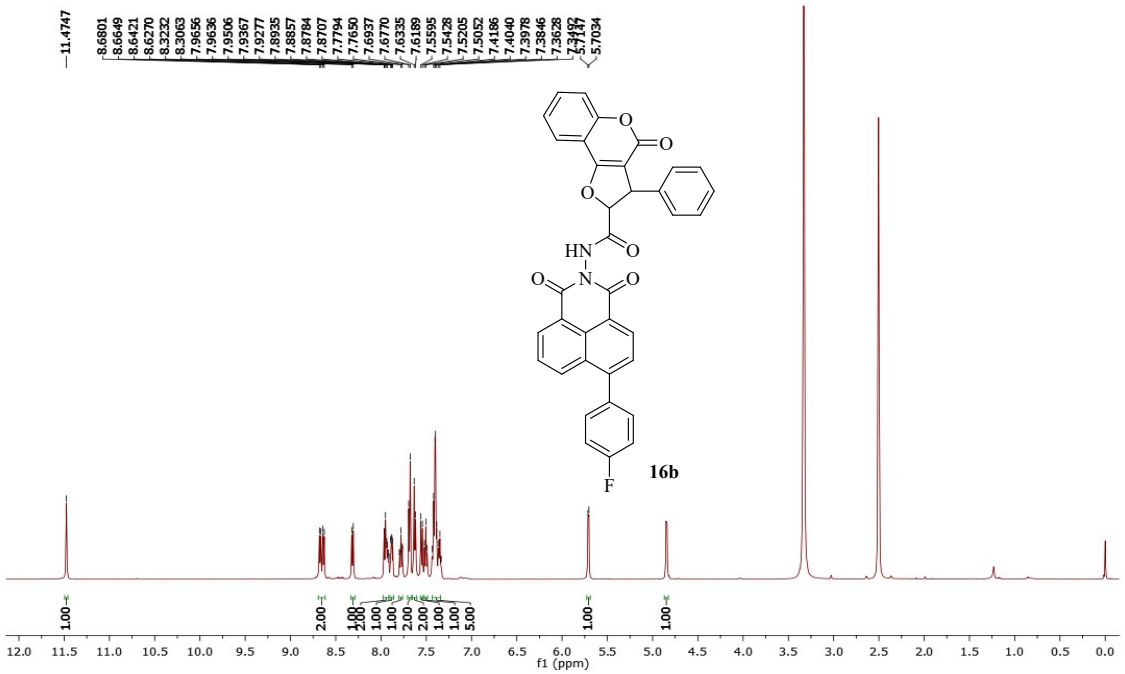

Figure S33: ^{1}H NMR spectrum of *N*-(6-(4-fluorophenyl)-1,3-dioxo-1*H*-benzo[*de*]isoquinolin -2(3*H*)-yl)-4-oxo-3-phenyl-2,3-dihydro-4*H*-furo[3,2-*c*]chromene-2-carboxamide (16b)

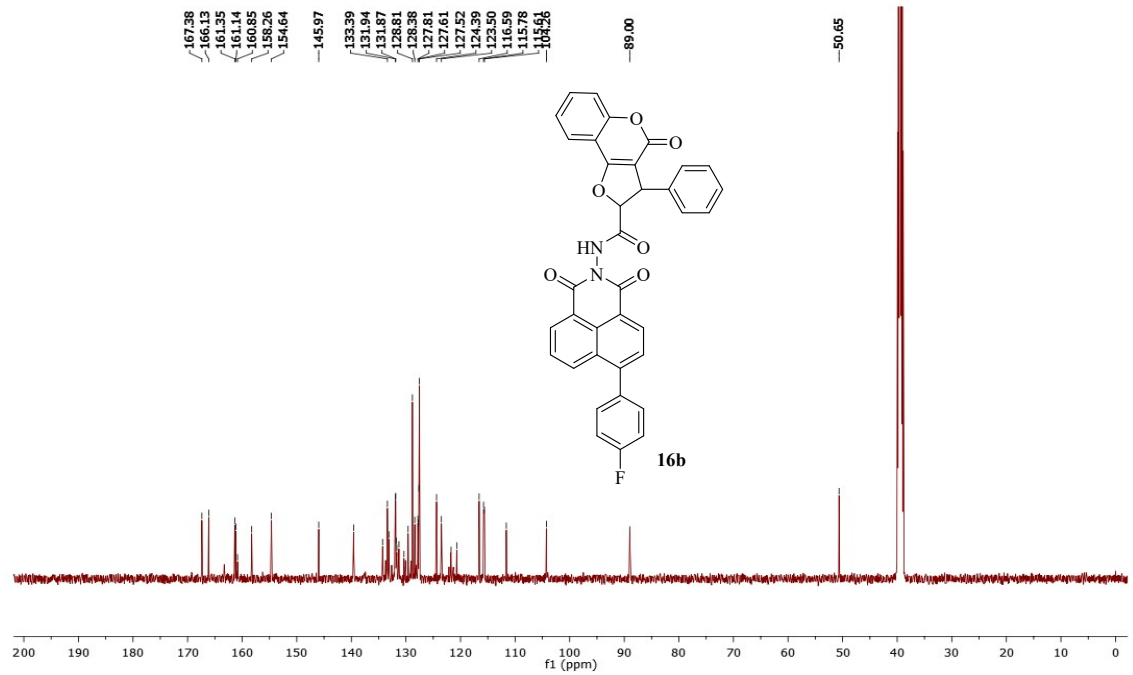

Figure S34: ^{13}C NMR spectrum of *N*-(6-(4-fluorophenyl)-1,3-dioxo-1*H*-benzo[*de*] isoquinolin-2(3*H*)-yl)-4-oxo-3-phenyl-2,3-dihydro-4*H*-furo[3,2-*c*]chromene-2-carboxamide(16b)

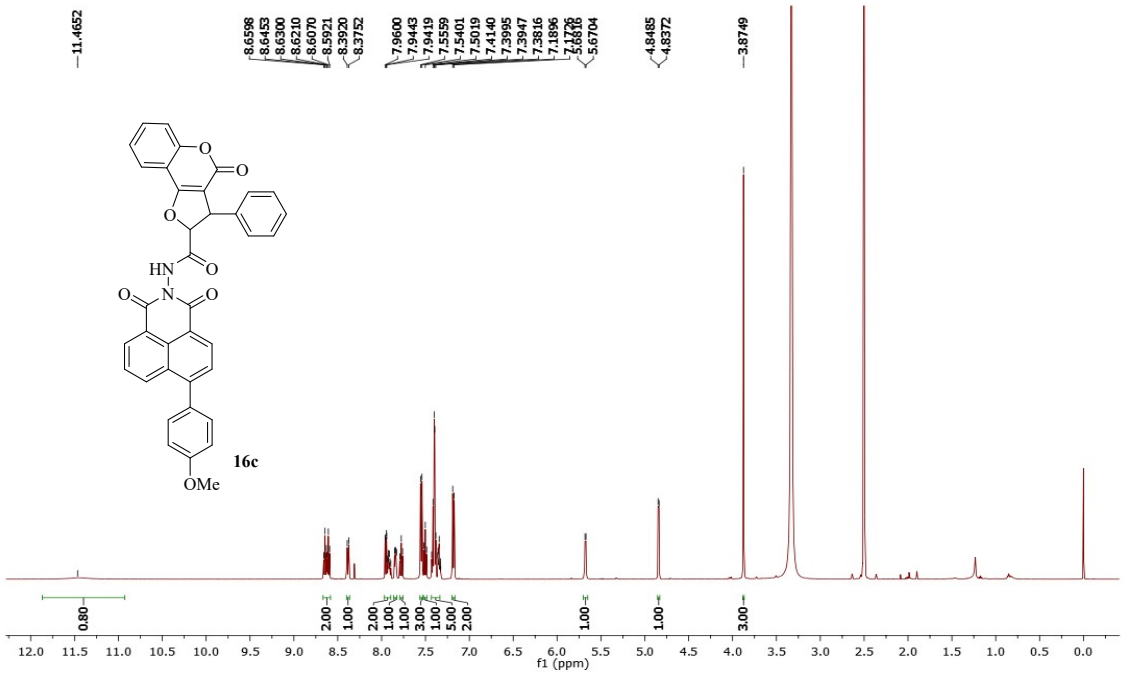

Figure S35: ^{1}H NMR spectrum of *N*-(6-(4-methoxyphenyl)-1,3-dioxo-1*H*-benzo[*de*]isoquinolin-2(3*H*)-yl)-4-oxo-3-phenyl-2,3-dihydro-4*H*-furo[3,2-*c*]chromene-2-carboxamide (16c)

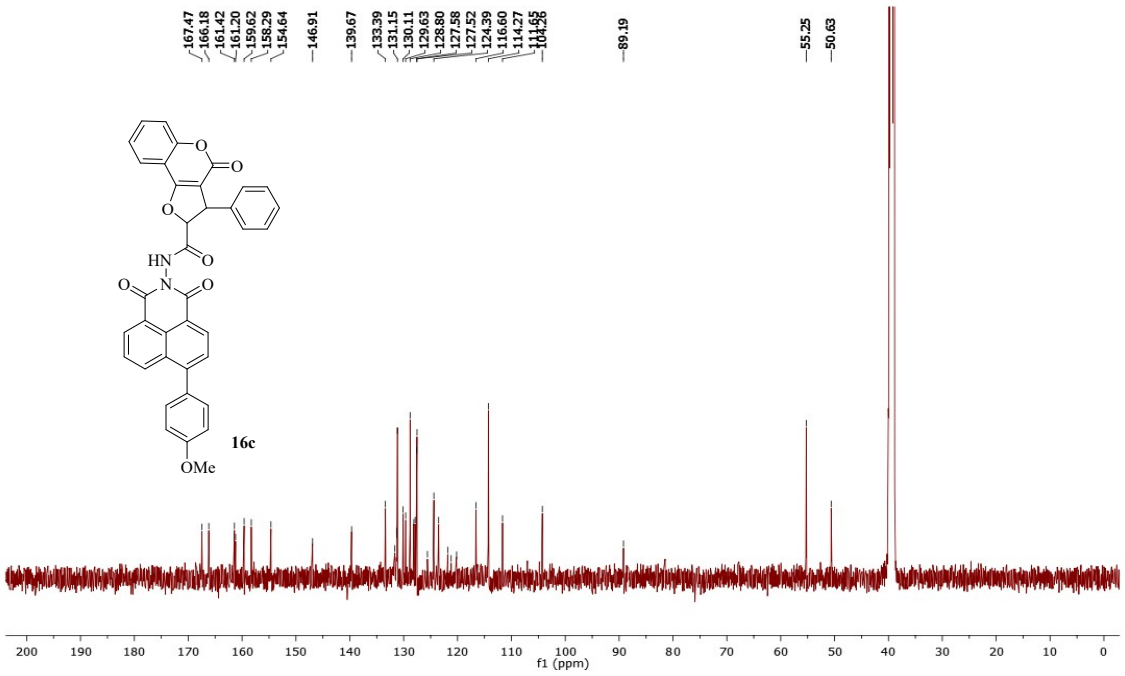

Figure S36: ^{13}C NMR spectrum of *N*-(6-(4-methoxyphenyl)-1,3-dioxo-1*H*-benzo[*de*]isoquinolin-2(3*H*)-yl)-4-oxo-3-phenyl-2,3-dihydro-4*H*-furo[3,2-*c*]chromene-2-carboxamide (16c)

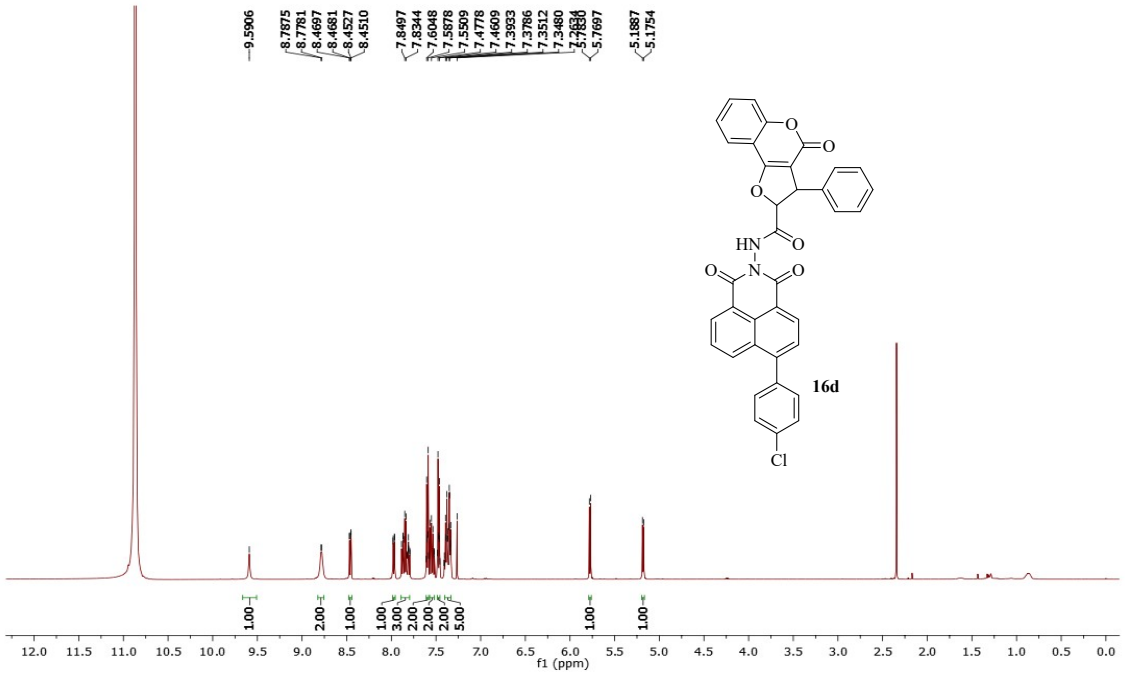

Figure S37: ^{1}H NMR spectrum of *N*-(6-(4-chlorophenyl)-1,3-dioxo-1*H*-benzo[*de*]isoquinolin -2(3*H*)-yl)-4-oxo-3-phenyl-2,3-dihydro-4*H*-furo[3,2-*c*]chromene-2-carboxamide (16d)

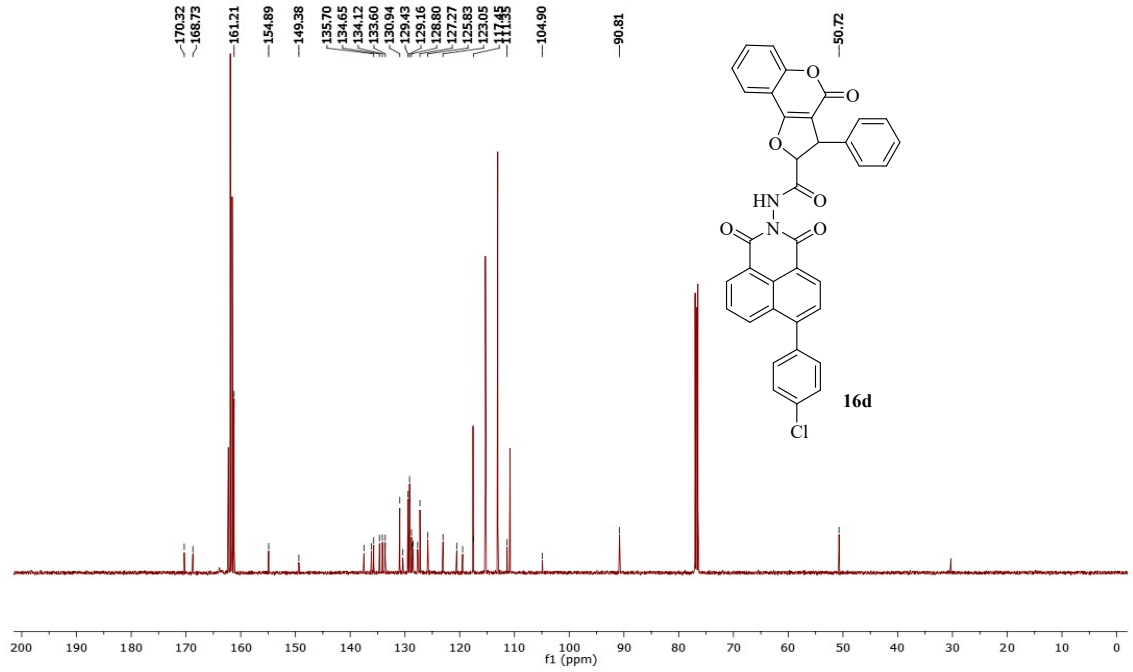

Figure S38: ^{13}C NMR spectrum of *N*-(6-(4-chlorophenyl)-1,3-dioxo-1*H*-benzo[*de*]isoquinolin-2(3*H*)-yl)-4-oxo-3-phenyl-2,3-dihydro-4*H*-furo[3,2-*c*]chromene-2-carboxamide (16d)

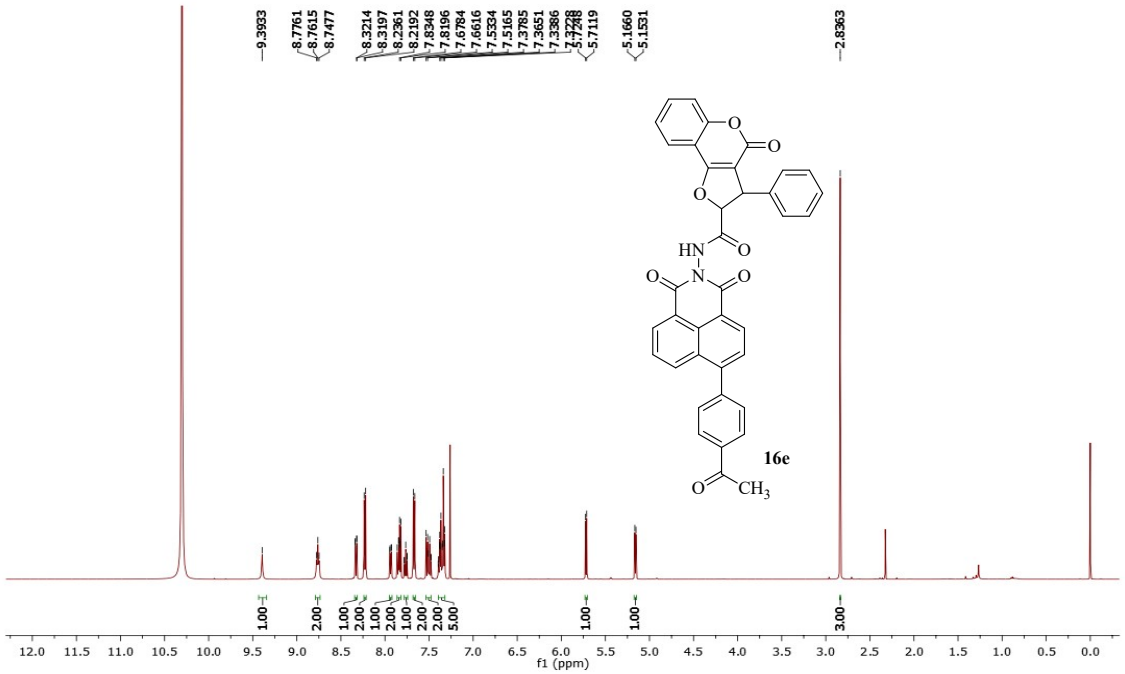

Figure S39: ^{1}H NMR spectrum of *N*-(6-(4-acetylphenyl)-1,3-dioxo-1*H*-benzo[*de*]isoquinolin -2(3*H*)-yl)-4-oxo-3-phenyl-2,3-dihydro-4*H*-furo[3,2-*c*]chromene-2-carboxamide (16e)

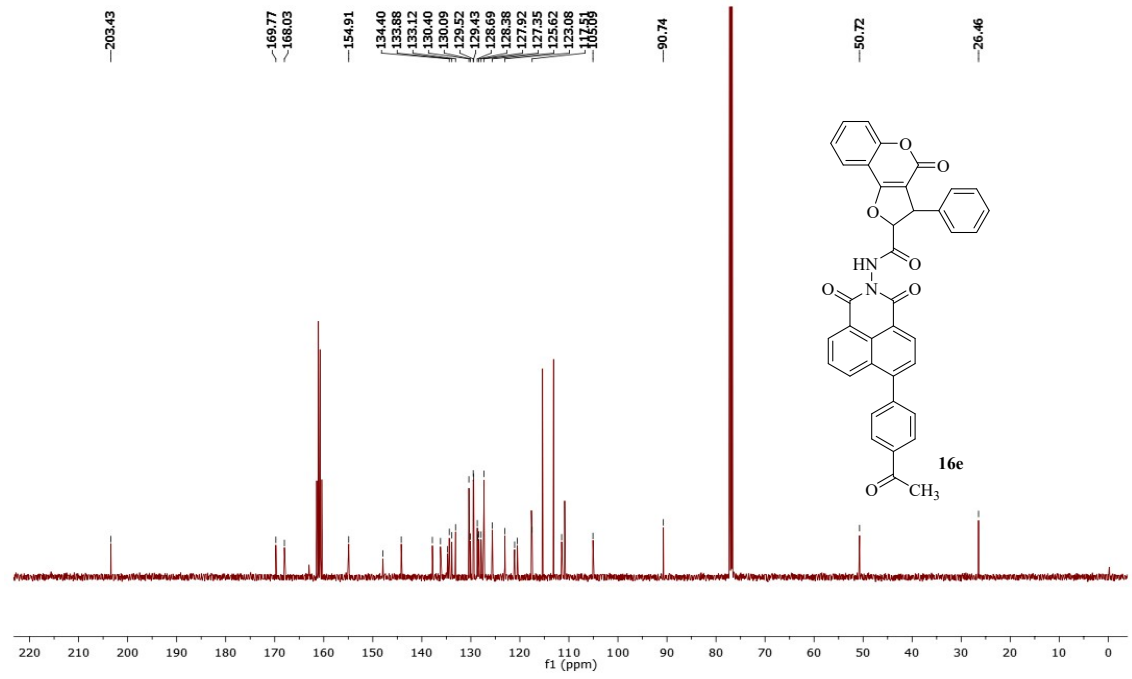

Figure S40: ^{13}C NMR spectrum of *N*-(6-(4-acetylphenyl)-1,3-dioxo-1*H*-benzo[*de*]isoquinolin -2(3*H*)-yl)-4-oxo-3-phenyl-2,3-dihydro-4*H*-furo[3,2-*c*]chromene-2-carboxamide (16e)

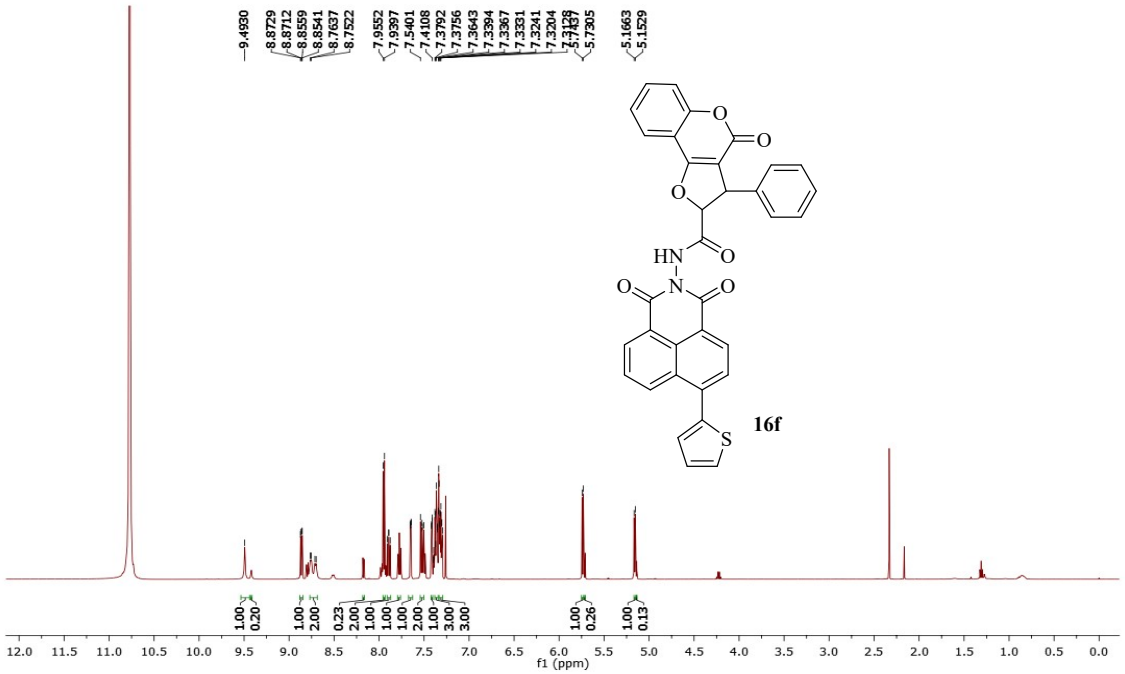

Figure S41: ^{1}H NMR spectrum of *N*-(1,3-dioxo-6-(thiophen-2-yl)-1*H*-benzo[*de*]isoquinolin-2(3H)-yl)-4-oxo-3-phenyl-2,3-dihydro-4*H*-furo[3,2-*c*]chromene-2-carboxamide (16f)

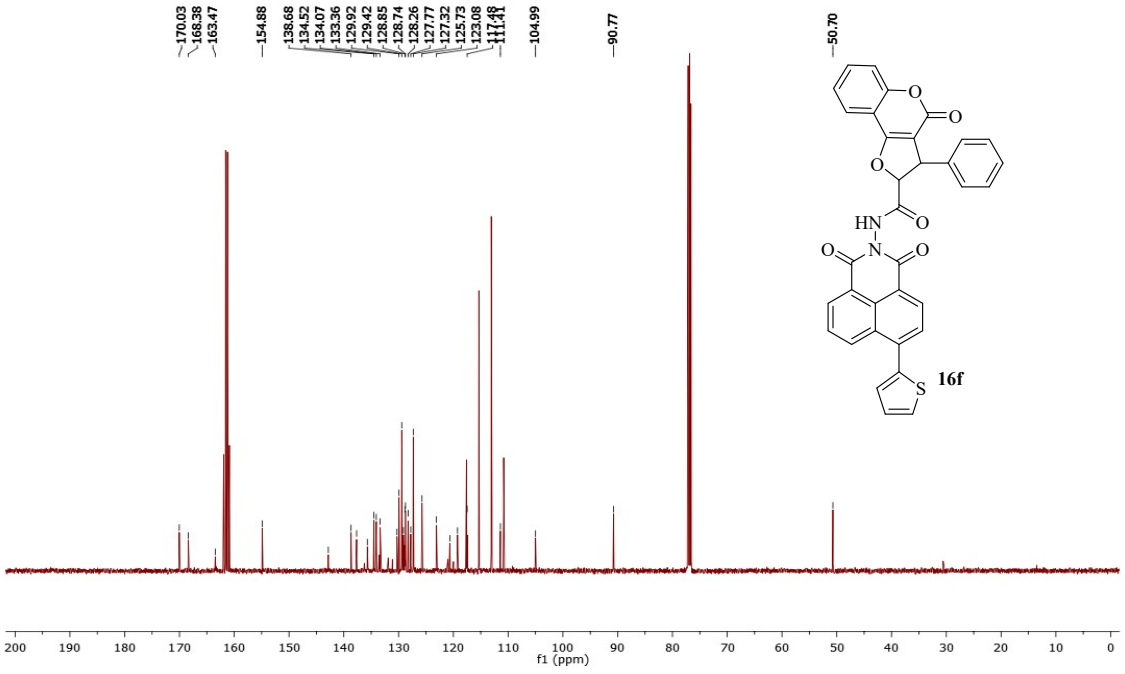

Figure S42: ^{13}C NMR spectrum of *N*-(1,3-dioxo-6-(thiophen-2-yl)-1*H*-benzo[*de*]isoquinolin-2(3H)-yl)-4-oxo-3-phenyl-2,3-dihydro-4*H*-furo[3,2-*c*]chromene-2-carboxamide (16f)

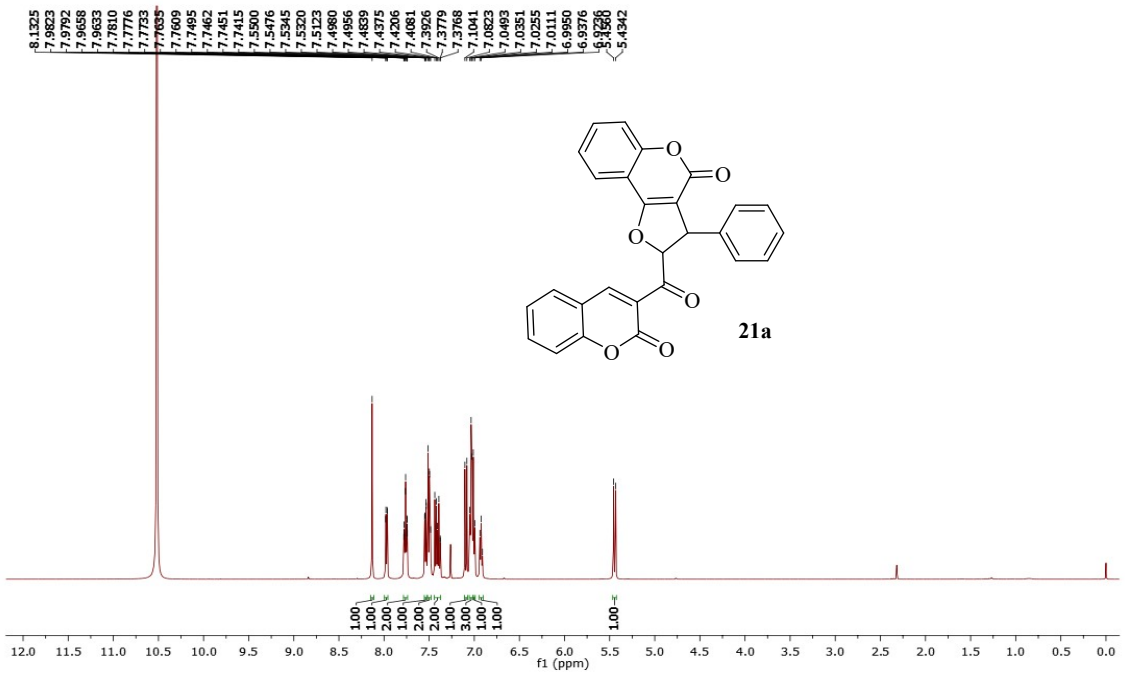

Figure S43: ^{1}H NMR spectrum of 2-(2-oxo-2*H*-chromene-3-carbonyl)-3-phenyl-2,3-dihydro-4*H*-furo[3,2-*c*]chromen-4-one (21a)

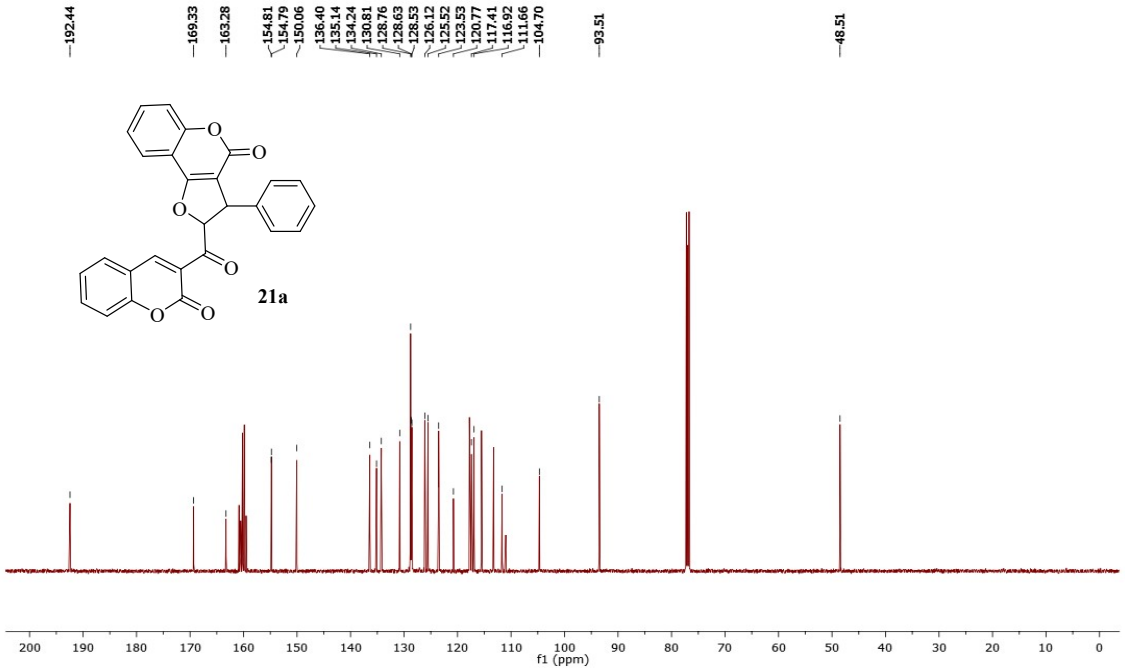

Figure S44: ^{13}C NMR spectrum of 2-(2-oxo-2*H*-chromene-3-carbonyl)-3-phenyl-2,3-dihydro-4*H*-furo[3,2-*c*]chromen-4-one (21a)

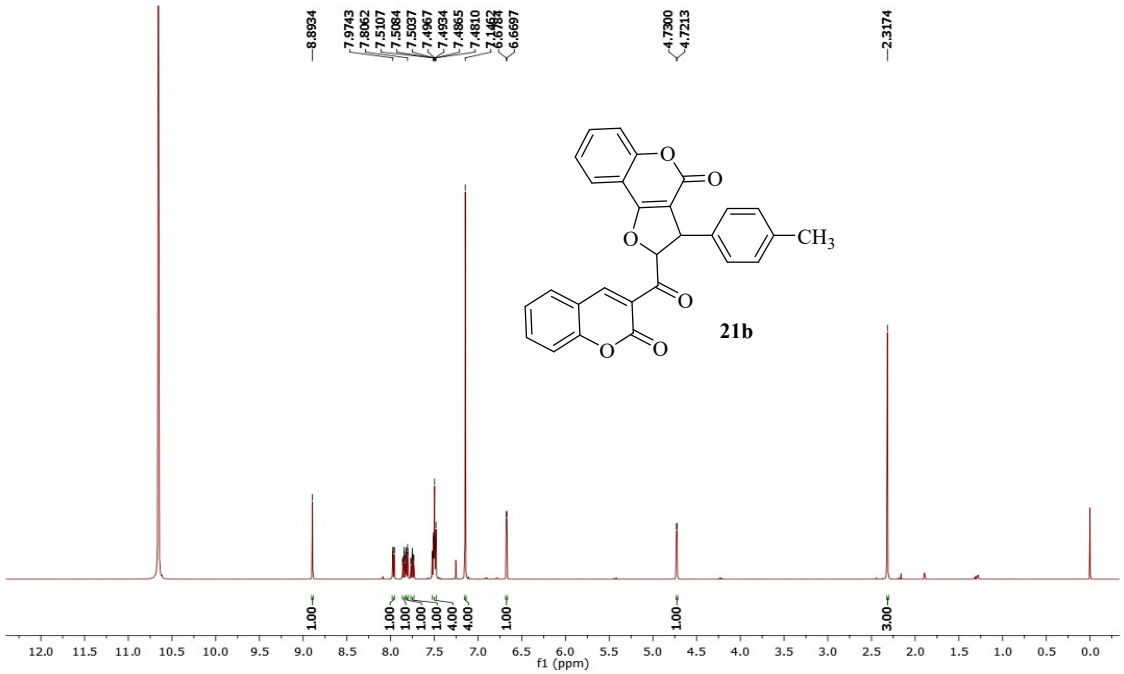

Figure S45: ^{1}H NMR spectrum of 2-(2-oxo-2*H*-chromene-3-carbonyl)-3-(*p*-tolyl)-2,3-dihydro-4*H*-furo[3,2-*c*]chromen-4-one (21b)

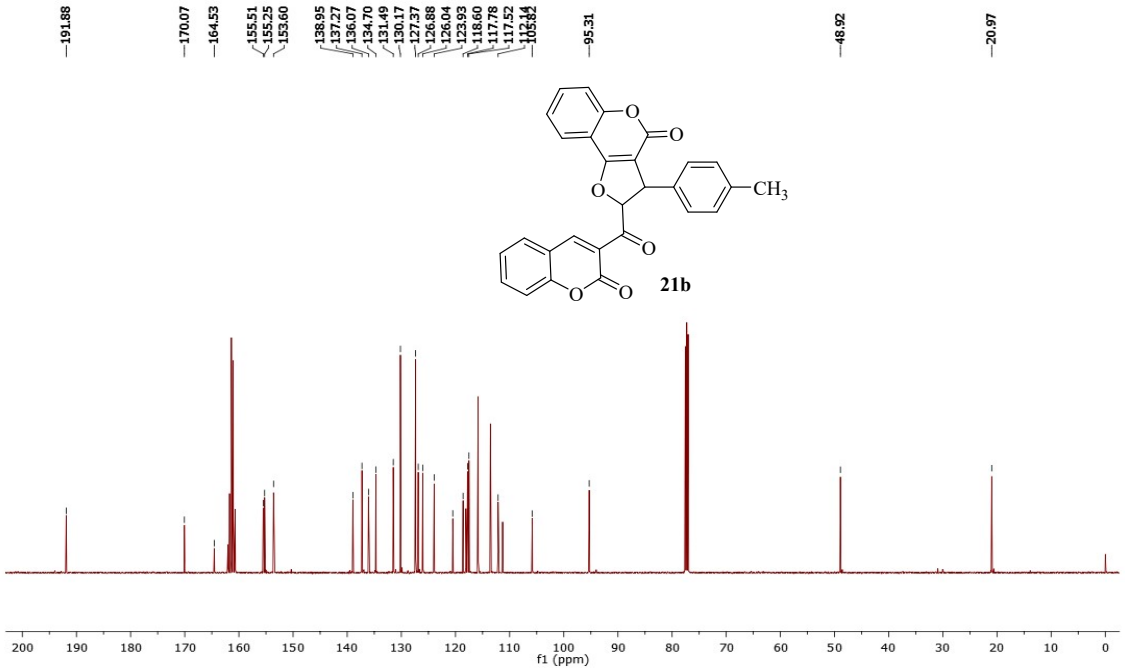

Figure S46: ^{13}C NMR spectrum of 2-(2-oxo-2*H*-chromene-3-carbonyl)-3-(*p*-tolyl)-2,3-dihydro-4*H*-furo[3,2-*c*]chromen-4-one (21b)

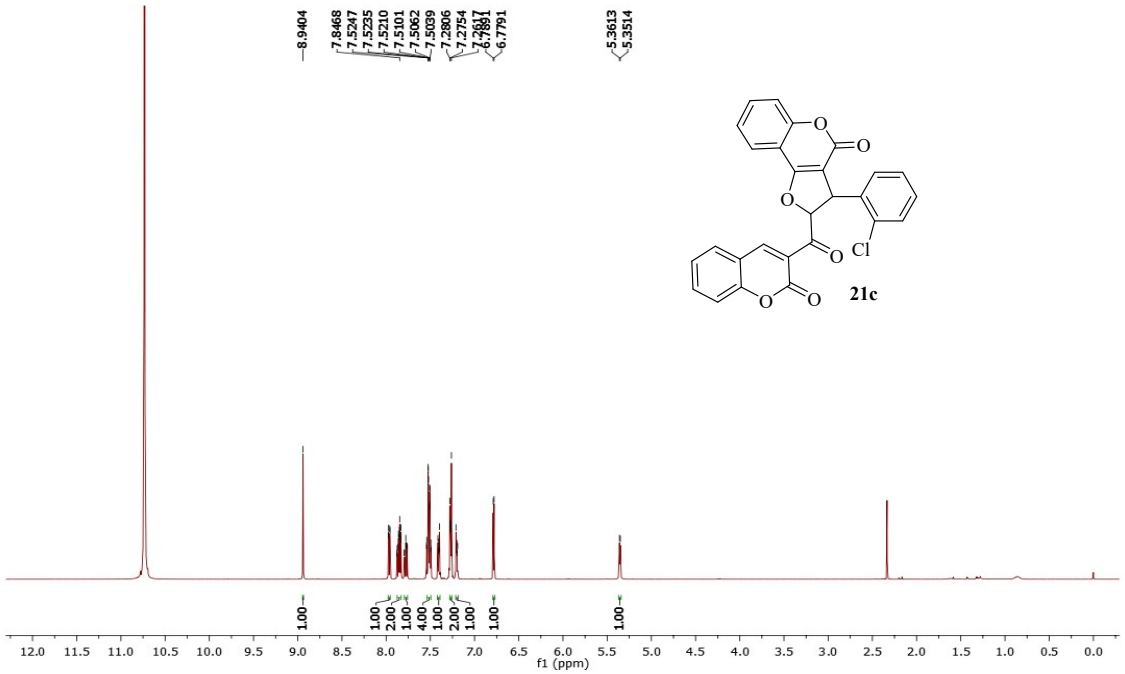

Figure S47: ^{1}H NMR spectrum of 3-(2-chlorophenyl)-2-(2-oxo-2*H*-chromene-3-carbonyl)-2,3-dihydro-4*H*-furo[3,2-*c*]chromen-4-one (21c)

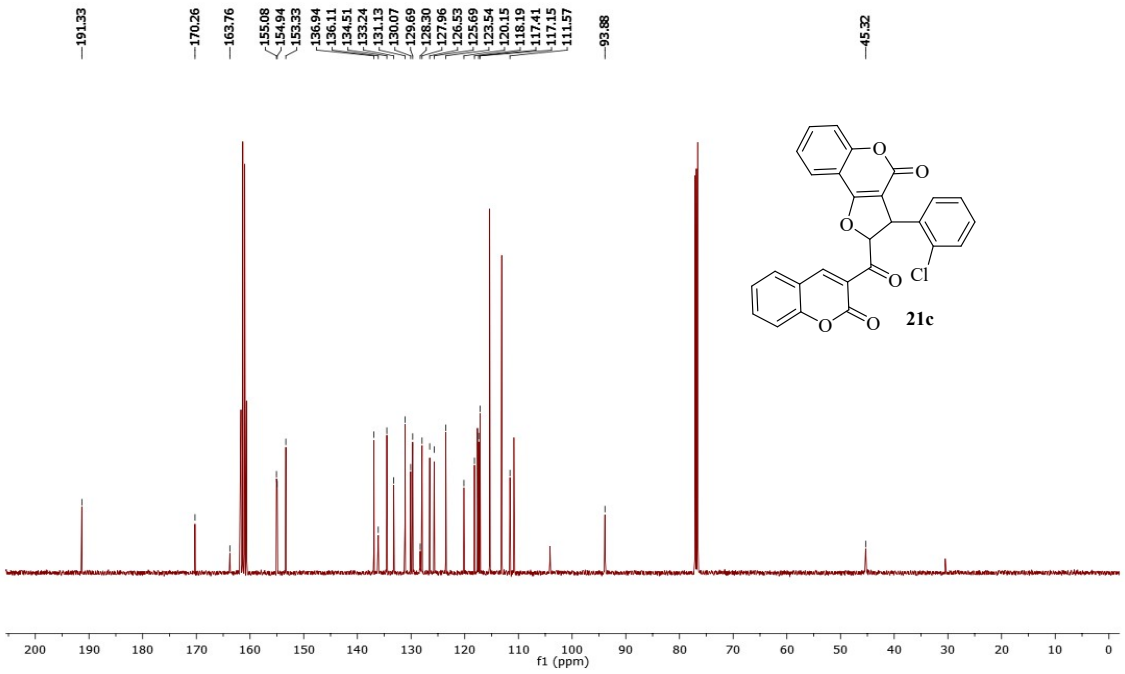

Figure S48: ^{13}C NMR spectrum of 3-(2-chlorophenyl)-2-(2-oxo-2*H*-chromene-3-carbonyl)-2,3-dihydro-4*H*-furo[3,2-*c*]chromen-4-one (21c)

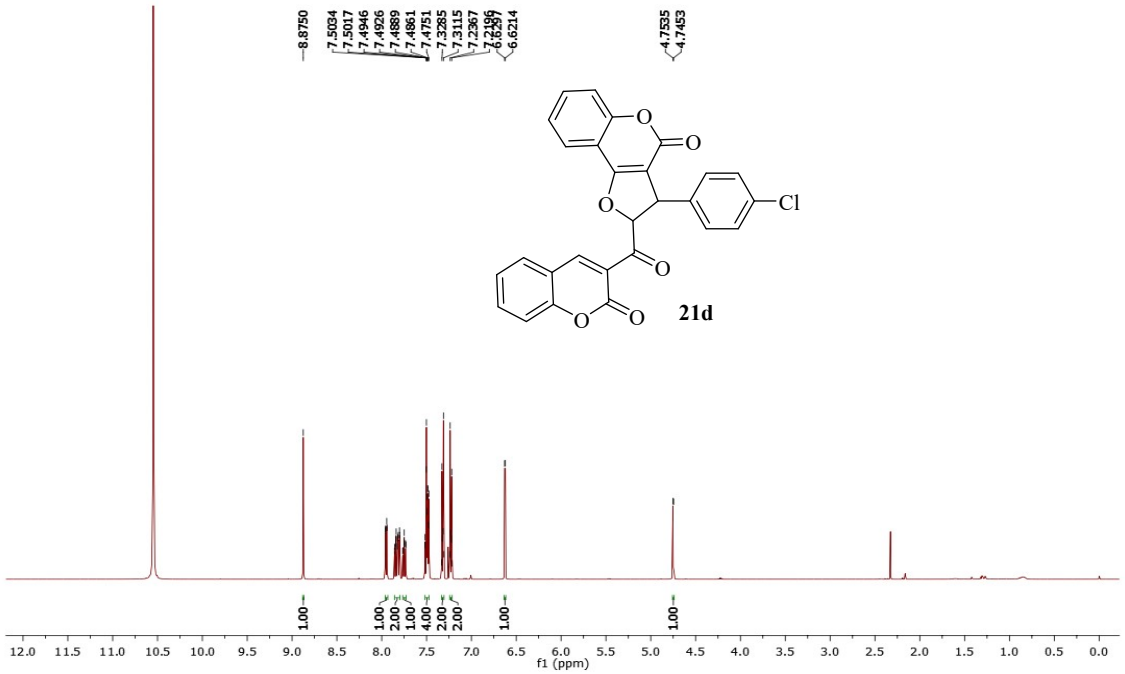

Figure S49: ^{1}H NMR spectrum of 3-(4-chlorophenyl)-2-(2-oxo-2*H*-chromene-3-carbonyl)-2,3-dihydro-4*H*-furo[3,2-*c*]chromen-4-one (21d)

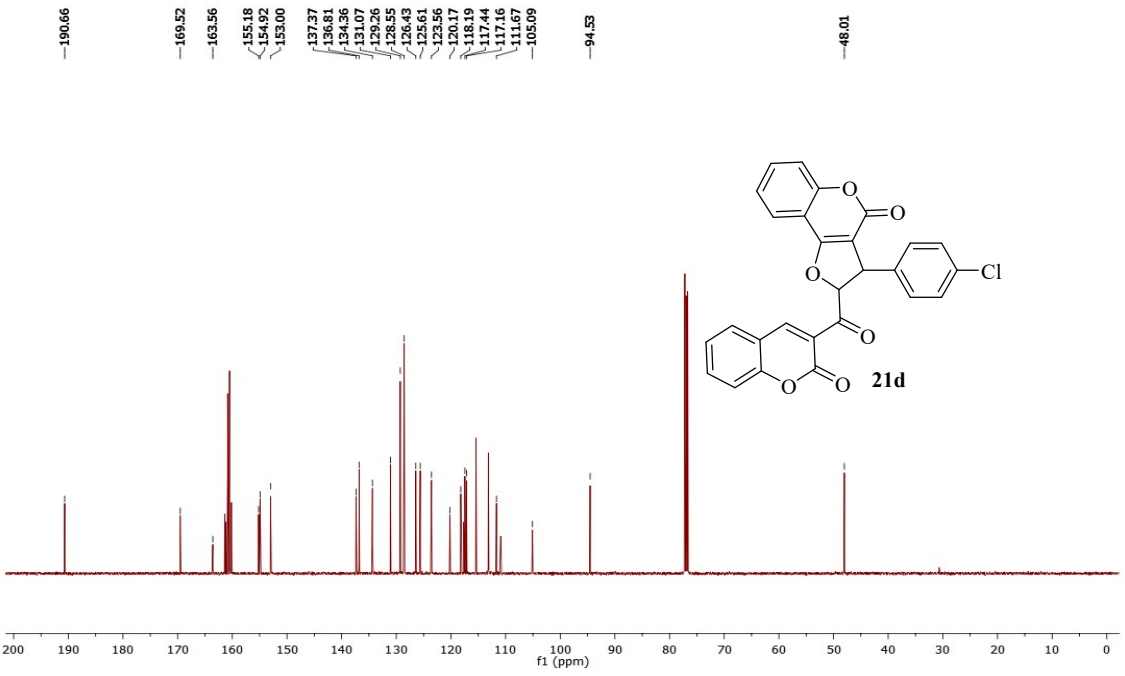

Figure S50: ^{13}C NMR spectrum of 3-(4-chlorophenyl)-2-(2-oxo-2*H*-chromene-3-carbonyl)-2,3-dihydro-4*H*-furo[3,2-*c*]chromen-4-one (21d)

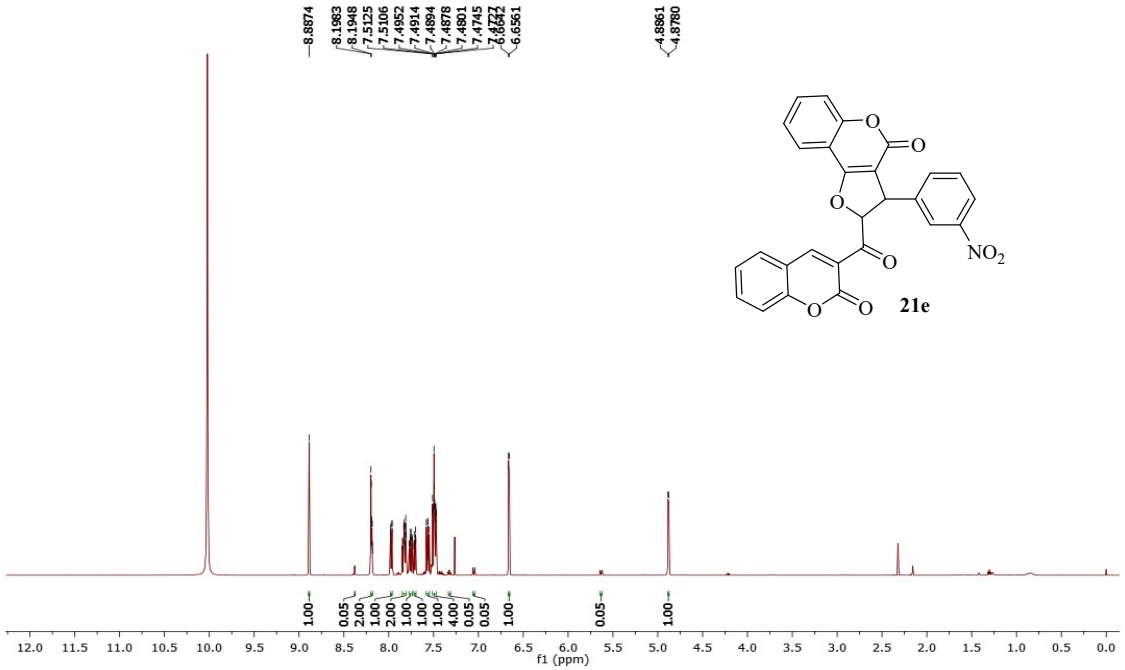

Figure S51: ^{1}H NMR spectrum of 3-(3-nitrophenyl)-2-(2-oxo-2*H*-chromene-3-carbonyl)-2,3-dihydro-4*H*-furo[3,2-*c*]chromen-4-one (21e)

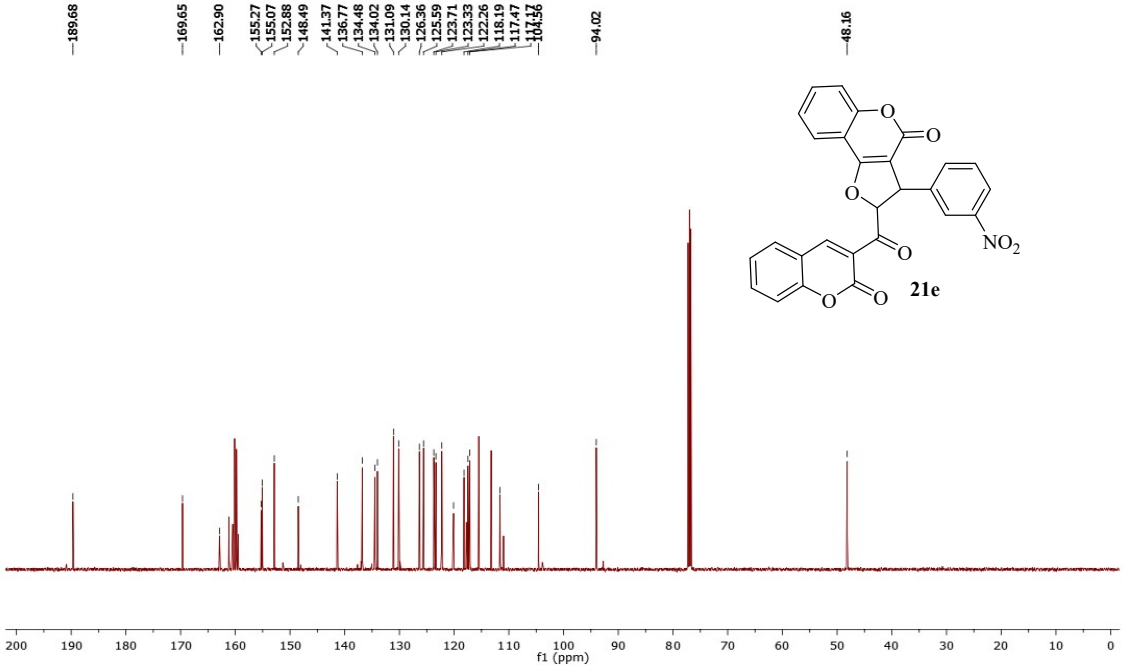

Figure S52: ^{13}C NMR spectrum of 3-(3-nitrophenyl)-2-(2-oxo-2*H*-chromene-3-carbonyl)-2,3-dihydro-4*H*-furo[3,2-*c*]chromen-4-one (21e)

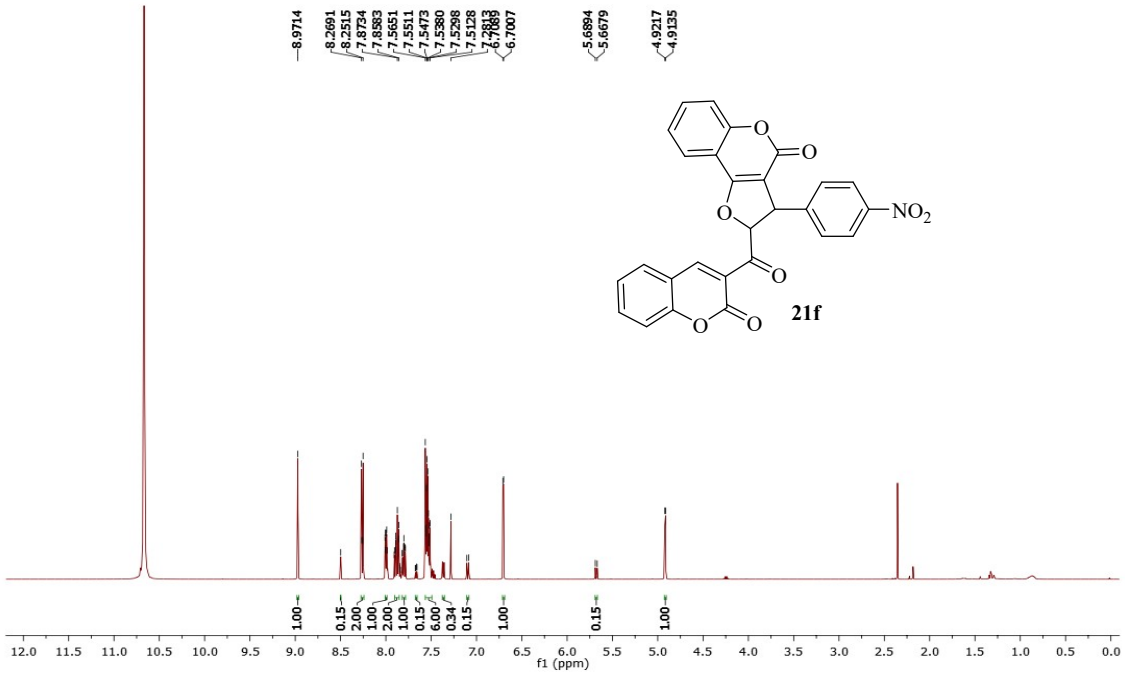

Figure S53: ^{1}H NMR spectrum of 3-(4-nitrophenyl)-2-(2-oxo-2*H*-chromene-3-carbonyl)-2,3-dihydro-4*H*-furo[3,2-*c*]chromen-4-one (21f)

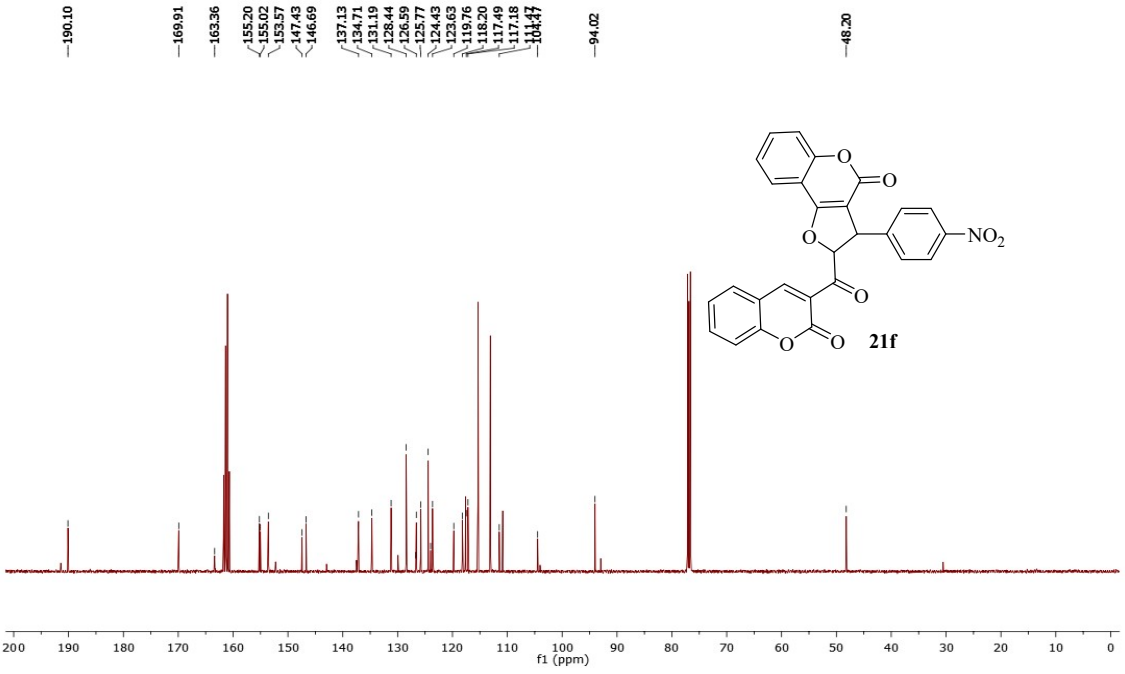

Figure S54: ^{13}C NMR spectrum of 3-(4-nitrophenyl)-2-(2-oxo-2*H*-chromene-3-carbonyl)-2,3-dihydro-4*H*-furo[3,2-*c*]chromen-4-one (21f)

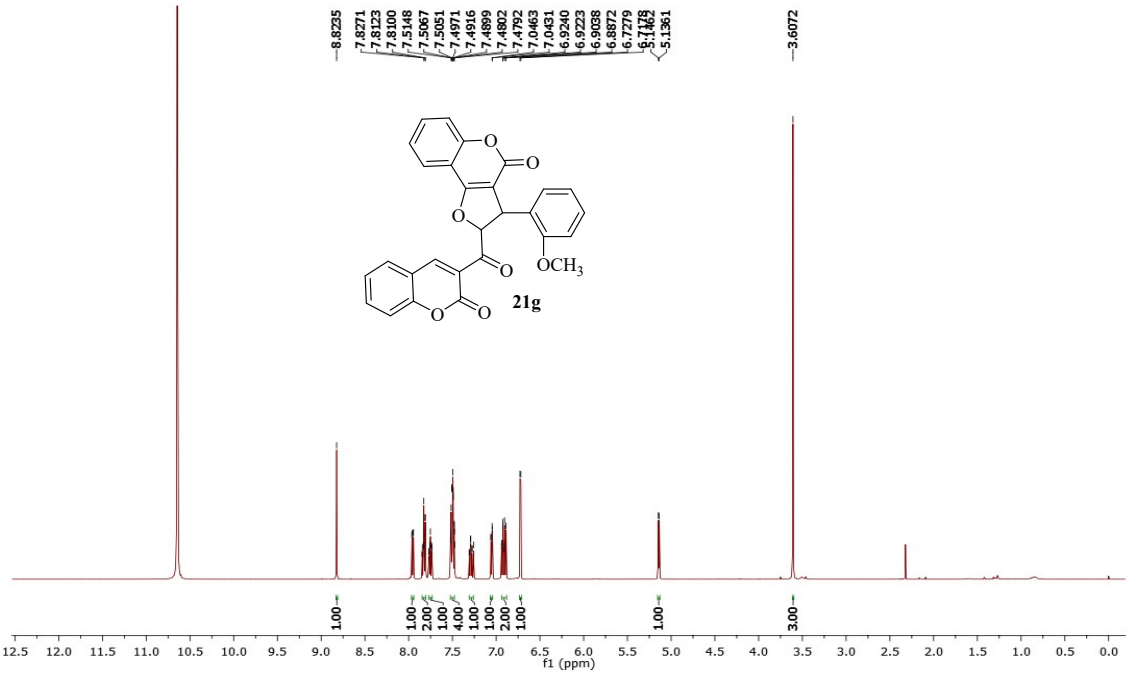

Figure S55: ^{1}H NMR spectrum of 3-(2-methoxyphenyl)-2-(2-oxo-2*H*-chromene-3-carbonyl)-2,3-dihydro-4*H*-furo[3,2-*c*]chromen-4-one (21g)

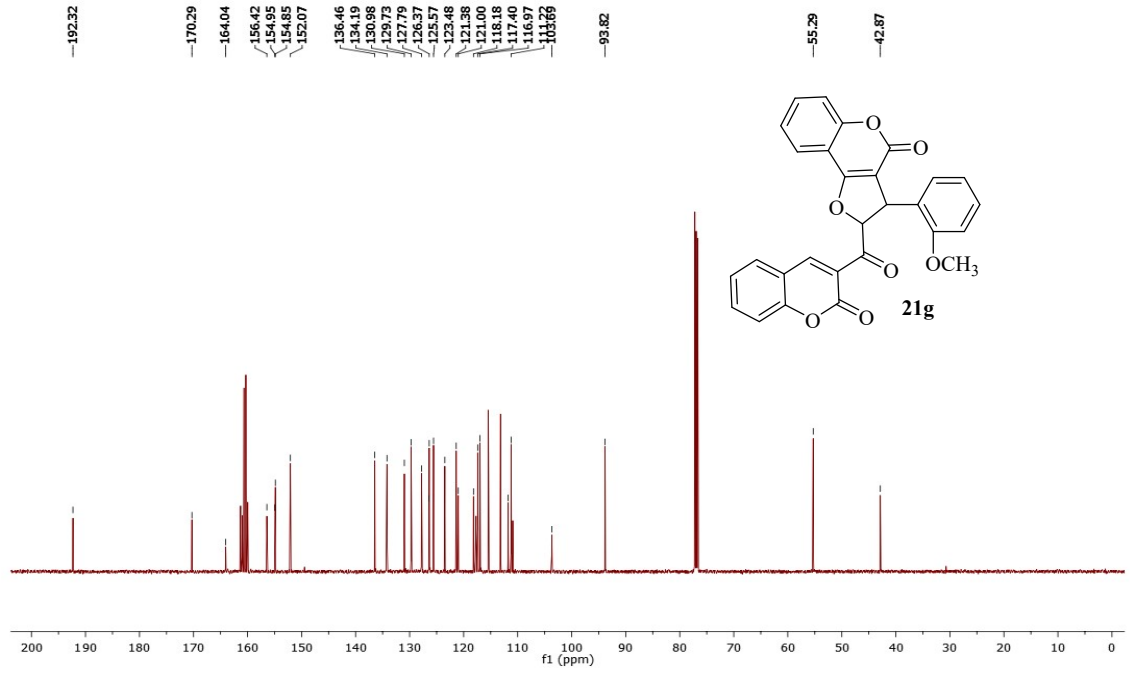

Figure S56: ^{13}C NMR spectrum of 3-(2-methoxyphenyl)-2-(2-oxo-2*H*-chromene-3-carbonyl)-2,3-dihydro-4*H*-furo[3,2-*c*]chromen-4-one (21g)

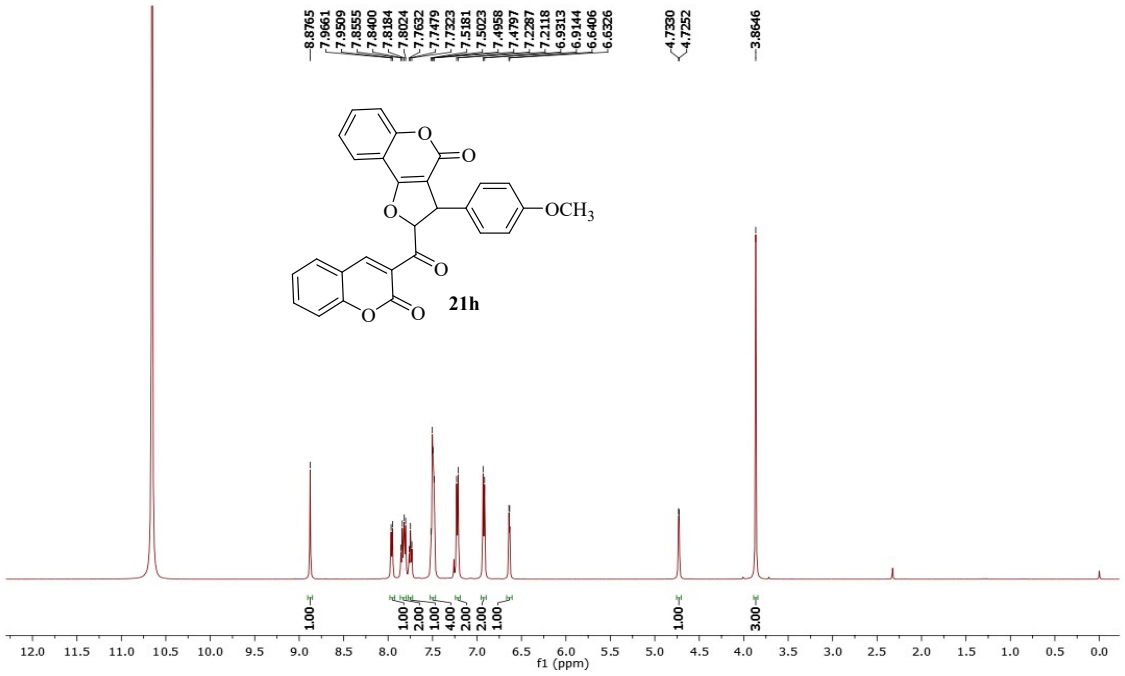

Figure S57: ^{1}H NMR spectrum of 3-(4-methoxyphenyl)-2-(2-oxo-2*H*-chromene-3-carbonyl)-2,3-dihydro-4*H*-furo[3,2-*c*]chromen-4-one (21h)

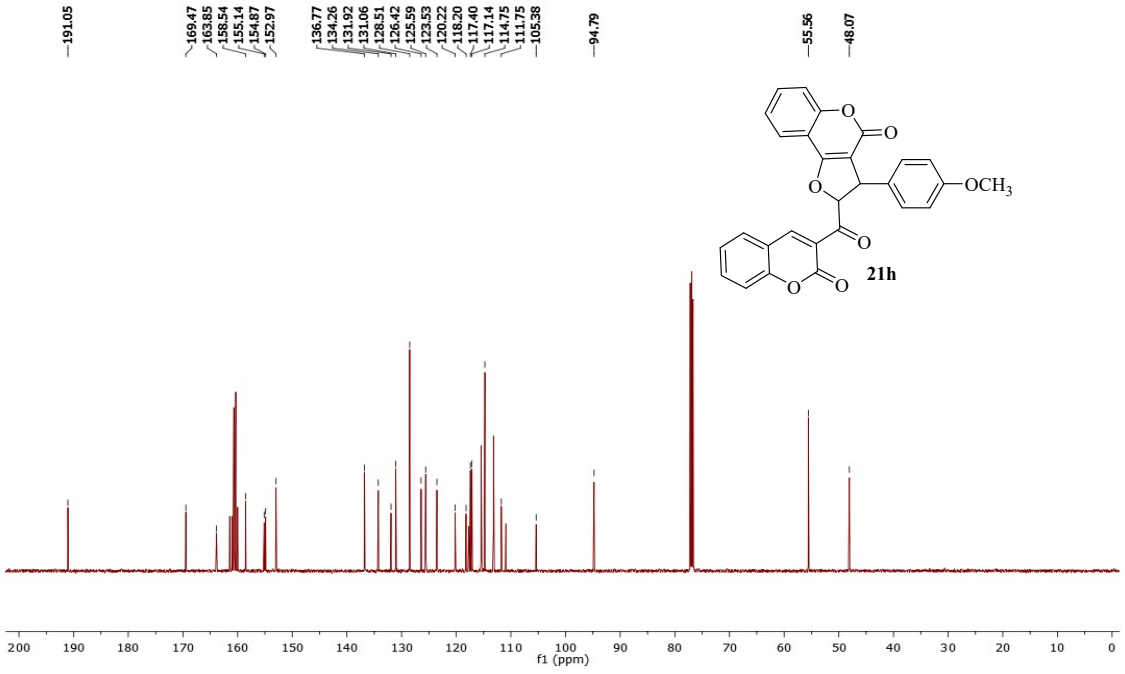

Figure S58: ^{13}C NMR spectrum of 3-(4-methoxyphenyl)-2-(2-oxo-2*H*-chromene-3-carbonyl)-2,3-dihydro-4*H*-furo[3,2-*c*]chromen-4-one (21h)

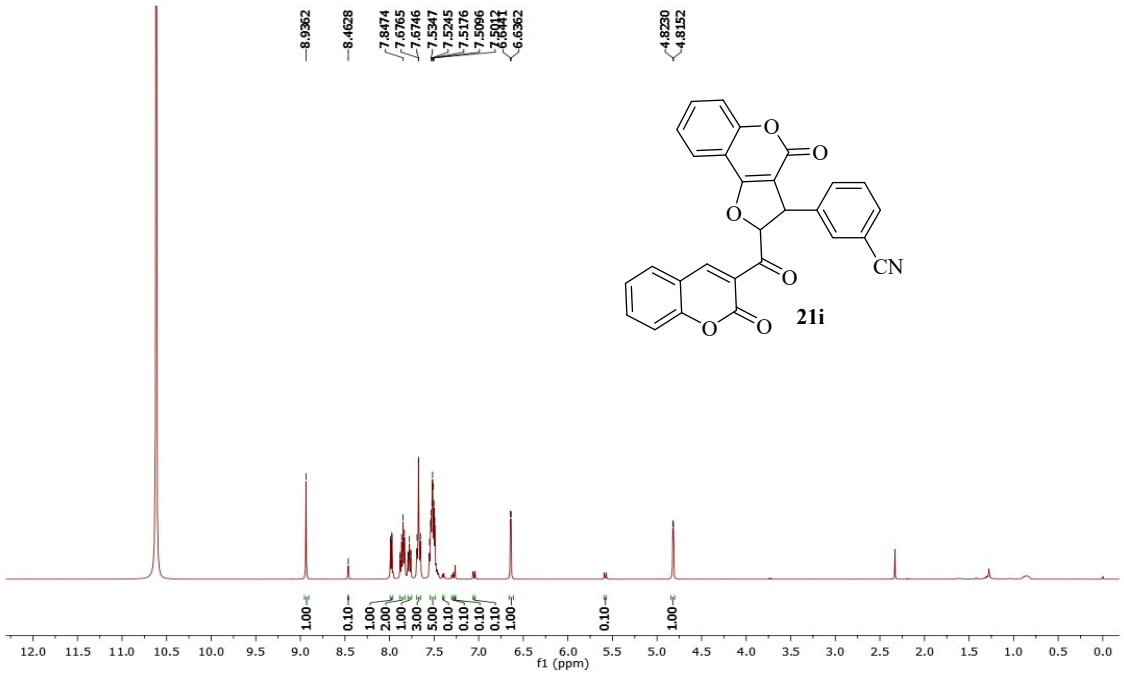

Figure S59: ^{1}H NMR spectrum of 3-(4-oxo-2-(2-oxo-2*H*-chromene-3-carbonyl)-2,3-dihydro-4*H*-furo[3,2-*c*]chromen-3-yl)benzonitrile (21i)

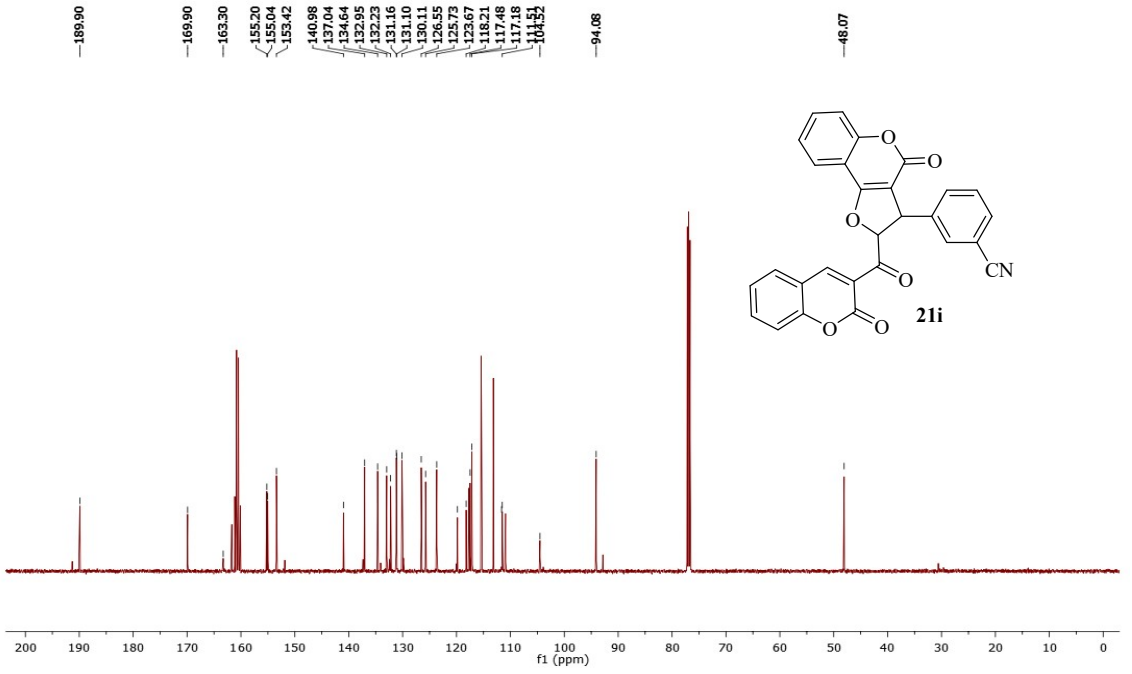

Figure S60: ^{13}C NMR spectrum of 3-(4-oxo-2-(2-oxo-2*H*-chromene-3-carbonyl)-2,3-dihydro-4*H*-furo[3,2-*c*]chromen-3-yl)benzonitrile (21i)

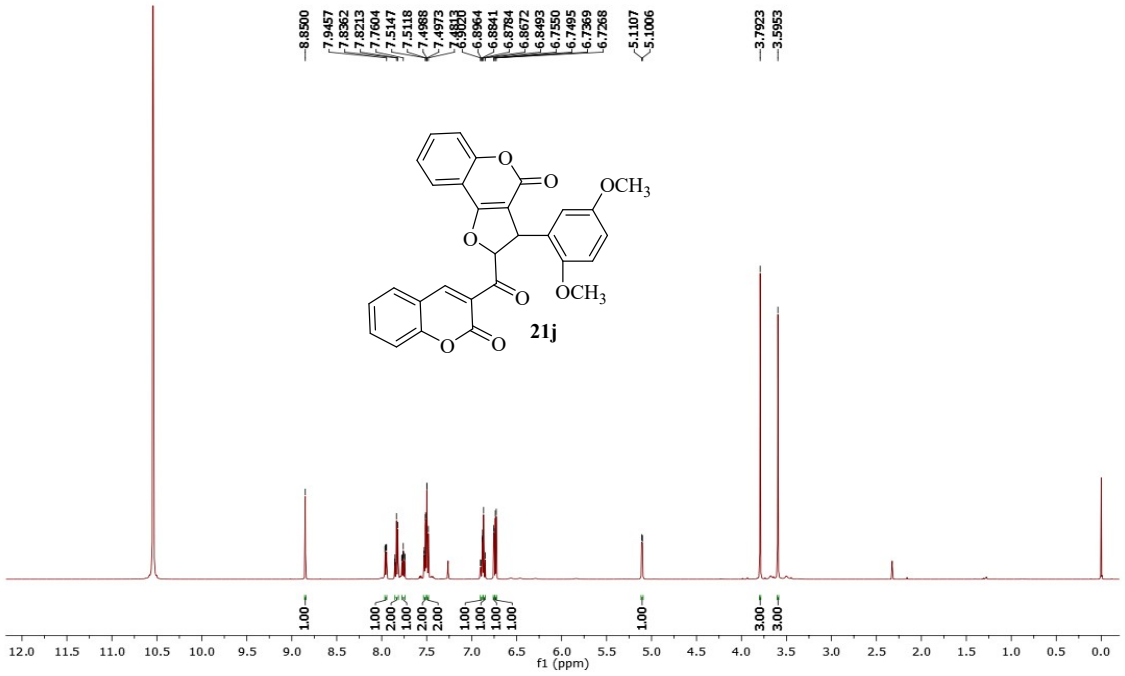

Figure S61: ^{1}H NMR spectrum of 3-(2,5-dimethoxyphenyl)-2-(2-oxo-2*H*-chromene-3-carbonyl)-2,3-dihydro-4*H*-furo[3,2-*c*]chromen-4-one (21j)

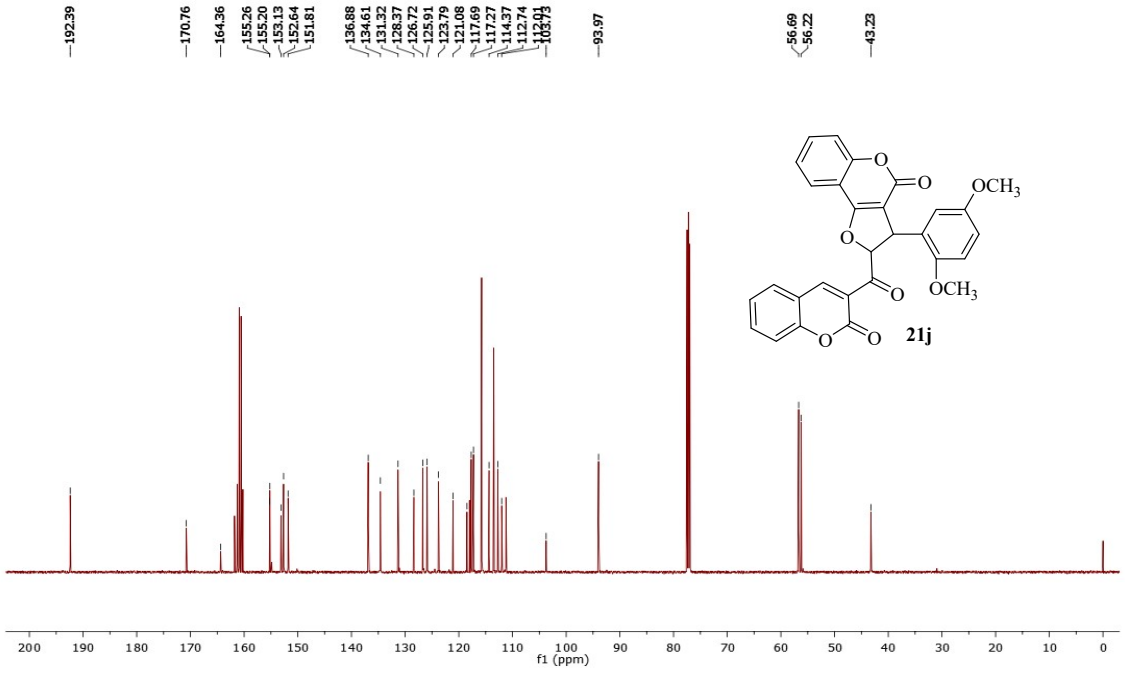

Figure S62: ^{13}C NMR spectrum of 3-(2,5-dimethoxyphenyl)-2-(2-oxo-2*H*-chromene-3-carbonyl)-2,3-dihydro-4*H*-furo[3,2-*c*]chromen-4-one (21j)

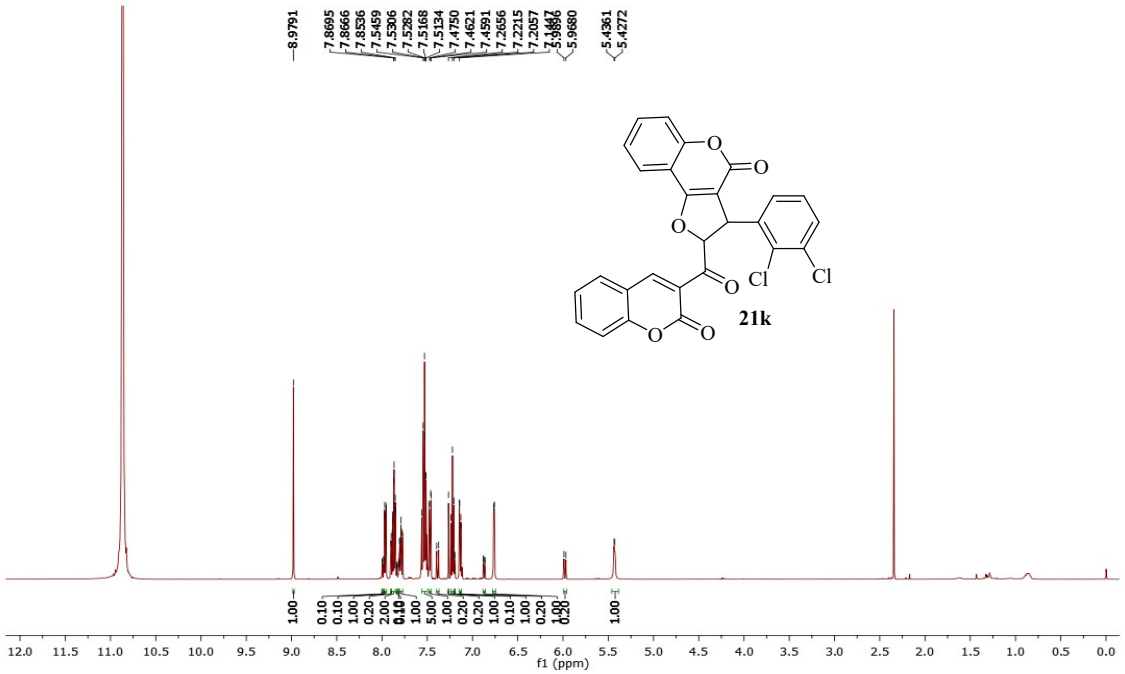

Figure S63: ^{1}H NMR spectrum of 3-(2,3-dichlorophenyl)-2-(2-oxo-2*H*-chromene-3-carbonyl)-2,3-dihydro-4*H*-furo[3,2-*c*]chromen-4-one (21k)

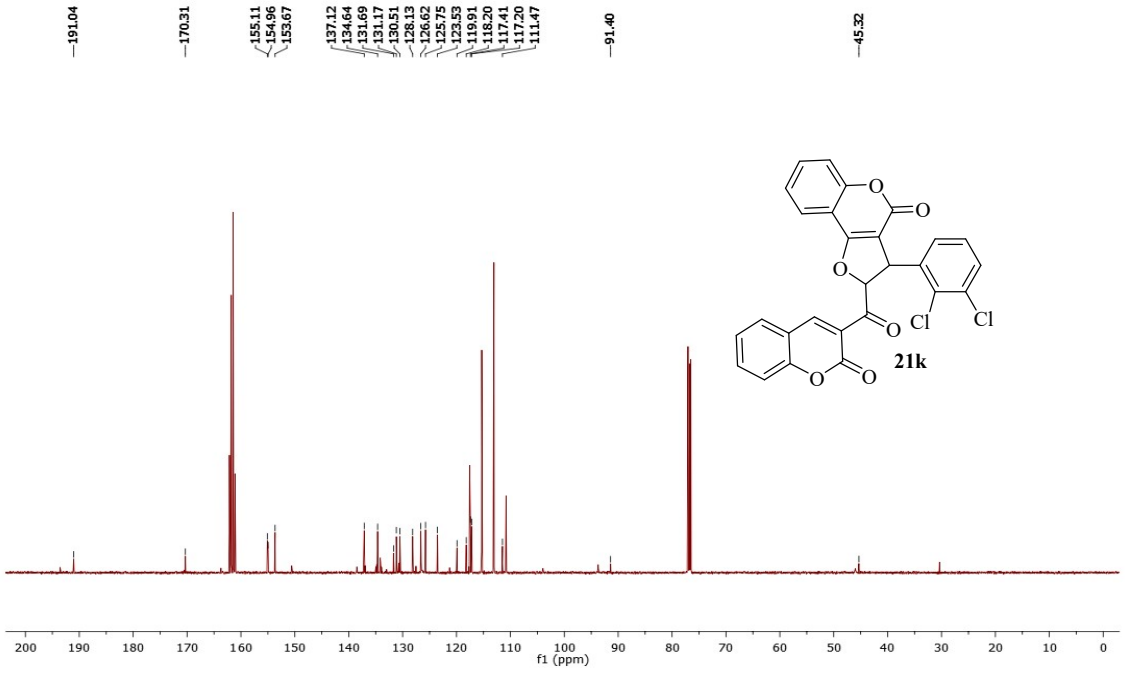

Figure S64: ^{13}C NMR spectrum of 3-(2,3-dichlorophenyl)-2-(2-oxo-2*H*-chromene-3-carbonyl)-2,3-dihydro-4*H*-furo[3,2-*c*]chromen-4-one (21k)

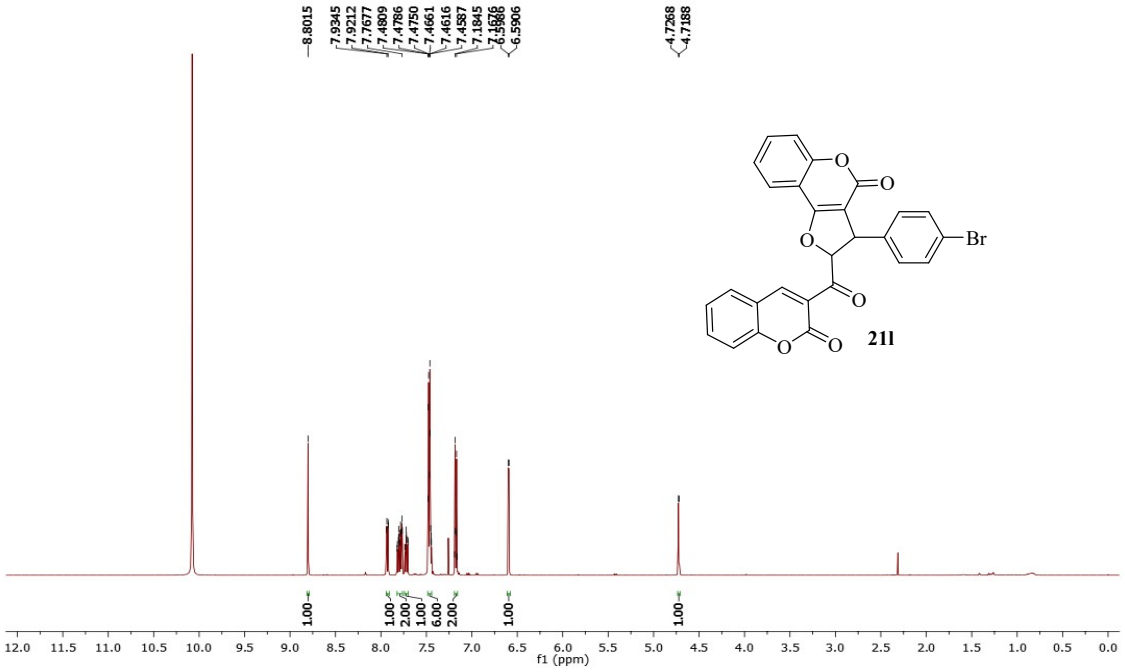

Figure S65: ^{1}H NMR spectrum of 3-(4-bromophenyl)-2-(2-oxo-2*H*-chromene-3-carbonyl)-2,3-dihydro-4*H*-furo[3,2-*c*]chromen-4-one (21l)

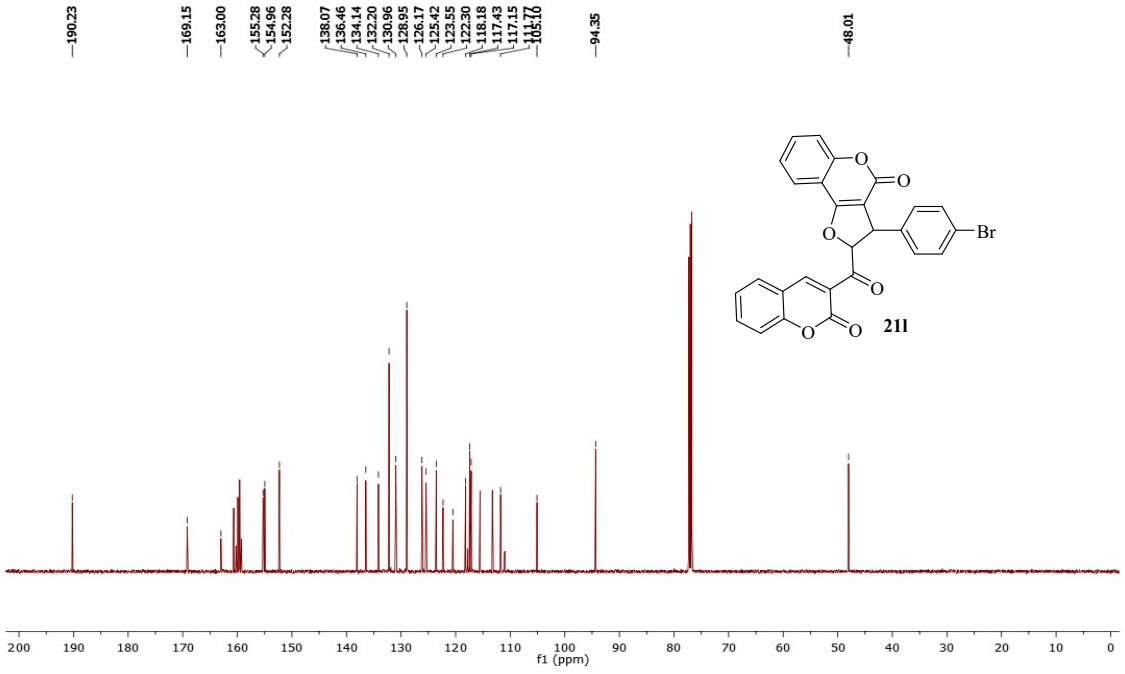

Figure S66: ^{13}C NMR spectrum of 3-(4-bromophenyl)-2-(2-oxo-2*H*-chromene-3-carbonyl)-2,3-dihydro-4*H*-furo[3,2-*c*]chromen-4-one (21l)

Experimental Protocols

Antibacterial and Biological Assays

The antibacterial activity of all the newly synthesized target compounds was tested *in vitro* against four Gram-positive (*Staphylococcus aureus* (MTCC No-902), *Enterococcus faecalis* (MTCC No-6845), *Bacillus subtilis* (MTCC No-441), *Listeria* (MTCC No-4214) and four Gram-negative bacteria (*Escherichia coli* (MTCC No-448), *Salmonella enterica* (MTCC No-1165), *Acinetobacter calcoaceticus* (MTCC No-1948), *Serratia marcescens* (MTCC No-2645). using the two-fold serial dilution method in 96-well micro test plates, following the guidelines provided by the National Committee for Clinical Laboratory Standards (NCCLS). The minimal inhibitory concentration (MIC, μg/mL) is the lowest concentration, or highest dilution, of the new compounds required to completely prevent bacterial growth after overnight incubation in a 96-well plate at 37 °C. The bacterial strains used for testing were obtained from the Institute of Microbial Technology (IMTech), Chandigarh. Amoxicillin and Tetracycline were utilized as reference drugs. To verify that the solvent did not affect bacterial growth, a control test was conducted using a test medium supplemented with DMSO at the same dilutions as in the control experiment. Bacterial growth was observed both visually and spectrophotometrically, with all experiments conducted in triplicate for accuracy. The bacterial suspension was diluted with sterile saline to achieve a concentration of 1×10^5 CFU/mL, while the stock solutions were made by dissolving the target compounds in DMSO. The compounds and reference drugs were prepared in nutrient broth using a two-fold serial dilution to achieve the desired concentrations of 800, 400, 200, 100, 50, 25, 12.5, 6.25, 3.125, and 1.56 μg/mL.

Biofilm Inhibition Assay

E. coli bacterial suspension was incubated with active analogues **16b** and **21e** at various concentrations in 96-well plate at 37 °C for 72 hours. After the incubation period, the supernatant was discarded, and the sediment was washed with phosphate buffer. The plate was then incubated at 60 °C for 1 hour to fix the biofilm. Following this, 0.1% crystal violet solution was added and left to incubate at room temperature for 1 hour. The wells were then rinsed with distilled water to remove excess dye. Finally, 33% acetic acid was used to elute the stained biofilm, and absorbance was measured at 600 nm using a microplate reader.

Kinetics of Bactericidal Activity

E. coli cells were incubated with biological active compounds **16b** and **21e** at different concentrations of (1 ×, 2 ×, 4 ×, and 8 × MICs) in a 96-well plate at 37 ºC. The absorbance of treated and untreated cells was noted for 8 hours at an interval of 1 hour, using an Elisa plate reader (Biotek, Power-Wave XS2). The reduction in absorbance of treated cells were recorded

Bacterial Susceptibility Evaluation

After determining the MIC values, multiple passaging was performed by transferring bacterial suspension grown at sub-MIC. After the growth of *E. coli,* new MIC value was calculated towards each passage of the strain; tetracycline was taken as control. The experiment was continued for 20 days.

Outer Membrane Permeability

The cultured *E. coli* was harvested by centrifugation at 3500 rpm for 5–10 minutes, followed by washing and resuspension in 1:1 mixture of 5 mM glucose and 5 mM HEPES buffer (*p*H 7.2) to achieve a final concentration of 10^8 CFU/mL. The *N*-phenyl naphthylamine (NPN) dye (10 μM, 50 μL) was added to the cell containing bacterial suspension (10^5 CFU/mL, 150 μL) and pre-incubated for about 1 h. Fluorescence intensity was recorded with an excitation wavelength of 350 nm and an emission wavelength of 420 nm (control group). Subsequently, analogues **16b** and **21e** were introduced at varying concentrations (1 ×, 2 ×, 4 ×, and 8 × MICs), and fluorescence intensity was measured under the same conditions using dimethyl sulfoxide as a negative control.

Inner Membrane Permeability

The *E. coli* bacterial culture was subjected to centrifugation at 3500 rpm for 5–10 minutes, followed by washing and resuspension in a 1:1 mixture of 5 mM glucose and 5 mM HEPES buffer (*p*H 7.2). Then propidium iodide (PI, 10 μM) was added to the wells containing bacterial suspension (~10^5 CFU/mL) and the formed suspension was incubated for 30 min at 37 ℃. Fluorescence intensity was recorded with an excitation wavelength of 535 nm and an emission wavelength of 617 nm (control group). Following this, analogues **16b** and **21e** were added at varying concentrations (1 ×, 2 ×, 4 ×, and 8 × MIC), and fluorescence intensity was evaluated under identical conditions using dimethyl sulfoxide as a negative control.

Leakage of Cytoplasmic Contents

E. coli cells were collected by centrifugation at 8000 rpm for 6 min and washed with PBS (0.1 mM, *p*H 7.2). Cell suspensions (100 μL) were incubated at 37 °C under agitation treated with

compounds **16b** and **21e** at (1 ×, 2 ×, 4 ×, and 8 × MIC), and DMSO was used as negative control. The amounts of DNA from the cytoplasm into supernatant were estimated by detection of absorbance at 260 nm.

Changes in Cell Morphology

The bacteria *E. coli* in the exponential phase was centrifuged at 3500 rpm for 5 min, and the supernatant was discarded. The bacteria cell was washed three times with PBS and re-suspended with PBS. The bacterial suspension was incubated with compounds **16b** and **21e** (1 × MIC) for 6 h at 37 ˚C and centrifuged at 3500 rpm for 5 min and then again washed thrice with PBS. The cells were fixed with 2.5% glutaraldehyde overnight at 4 ^{o}C and washed with PBS buffer and dehydrated with different concentrations of ethanol (45, 55, 65, 75, 95 and 100%). Then, the obtained pellets were dried and visualized under a scanning electron microscope.

Measurement of Metabolic activity

E. coli cultures were treated with varying concentrations of analogues **16b** and **21e** for 6 hours at 37 °C. Afterward, untreated and treated cells were incubated with resazurin dye (50 μg/mL, 25 μL) at 37 °C for 1 hour. Absorbance at 570 nm was measured using an ELISA plate reader, and the metabolic activity was assessed using the average percentage reduction.

Evaluation of Intracellular Reactive Oxygen Species (ROS)

A 2,7-dichlorofluorescein diacetate (DCFH-DA) assay was employed to quantify intracellular ROS. *E. coli* ells at 10^6 CFU/mL were then treated with increasing concentrations of analogues **16b** and **21e** for 6 hours at 37 °C. Following treatment, control and treated cells were harvested, rinsed with PBS, and subsequently incubated with 100 μM DCFH-DA probe for 30 minutes in dark at 37 °C. The oxidative cleavage of DCFH-DA to DCF generated fluorescence, which was detected using a fluorescence spectrophotometer with excitation and emission wavelengths of 485 nm and 528 nm, respectively. The enhancement in intracellular ROS levels in cells exposed to compounds **16b** and **21e**, relative to control cells, was analyzed and plotted.

Determination of Glutathione Activity

The standard Ellman's assay was employed to assess intracellular GSH activity. *E. coli* suspensions (~10^5 CFU/mL) underwent treatment with increasing concentrations of analogues **16b** and **21e** for 6 hours at 37 °C. After centrifugation at 5000 rpm for 5 minutes, control and treated cells were washed with PBS and lysed. The clear supernatant was carefully collected. Tris-HCl (50 mM) and 5,5-dithiobis(2-nitrobenzoic acid) (DTNB) (100 mM) were then added and incubated

in the dark at 37 °C for 30 minutes. The resulting solution was measured at 412 nm by spectrophotometry (**eq 7**).

$$\left(1-\frac{OD@412\ nm\ of\ treated}{OD@412\ nm\ of\ control}\right) \times 100 \quad (7)$$

Lipid peroxidation

Malondialdehyde (MDA) is a natural product of lipid oxidation in organisms. Some aliphatic acids are gradually decomposed into complex compounds after oxidation, including MDA. Hence, the extent of lipid oxidation can be determined by quantifying MDA levels. The *E. coli* suspensions (~10^5 CFU/mL) were treated with increasing concentrations of analogues for 4 hours at 37 °C. Trichloroacetic acid (TCA) was used to stop the reaction under dark conditions, followed by the addition of 0.5% thiobarbituric acid. Following heating at 80 °C for 30 min, the mixture was cooled using an ice bath. Control and treated cells were then centrifuged at 5000 rpm for 5 min, and the supernatant was collected for analysis and tested by microplate reader at 535 nm.

Circular Dichroism (CD) Spectroscopy

Circular dichroism (CD) data were expressed as mean residue ellipticity (MRE) using the equation:

$$MRE = \frac{Observed\ CD\ (m\ degree)}{C_p nl \times 10} \quad (8)$$

Here, C_p denotes the HSA concentration, *n* corresponds to the number of amino acid residues in the protein (585), and *l* represents the path length of the cuvette (2 mm). The α-helical fraction of native HSA as well as HSA in the presence of analogues **16b** and **21e** was calculated from the MRE at 208 nm by applying the equation:

$$\alpha - helix\ \% = \frac{MRE_{208} - 4000}{33000 - 4000} \times 100 \quad (9)$$

Where, MRE_{208} is the observed MRE value at 208 nm, 4000 is the MRE of the β-sheet and random coil conformation at 208 nm, and 33,000 is the MRE for pure α-helix at the same wavelength.

Cytotoxicity Assay

Human embryonic kidney cells (HEK293) were cultured in DMEM along with 10% FBS, 100 mg/mL streptomycin, 100 U/mL penicillin, and 50 mM glutamine. The experiment was conducted in triplicate by seeding the cells in 96 well plates at the density of 1×10^{-5} in DMEM media

supplemented with 10 % FBS cells. In 5% CO_2 incubator cells were incubated at 37 °C. Cells were treated with five different concentrations (0.01, 0.1, 1, 10, and 100 μM) of compounds **16b** and **21e** at 37 °C for 48 h. From 5 mg/mL stock of MTT (prepared in 1* PBS buffer), 10 μL was pipetted out and added in each well then incubated at 37 °C for 4 hours in the dark. The formazan crystals were dissolved in 100 μL of DMSO. Formazan crystal formation was assessed by measuring absorbance using a Bio-Tek ELISA plate reader at a reference wavelength of 570 nm. The MTT assay was performed in three independent replicates to validate the consistency of the findings. The average values were calculated, and the data were represented with error bars indicating the standard deviation. To calculate the inhibition percentage, the following equation **(8)** was used

$$\% \text{ inhibition} = [1 - (A_t/A_c) \times 100]\% \quad (10)$$

where A_t is the test substance absorbance and A_c is the control solvent absorbance.

Quantum Chemical Studies

Quantum chemical calculations were executed using density functional theory (DFT) with the B3LYP method and a 6-311+g** basis set. The active analogues, **16b** and **21e**, underwent geometry optimization using GaussView 5.0.8 for molecular structure sketching. The HOMO − LUMO surface of the investigated molecules was graphically represented using Chemcraft, offering a visual depiction of electron distribution and energy gaps.

Sample preparation: A stock solution of calf thymus (ct) DNA was prepared by dissolving the DNA in a buffer consisting of 10 mM Tris and 1 mM EDTA at pH 7.4 at room temperature and stored at 4 °C for 24 h. The absorbance ratio at 260 nm to 280 nm was measured to assess the DNA solution's purity. The concentration of the DNA stock solution was calculated using the average extinction coefficient of 6600 $M^{-1}cm^{-1}$ for a single nucleotide at 260 nm. The stock solution of the analogues (10^{-3} M) were prepared in DMSO, and HSA (10 μM) was prepared in distilled water.

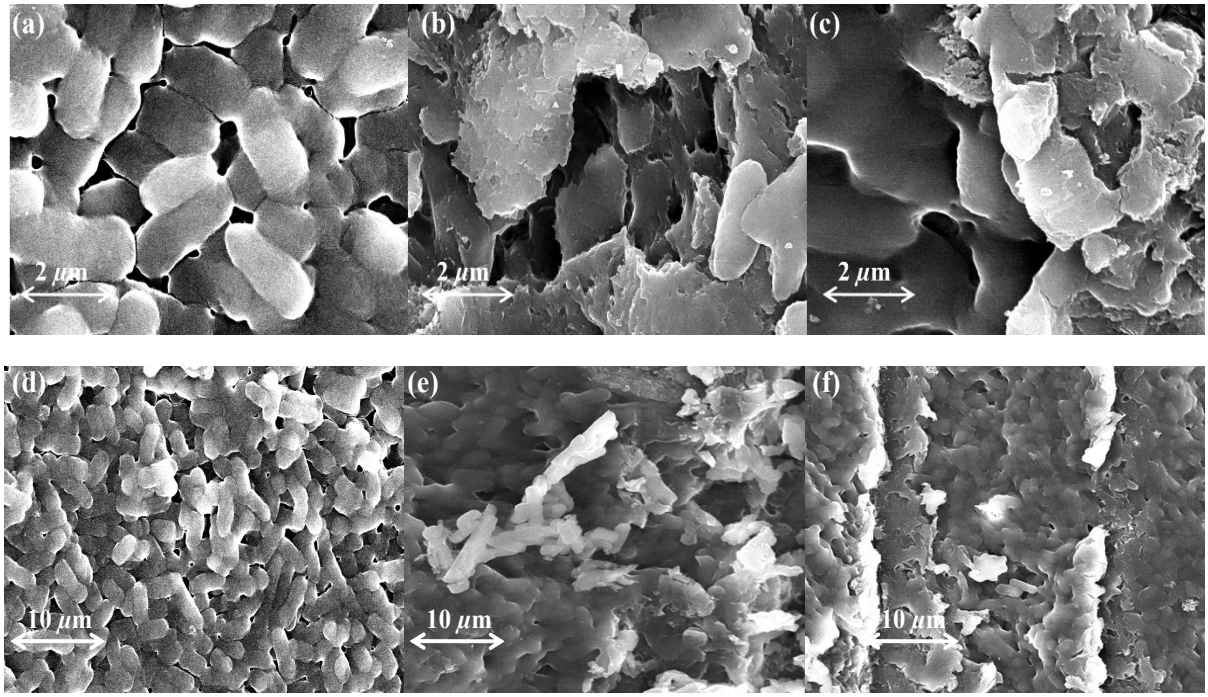

Figure S67. SEM images of (a, d) untreated *E. coli* and treated *E. coli* with analogues (b, e) **16b** and (c, f) **21e** at 1 × MIC. Scale bars: (a, b, c) 2 μm; (d, e, f) 10 μm.

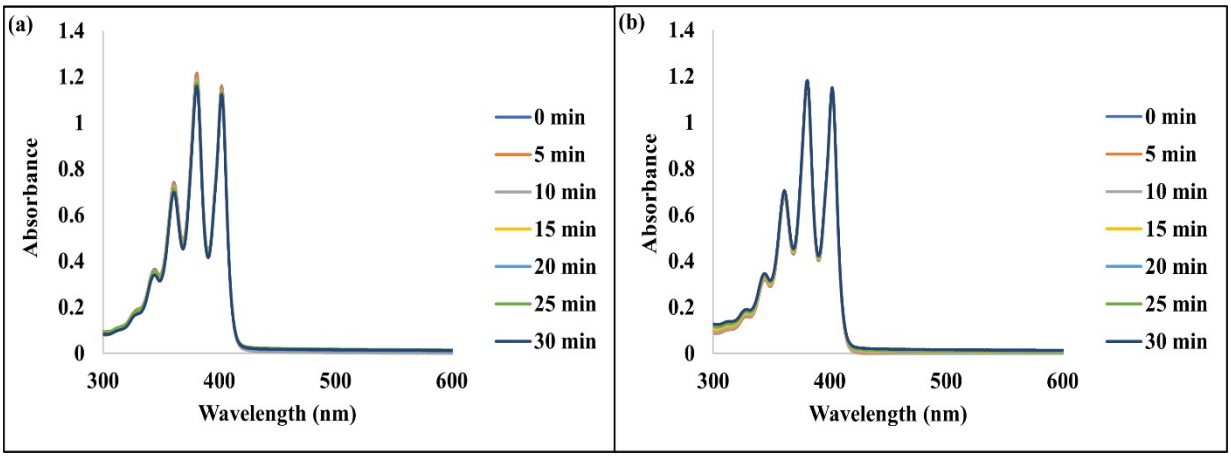

Figure S68. UV–Vis spectra of ABDA in the presence of (a) **16b** and (b) **21e** (5 μM) in PBS containing 0.5% DMSO, upon irradiation with a UV light (365-367 nm, 10 W).

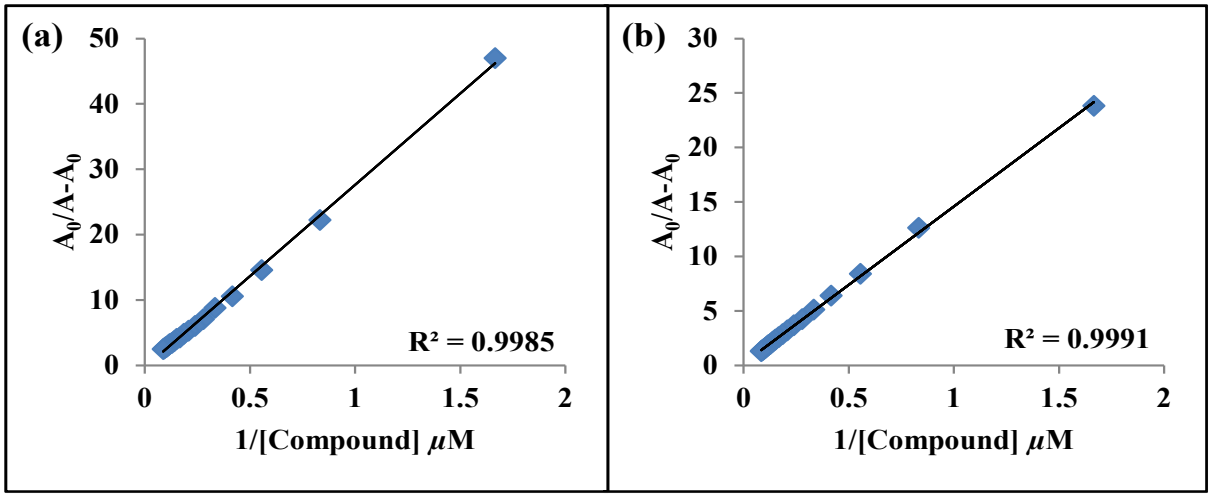

Figure S69. Benesi-Hildebrand plots of absorption spectra of HSA with (a) **16b** and (b) **21e** at 298 K.

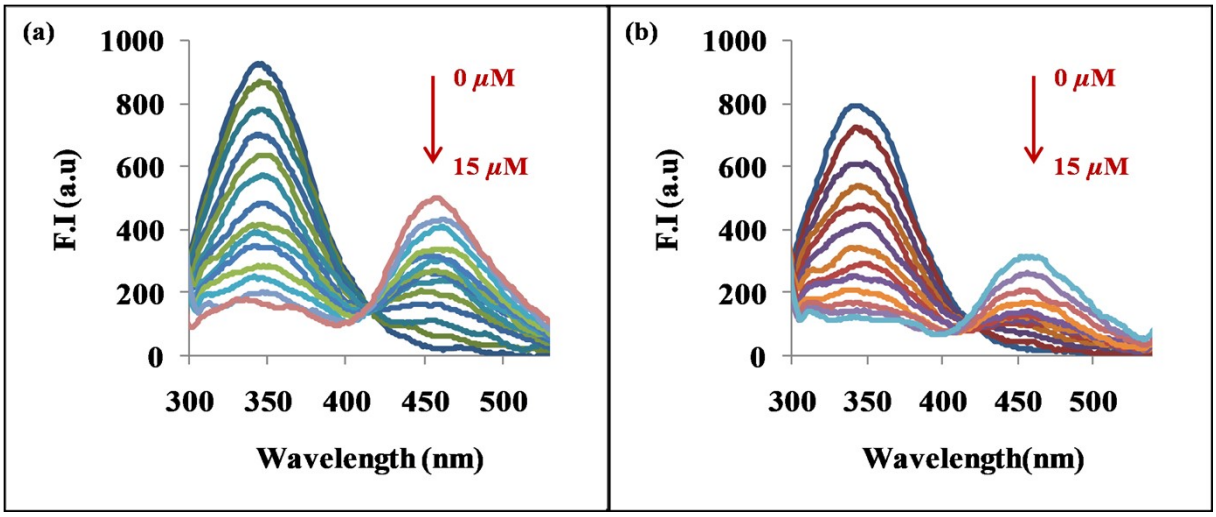

Figure S70. Emission spectra of HSA with **16b** at (a) 308 K and (b) 318 K.

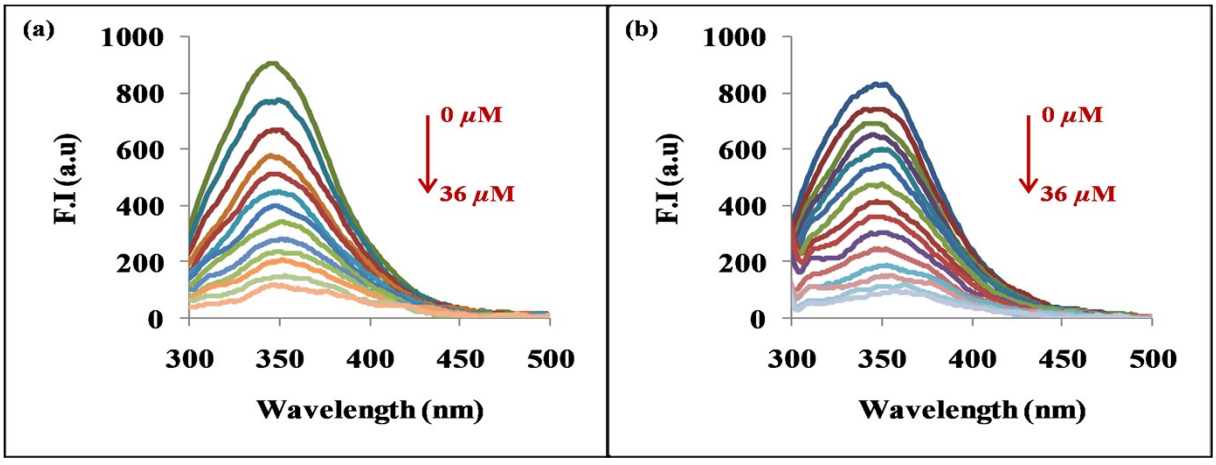

Figure S71. Emission spectra of HSA with **21e** at (a) 308 K and (b) 318 K.

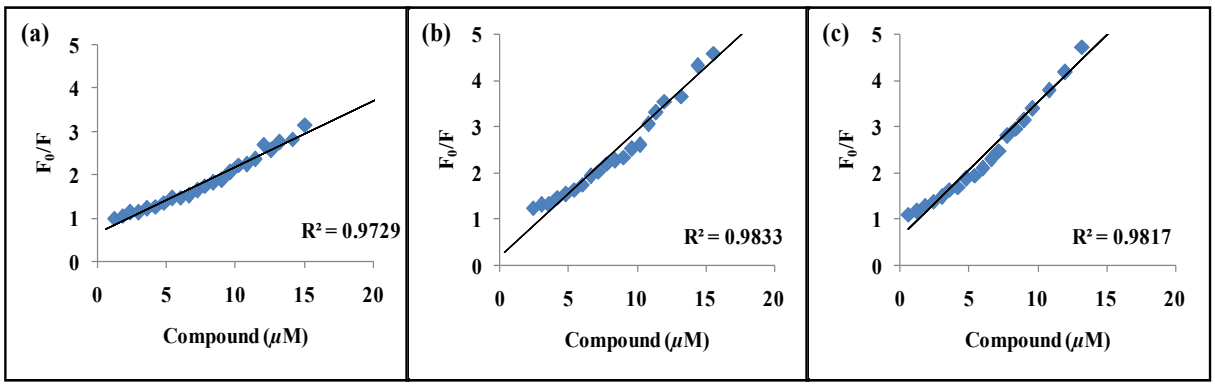

Figure S72.The Stern-Volmer plots of emission spectra of HSA with **16b** at (a) 298 K, (b) 308 K and (c) 318 K.

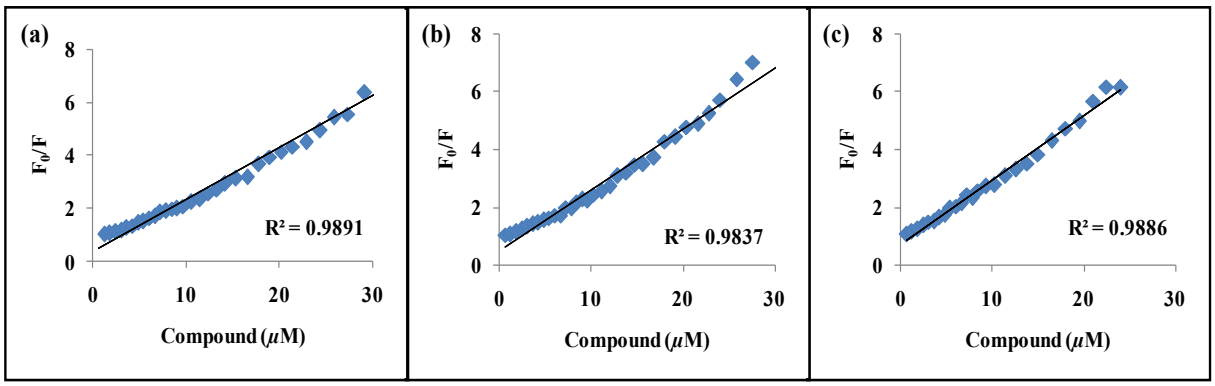

Figure S73.The Stern-Volmer plots of emission spectra of HSA with **21e** at (a) 298 K, (b) 308 K and (c) 318 K.

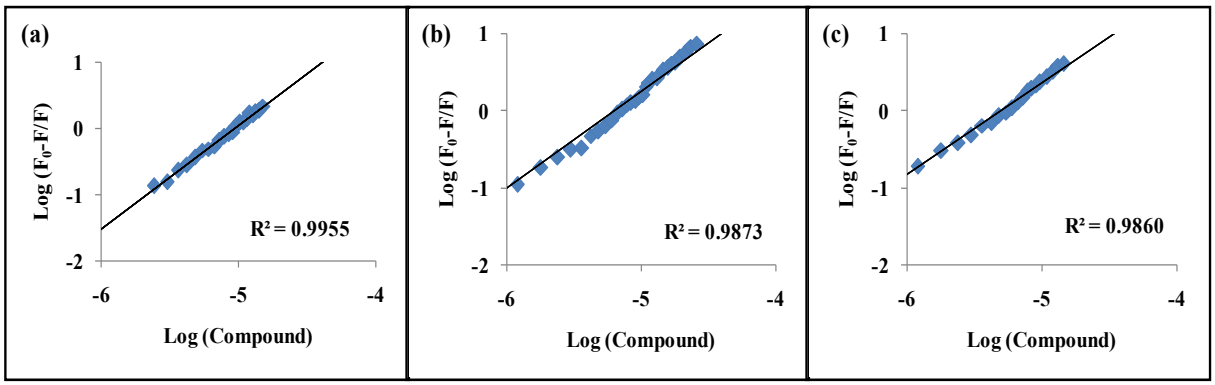

Figure S74. Modified Stern-Volmer plots of emission spectra of HSA with **16b** at (a) 298 K, (b) 308 K and (c) 318 K.

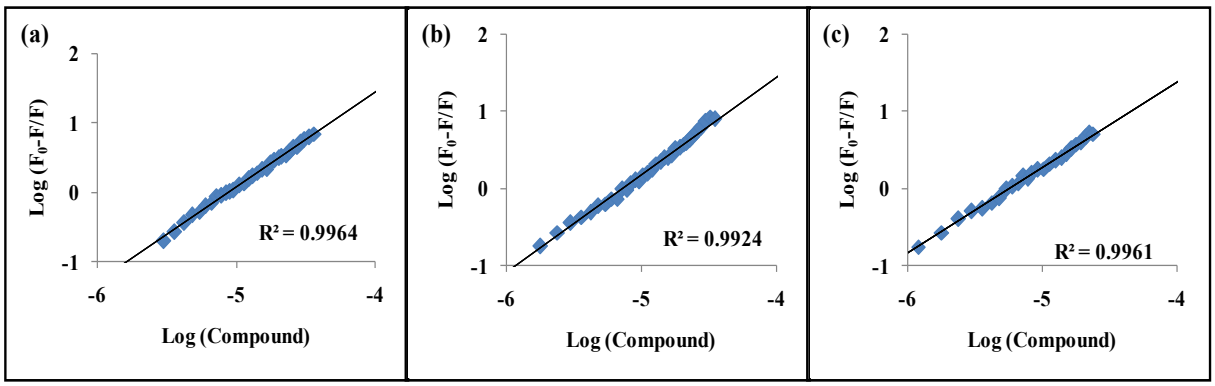

Figure S75. Modified Stern-Volmer plots of emission spectra of HSA with **21e** at (a) 298 K, (b) 308 K and (c) 318 K.

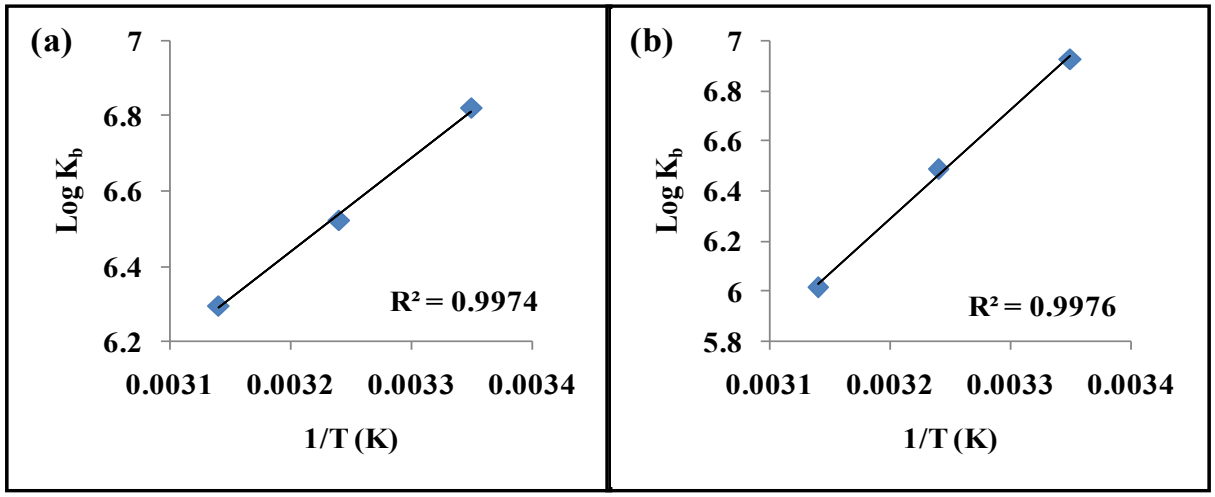

Figure S76. Van't Hoff plots of emission spectra of HSA with (a) **16b** and (b) **21e.**

Table S1. Lifetime fluorescence decay of HSA on interaction with **16b** and **21c**

System	Conc.	τ_1[ns]	τ_2[ns]	τ_3[ns]	α_1	α_2	α_3	τ_{av}	χ^2
HSA		3.12	0.32	7.26	0.29	0.03	0.68	5.84	1.05
HSA-16b	1:1	3.09	7.19	0.74	0.31	0.58	0.11	5.24	1.10
	1:2	3.64	7.44	0.85	0.34	0.38	0.28	4.29	1.06
	1:3	2.20	6.54	0.60	0.26	0.38	0.37	3.24	1.03
	1:4	2.14	6.09	0.53	0.25	0.27	0.48	2.44	1.01
HSA-21e	1:1	5.42	1.56	13.55	0.73	0.20	0.06	5.08	1.03
	1:2	3.35	6.82	0.87	0.43	0.37	0.20	4.14	1.06
	1:3	3.20	7.66	0.77	0.44	0.19	0.38	3.16	1.01
	1:4	1.91	0.63	4.98	0.27	0.48	0.25	2.06	1.04

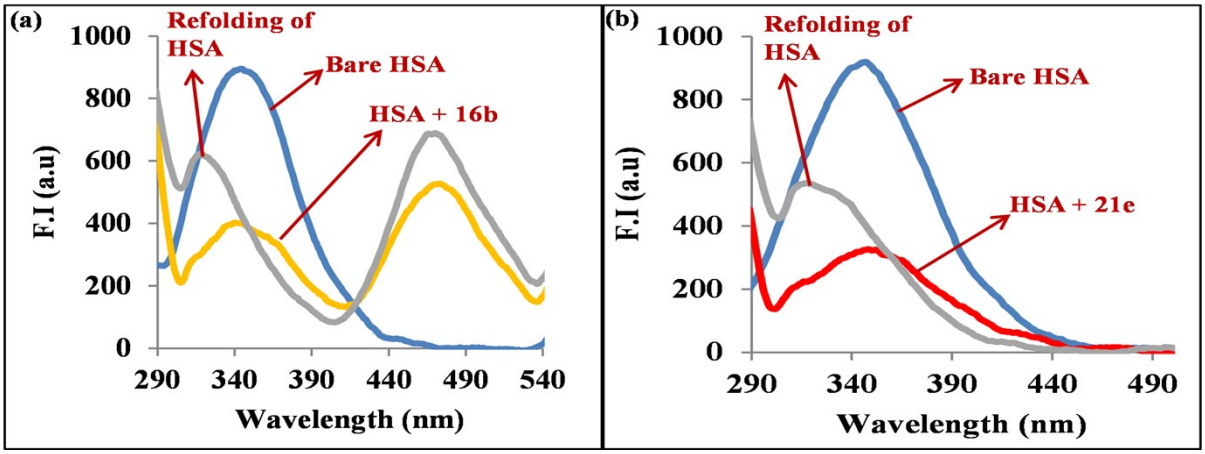

Figure S77. Fluorescence spectra of bare HSA (blue) in the presence of compounds (a) **16b** (orange) and (b) **21e** (red) and in the presence of SDS (grey).

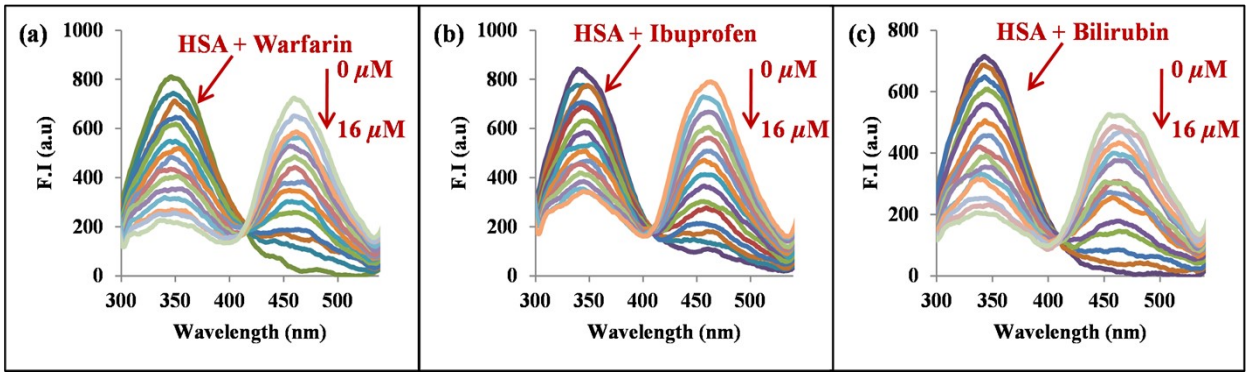

Figure S78. Effect of incremental addition of analogue **16b** on the emission spectra of (a) HSA-Warfarin complex, (b) HSA-Ibuprofen complex and (c) HSA-Bilirubin complex in phosphate buffer (*p*H = 7.4) at 298 K.

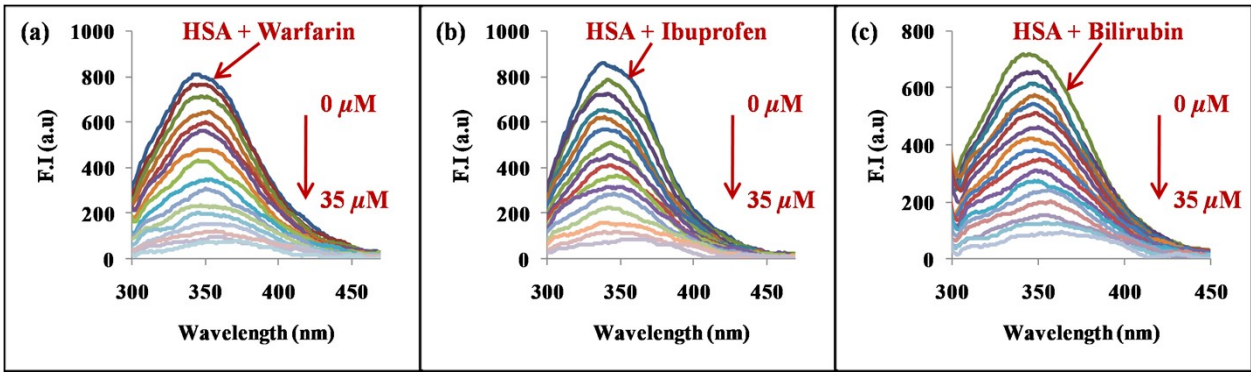

Figure S79. Effect of incremental addition of analogue **21e** on the emission spectra of (a) HSA-Warfarin complex, (b) HSA-Ibuprofen complex and (c) HSA-Bilirubin complex in phosphate buffer (*p*H = 7.4) at 298 K.

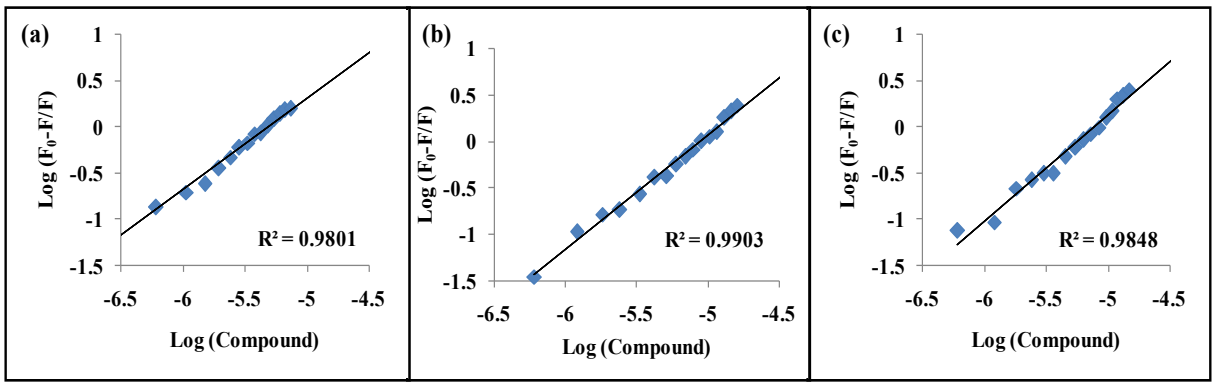

Figure S80. Modified Stern-Volmer plots of **16b** for determination of binding constant in drug displacement studies of (a) HSA–Warfarin complex, (b) HSA–Ibuprofen complex, and (c) HSA–Bilirubin complex in phosphate buffer (pH 7.4) at 298 K.

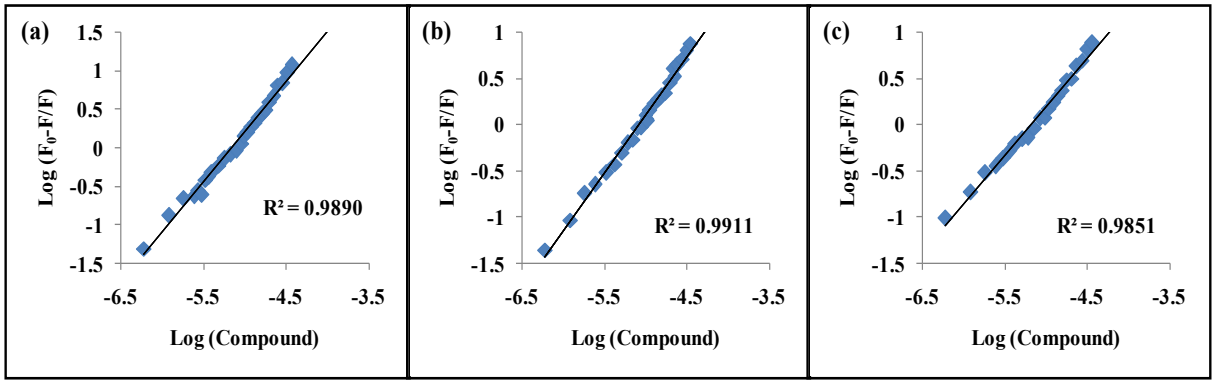

Figure S81. Modified Stern-Volmer plots of **21e** for determination of binding constant in drug displacement studies of (a) HSA–Warfarin complex, (b) HSA–Ibuprofen complex, and (c) HSA–Bilirubin complex in phosphate buffer (pH 7.4) at 298 K.

Table S2. Binding constants (K_{bin}) of the HSA–**16b**/**21e** systems at 298 K in the absence and presence of site markers.

HSA/Site Markers	**Binding constant (K_{bin} [M^{-1}])**		**Binding stoichiometry (n)**	
	16b	**21e**	**16b**	**21e**
HSA	6.06×10^6	8.39×10^6	1.55	1.36
Warfarin	1.65×10^5	4.97×10^5	0.98	1.29
Ibuprofen	1.66×10^6	2.26×10^6	1.23	1.25
Bilirubin	7.19×10^5	2.69×10^5	1.14	1.04

Table S3. Docking results based on the binding free energies of analogues **16b** and **21e** at the entire HSA, and their Subdomains IIA, IIIA, and IB

	16b				21e			
Mode	**Entire**	**IIA**	**IIIA**	**IB**	**Entire**	**IIA**	**IIIA**	**IB**
1	-7.26	-8.86	-6.65	-8.35	-10.36	-8.88	-8.96	-10.80
2	-6.73	-.8.64	-6.33	-8.17	-8.02	-8.81	-7.84	-10.64
3	-6.69	-8.61	-6.32	-7.79	-6.89	-8.64	-7.74	-10.62
4	-6.23	-8.60	-6.31	-6.96	-6.16	-8.46	-7.52	-9.71
5	-6.00	-6.99	-6.26	-6.85	-5.98	-8.45	-7.52	-9.68
6	-5.68	-6.66	-6.25	-5.92	-5.71	-8.14	-6.39	-9.64
7	-5.63	-6.87	-6.23	-5.76	-5.64	-7.69	-7.18	-9.54
8	-5.42	-6.84	-6.09	-5.36	-4.80	-7.68	-7.09	-9.54
9	-5.43	-6.80	-5.46	-4.84	-4.46	-6.50	-6.54	-9.25

Table S4. Amino acid residue involved in the ligand-protein interaction and free binding energy

Analogue	**ΔG (kcal mol-1)**	**Site**	**Amino acid residue involved in interaction**	**Type of interaction**	**Bond distance**
16b	-8.86	Subdomain IIA	ALA A:291	π–Alkyl	5.20,5.18
			ILE A:290	π–Alkyl	5.19
			SER A:287	π–Sigma	3.74
			LEU A:260	π–Alkyl	4.72
			ALA A:261	π–Alkyl	5.12
			ARG A:257	π–Alkyl, π–Cation,	5.37,4.69, 4.75
			VAL A:241	π–Alkyl	5.14
			LEU A:238	π–Sigma	3.56
			ARG A:218	π–Alkyl	5.12

			TRP A:214	π– π T-shaped	5.16,5.03
			LYS A:199	π-Cation, Conventional Hydrogen Bond,	4.18, 3.39
21e	-10.80	Subdomain IB	PHE A:157	π– π T -shaped	4.80
			LYS A:190	π-Alkyl, π-Donor Hydrogen Bond, Conventional Hydrogen Bond,	4.93,3.98,3.21
			LEU A:115	π-Alkyl, Conventional Hydrogen Bond,	5.25,3.39
			ILE A:142	π-Alkyl	5.04,4.58
			HIS A:146	π– π T -shaped	4.91
			ARG A:186	π-Alkyl, Carbon Hydrogen Bond	5.35,4.86,3.38
			ARG A:145	π-Alkyl	4.92
			ARG A:114	π-Alkyl	4.82,4.54

(A) Suldow Site I (16b)

(a)

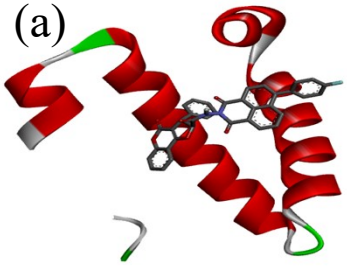

(b)

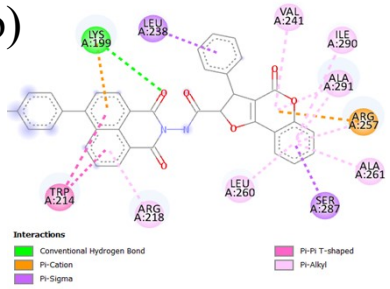

(c)

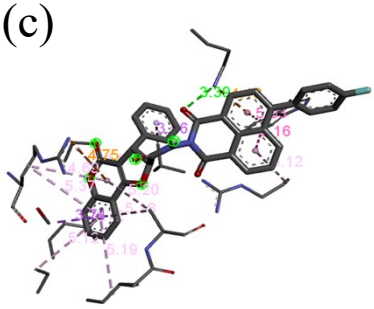

(d)

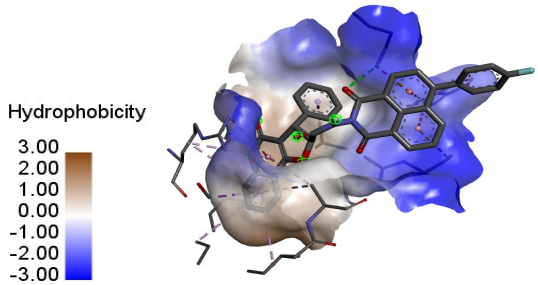

(B) Suldow Site II (16b)

(a)

(b)

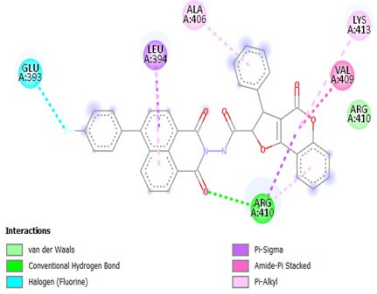

(c)

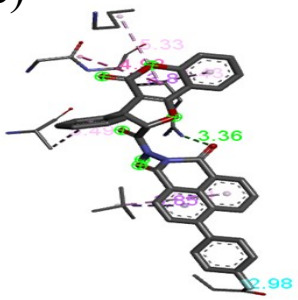

(d)

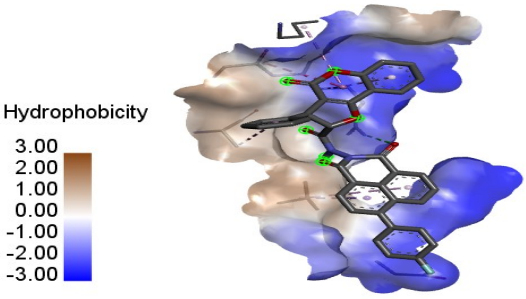

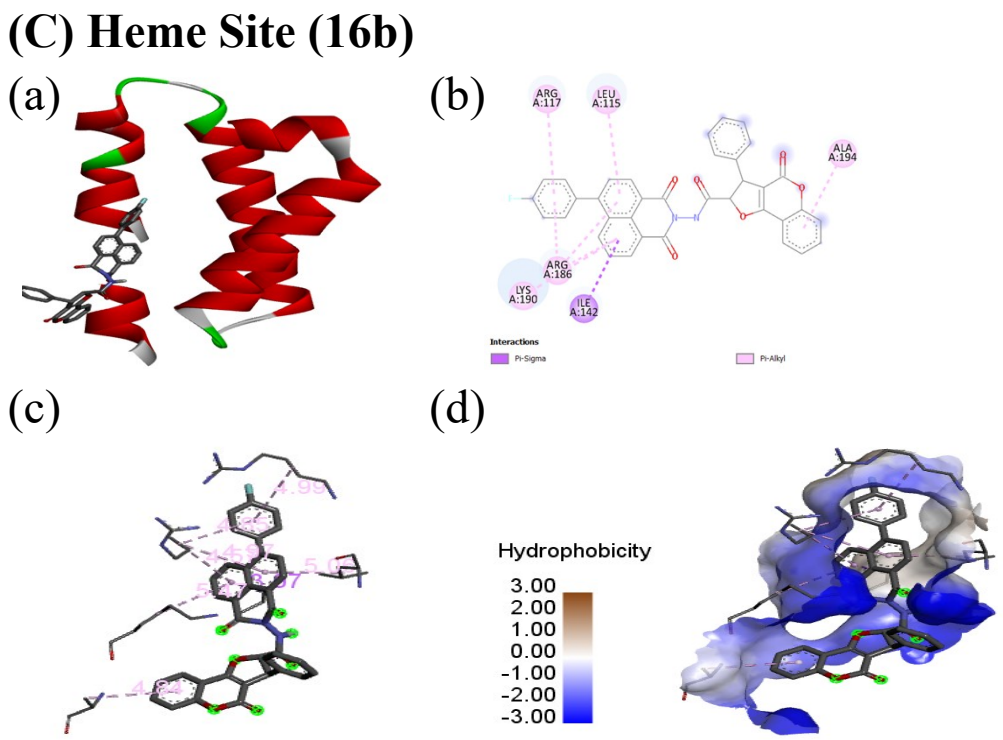

Figure S82. (a) **16b** docked in the binding pocket, (b) 2D representation of the interaction, (c) 3D portrait of the optimum conformation, and (d) location in the hydrophobic cavity at each respective site: (A) Suldow site I, (B) Suldow site II, and (C) Heme site.

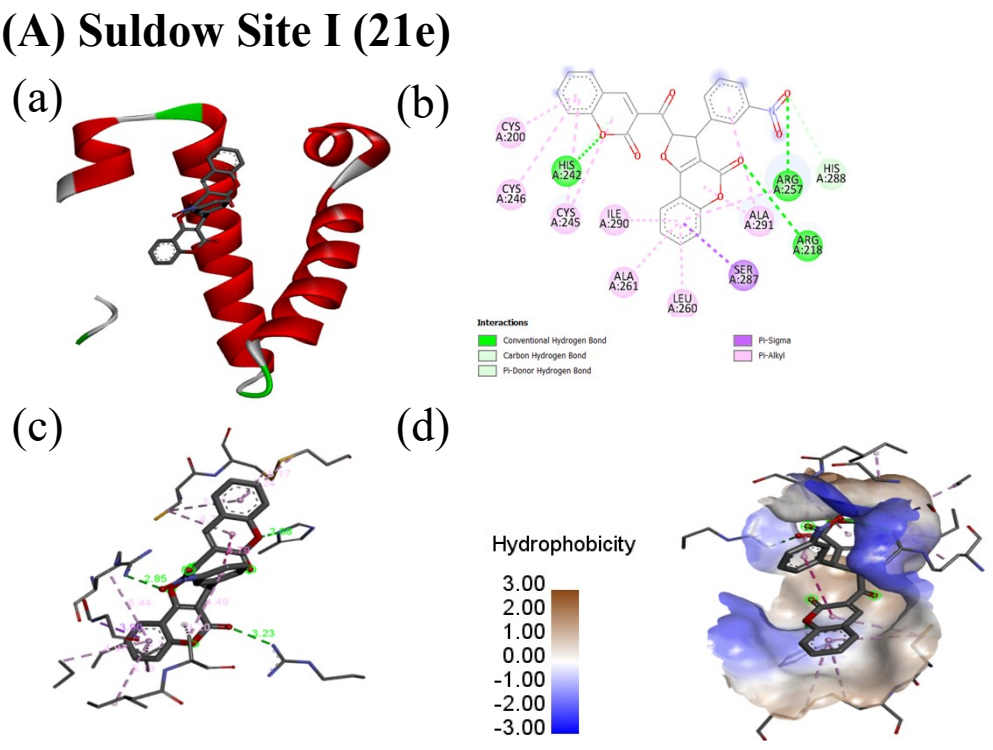

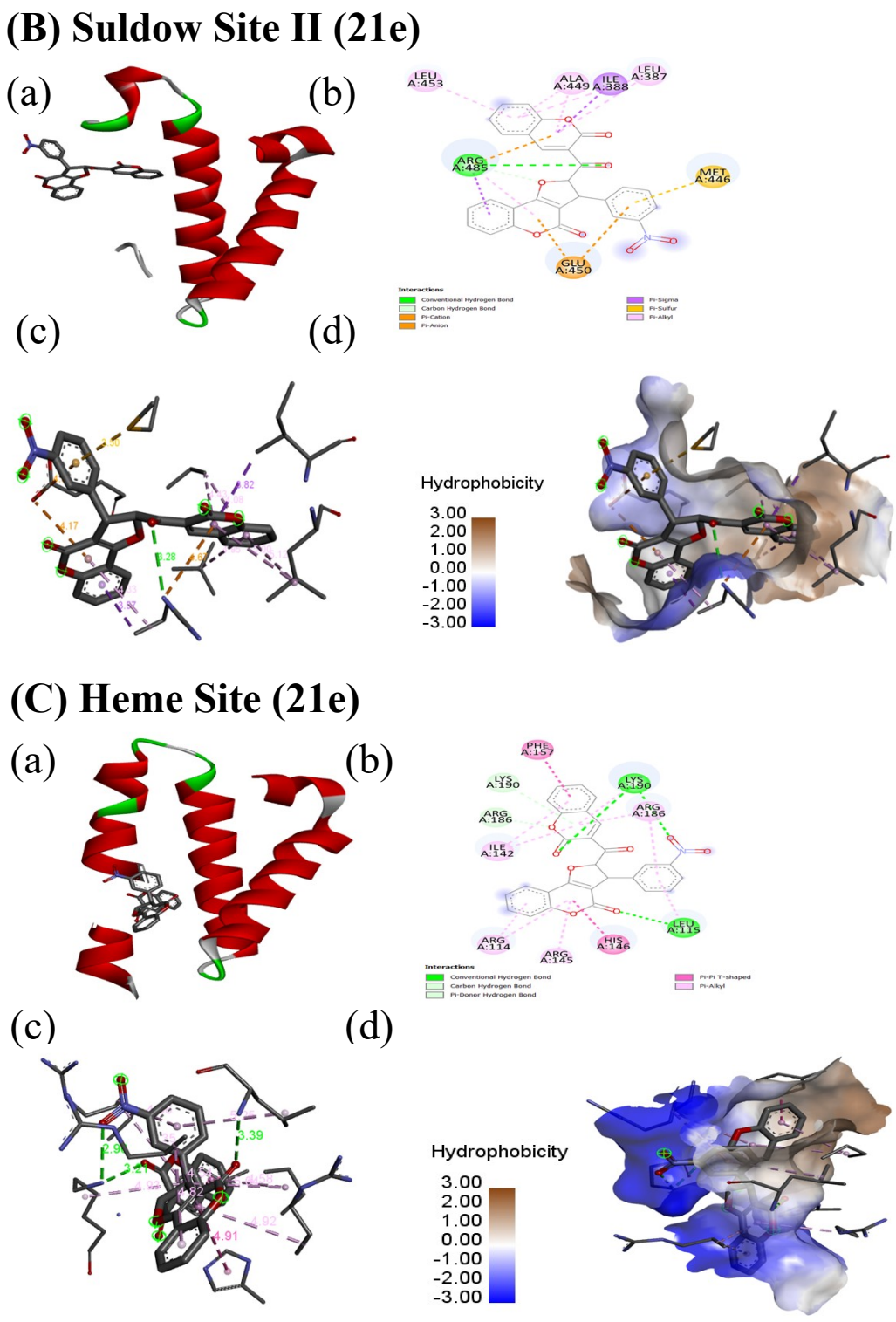

Figure S83. (a) **21e** docked in the binding pocket, (b) 2D representation of the interaction, (c) 3D portrait of the optimum conformation, and (d) location in the hydrophobic cavity at each respective site: (A) Suldow site I, (B) Suldow site II, and (C) Heme site.

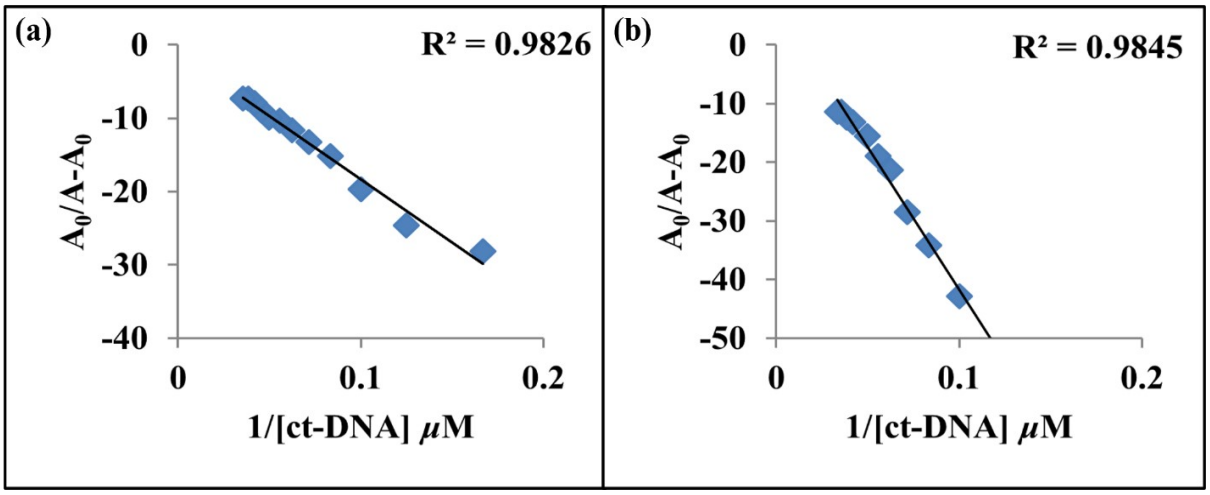

Figure S84. Benesi-Hildebrand plots of absorption spectra of ct-DNA with (a) **16b** and (b) **21e** at 298 K.

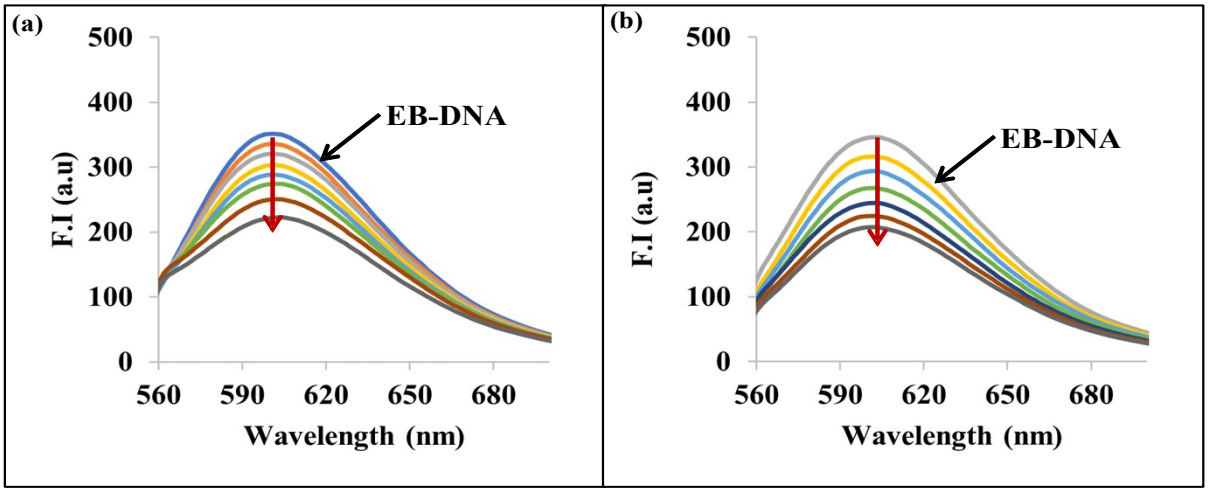

Figure S85. Emission spectra of ethidium bromide (EB) displacement assay with ct-DNA upon increasing concentration of analogues (a) **16b**, and (b) **21e** in phosphate buffer (pH 7.4) at 298 K.

Table S5. The docking results based on the binding free energies of analogues **16b** and **21e** docked into 1BNA from the co-crystallized ligand

Mode	Affinity (kcal/mol)	
	16b	**21e**
1	-11.18	-10.22
2	-11.18	-9.36
3	-11.17	-9.14
4	-11.16	-9.04
5	-11.14	-7.91
6	-11.17	-8.89
7	-10.71	-8.69
8	-10.54	-8.57
9	-10.32	-8.07
10	-8.78	-7.37

Table S6: Cartesian Coordinates of analogues **16b** and **21e**

Cartesian Coordinate of Compound 16b				**Cartesian Coordinate of Compound 21e**			
C	3.127431000	1.003486000	-1.256816000	C	4.699421000	-1.547917000	1.863551000
C	2.557949000	0.633527000	-0.054500000	C	4.173135000	-1.239526000	0.593399000
C	3.348428000	0.010492000	0.943875000	C	5.061004000	-0.949577000	0.456972000
C	4.734599000	-0.243765000	0.695987000	C	6.440991000	-0.954828000	0.255325000
C	5.290767000	0.117524000	-0.575405000	C	6.933168000	-1.261469000	1.005402000
C	4.482554000	0.743917000	-1.510982000	C	6.066764000	-1.561147000	2.068614000
H	2.505377000	1.478113000	-2.005673000	C	2.774149000	-1.178451000	0.304038000
C	2.783314000	-0.352490000	2.194181000	C	2.293276000	-0.864233000	0.930416000
C	5.505801000	-0.813213000	1.743129000	C	3.235716000	-0.644093000	2.049083000
H	4.900083000	1.010595000	-2.474673000	O	4.600379000	-0.660246000	1.698383000
C	4.934805000	-1.147594000	2.951519000	O	2.977816000	-0.478475000	3.201554000
C	3.565539000	-0.927147000	3.177371000	C	0.829660000	-0.706742000	1.189880000
H	6.564509000	-0.974862000	1.588700000	C	-0.140663000	-1.300239000	0.145717000
H	5.544623000	-1.578432000	3.736686000	C	-0.537576000	-0.366649000	1.071271000

H	3.103992000	-1.192273000	4.120500000	C	-2.024625000	-0.634236000	1.101208000
C	1.346959000	-0.120535000	2.478757000	C	-2.393953000	-1.305423000	0.017455000
C	1.122130000	0.897394000	0.169027000	O	-1.376646000	-1.634579000	0.831441000
N	0.614818000	0.492831000	1.427706000	C	-0.796328000	1.925062000	0.006736000
O	0.392127000	1.434657000	-0.638444000	C	-0.457027000	3.269649000	0.066038000
O	0.806894000	-0.408763000	3.521260000	C	0.465727000	3.848716000	0.798948000
N	-0.744980000	0.629975000	1.616591000	C	1.056908000	3.039668000	1.761431000
C	-1.599503000	-0.309572000	1.075009000	C	0.729201000	1.686462000	1.837111000
C	-3.051508000	0.167277000	1.062399000	C	-0.190100000	1.112445000	0.954396000
C	-3.393153000	0.907108000	-0.292200000	O	0.388212000	-0.135861000	2.155537000
C	-4.468117000	-0.013111000	-0.820542000	N	-1.115141000	4.123684000	1.083773000
C	-4.676993000	-1.030980000	0.049373000	O	-0.730548000	5.282202000	1.182652000
O	-3.924572000	-0.982894000	1.164535000	O	-2.003511000	3.622817000	1.758647000
O	-1.233833000	-1.367798000	0.624531000	C	-6.045613000	-1.473627000	0.495999000
H	-1.072764000	1.559669000	1.840394000	C	-4.684842000	-1.218589000	0.666254000
C	-5.333392000	4.051998000	0.698700000	C	-3.757426000	-1.631363000	0.310450000
C	-5.014764000	2.715236000	0.474353000	C	-4.207259000	-2.299266000	1.460560000
C	-3.781005000	2.361624000	-0.082369000	C	-5.558880000	-2.548648000	1.627359000
C	-2.873007000	3.372428000	-0.411430000	C	-6.472399000	-2.134883000	0.647402000
C	-3.191153000	4.711684000	-0.185992000	H	-6.740028000	-1.146468000	1.259395000
C	-4.421116000	5.054846000	0.370397000	H	-3.483996000	-2.603969000	2.206765000
H	-6.296871000	4.311872000	1.122895000	H	-5.911051000	-3.059511000	2.515017000
H	-5.737073000	1.943613000	0.720434000	H	-7.529935000	-2.330541000	0.782103000
H	-1.917799000	3.107651000	-0.853071000	O	-4.306592000	-0.568568000	1.804422000
H	-2.480233000	5.485470000	-0.453772000	C	-2.973596000	-0.225320000	2.098020000
C	-5.625923000	-2.078238000	-0.186115000	O	-2.753972000	0.349732000	3.133098000
C	-6.325309000	-1.977680000	-1.404024000	H	0.247874000	-2.245434000	0.240858000
O	-6.103423000	-0.966449000	-2.288524000	H	-0.054484000	-0.749071000	1.974175000
C	-5.153757000	0.060267000	-2.081048000	H	4.017568000	-1.773879000	2.676377000
O	-5.016377000	0.873901000	-2.956077000	H	6.470019000	-1.799503000	3.044971000
C	-5.887766000	-3.150991000	0.680412000	H	8.004647000	-1.270335000	1.168251000
C	-6.837483000	-4.099024000	0.337515000	H	7.096327000	-0.723898000	1.085483000
C	-7.531558000	-3.985886000	-0.875385000	H	2.091570000	-1.369681000	1.125199000
C	-7.281574000	-2.934646000	-1.746789000	H	1.182705000	1.072934000	2.608526000

H	-7.806211000	-2.836583000	-2.688783000	H	1.766061000	3.465443000	2.461031000
H	-8.273368000	-4.730056000	-1.141849000	H	0.695194000	4.901569000	0.713981000
H	-7.041736000	-4.928557000	1.003421000	H	-1.520584000	1.535723000	0.708930000
H	-5.334833000	-3.220891000	1.608907000				
H	-3.263674000	0.802622000	1.924018000				
H	-2.520596000	0.881990000	-0.950995000				
H	-4.671919000	6.095790000	0.540440000				
C	7.567663000	0.877948000	-1.297046000				
C	6.710479000	-0.165608000	-0.922402000				
C	7.207815000	-1.476864000	-0.933497000				
C	8.522453000	-1.743386000	-1.304971000				
C	9.339449000	-0.681011000	-1.659995000				
C	8.887873000	0.628904000	-1.663565000				
H	7.202675000	1.898480000	-1.288229000				
H	6.554692000	-2.301143000	-0.671708000				
H	8.911142000	-2.753758000	-1.329002000				
H	9.559513000	1.430258000	-1.944973000				
F	10.620169000	-0.932660000	-2.017065000				